論文 / 著書情報
Article / Book Information

題目(和文)	
Title(English)	Study on magnetic and electronic properties of activated carbon fibers
著者(和文)	中山敦子
Author(English)	Nakayama Atsuko
出典(和文)	学位:博士(理学), 学位授与機関:東京工業大学, 報告番号:甲第3213号, 授与年月日:1996年3月26日, 学位の種別:課程博士, 審査員:
Citation(English)	Degree:Doctor (Science), Conferring organization: Tokyo Institute of Technology, Report number:甲第3213号, Conferred date:1996/3/26, Degree Type:Course doctor, Examiner:
学位種別(和文)	博士論文
Type(English)	Doctoral Thesis

Study on Magnetic and Electronic Properties of Activated Carbon Fibers

-1996-

Atsuko Nakayama

Department of Chemistry

Tokyo Institute of Technology

What caused me to write about ACF?

Before talking about ACFs, in advance, I'd like to refer to activated carbons (AC) which are the root of activated carbon fibers (ACF). ACs are the products of social demands. They are useful for refining materials, catalysts, the withdrawal of solvents, pollution countermeasures, and the adsorbency of medical supplies. The industrial history of ACs started in the late 18th century and in time, human beings came to scientifically recognize the adsorbility of char. The gas adsorption phenomenon[1] and the decoloranity of the char[2] was studied, and these technologies were utilized for the technique of sugar refinement. However, systematic studies on the adsorption properties had not been started until the middle of the 19th century, when the first study of the production of AC to produce the drinkable water was done (Lipscomb[3], 1862) resulting in our ability to get clean water easily at present. At the same time, air cleaning was examined by using activated carbons (Stenhouse[4], 1872), and the mask was produced by using activated carbons. The examination of gas adsorption of the vapors of organic compounds was carried by Hunter[5] in 1865, who was one of the pioneers in the study of the gas adsorption. He had found that carbon from the endcarpe of coconut had the greatest absorbility among different activated carbons.

Recently, new activated carbons in the form of fibers named "Activated carbon fiber (ACF)" have been produced industrially. There are some ACFs which are separated pitch based, phenol resin based, poly-acrylic based, and cellulose based fibers, due to differences in pristine carbons. It is surprising to note that ACF's industrial products made in JAPAN account for more than 90% of the world's

total. Pitch based ACFs mentioned in this thesis have also originated in Japan. They were developed by Osaka Gas Corporation Ltd. and produced by Adore in 1986. ACF shows a higher adsorption speed and more excellent adsorption ability compared to former existing ACs. Another interesting factor of ACFs is its fiber form. The accepted forms of ACs have been granular powder carbons, and other properties besides adsorption have not been investigated and worked on. However, we expect further findings on the transport properties to ACFs which one is one of its several unknown characteristics of ACFs. Regarding the conduction mechanism and magnetic properties of carbon fibers (CF), especially, the relationship between the extension of microdomains by graphitization and the transport properties of CFs has been studied, and is explained in the text. We are now able to obtain ACF, and investigate its electronic properties. ACFs have a porous structure not found on CFs which will enable us to find new properties caused by the porous structure. What are the second and/or third outstanding features of ACFs demanded from the next age? Some possible answers to this question are going to be suggested in this thesis.

ACFs retain a lot of new properties which are not found in other materials. I am impressed by the fact that many of the ACFs in industrial products have their origin and their development in Japan, and I feel honored as a Japanese scientist to have had the opportunity to uncover certain characteristics of ACF.

Kawasaki, Kanagawa

December 1995 *Atsuko Nakayama*

Acknowledgements

The present thesis is summarized on the author's doctor course's study from April 1991 to March 1994 at Enoki's laboratory in Tokyo Institute of Technology. I would like to thank my thesis advisor Professor Toshiaki Enoki for his scientific guidance, as well as his continued support during the course of this thesis. As far as this thesis, the collaboration research with Dr. Stanislas Laurent di Vittorio who had been in the doctor course in Massachusetts Institute of Technology had given me the opportunity to study Activated carbon fibers (ACF), and a lot of meaningful results were obtained then.

I am deeply indebted to Professor Ko Sugihara of faculty of pharmacy of Nihon University for his theoretical supports and valuable discussions concerning "the spin-lattice relaxation mechanism of ACF", and Professor Katsumi Kaneo and Mr. Chiaki Ichii of faculty of science of Chiba University for the experimental support and valuable discussion concerning " characters of gas-adsorption of ACF and ACF's geometrical structure.

I acknowledge Mr. Norifumi Shindo of Osaka gas CO., LTD. for a gift of ACF samples.

As for the experimental part of this thesis, I got invaluable help and had valuable discussions from Dr. Kazuya Suzuki of Enoki's laboratory. I think Dr. Kei-ichi Koga of Institute of Solid State Physics of University of Tokyo for his support on the magnetic susceptibility measurements. The measurement of electron magnetic resonance spectra was performed in Professor Kaizu's laboratory of Tokyo Institute of Technology and Professor Sugawara's laboratory of University of Tokyo. The measurement of mass spectra through the thermal desorption was

performed in Professor Yashima's laboratory of Tokyo Institute of Technology. Scanning electron microscopy was performed in Professor Nishida's laboratory of Tokyo Institute of Technology.

I am grateful for many helpful discussion from the followings: Professor Mildred S. Dresselhaus of Massachusetts Institute of Technology, Professor Morinobu Endo of faculty of technology of Shinshu University, Professor Yuhei Shimoyama of Hokkaido University of Education, Professor Takuro Tsuzuku and Dr Keiko Matsubara of Nihon University, Dr. Mitsutaka Fujita of University of Tsukuba, Professor Hiroo Inokuchi, Professor Kyuya Yakushi and Dr. Syunji Bando of Institute of Molecular Science.

I would like to thank all the member of Enoki's laboratory for their various discussions and their kindness.

These acknowledgements would not be complete without mentioning the continued support and encouragement of my family, my friends, my apartment owner and neighbers, and all the member of International Center of Materials Research.

Contents

Part I

General Introduction

I-1 The Back Ground of The Geometrical Structures

There are many kinds of carbons which are classified by the difference in production processes. Carbon blacks[6], evaporated carbon films[7], anthracite carbon powders[8], glassy carbons[9], activated carbons[10], carbon fibers (CF)[11], and activated carbon fibers (ACF) mentioned as follows are typical carbons. They show unique phenomena observed in conductivities[12], ESR spectra[13], photoconductivities[14], and magnetresistance[15] reflecting their respective disordered structures not observed in graphite which has the ideal two dimensional structures. ACFs are one of the most modern materials in carbons. There are different kinds of ACFs determined by their respective precursors such as cellulose, pitch, polyacrylnitoril, and phenol. In particular, I have some interests and expectations in the point of the magnetic and the electron properties of ACFs, because of the highly disordered carbon materials with huge specific surface areas within their structure.

A total structure model of ACFs is shown in Fig. 1. ACFs consist of an assembly of many micrographites which are in turn composed of disordered stacks of three to four graphene sheets with a dimension of ca. $(20\text{-}30Å)^2$. These provide a microporous structure with ca. 10Å micropores.[16,17,18] The details are mentioned in the following part. The pore structure of ACFs attracts considerable attention due to high adsorptive activity, because one of its remarkable features is the enormous specific surface areas (SSA) ranging from 1000 to 3000 m^2/g. The

manufacturing process called "activation" gives rise to the porous structure, resulting in making SSA larger than other materials. The magnitude of SSA of ~3000 m^2/g exceeds the theoretical upper limit of SSA, which is 2630 m^2/g interpreted for a single layer of adsorbed molecules covering both surface of a single layer. It means that ACF has another gas-adsorption site in addition to the surface of graphene sheets.

The classification of the geometrical structure on ACF is summarized in Fig. 2. ACF structure is sorted out into textural structure and pore structure approximately. Textural structure is composed by π bonding structure consisting of micrographites and σ bonding structure corresponding to the dangling bonds and the bridges in order to link with micrographites as shown in Fig. 2 (a). Taking into account the differences of the functions shown in each part, ACF is characterized with inner structure and surface structure containing electrically active dangling bonds such as free radicals and electron attracting and/or donating groups, and electrically non-active dangling bonds like σ-bonding hydrocarbons expressed in Fig. 2 (b). ACF, where more than 40% of the constituent carbon atoms face to the surface[19], and though being solid, are very sensitive to gas adsorptions[16].

What is the basic sense of micrographites in ACFs? These are one of the amorphous carbons, and do not have an ordered structure like graphite, however, the results of X-ray diffraction give a broad peak of (002) which determines the stacking height of the graphene sheets[16]. The stacking height of the graphene

sheets composing of the micrographite is determined at ca. 1nm by using the peak width of (002) deflection. This result means that the micrographite consists of three to four graphene sheets. Micrographites are also found by transmission electron microscope observations (TEM)[18]. Figure 3 shows transmission electron micrographs of pitch based ACF1000 and 3000 taken by M. Endo[20]. There are the black color area as well as the white color area in TEM photographs, which are recognized as micrographite and the micropores, respectively. Many ordered micrographite consisting of the domain sized ca. 100 Å are found in ACF1000. However, ACF3000 has few ordered micrographites, and the domain sizes (ca. 30~40 Å) are smaller than that of ACF1000. Since th magnitude of SSA of ACF3000 is larger than that of graphite, the number of adsorption site and the pore structure of ACF3000 are different from those of ACF1000, resulting in the difference of the randomness in the configuration for micrographites. Thus, the structure of ACF3000 is supposed to be fundamentally different from that of ACF1000. Frankline[21] and Otani[22] modeled the structures of carbons having the crystallites shown in Fig. 4, which are referred to consider the difference of the randomness in structures between ACF3000 and ACF1000. There are two kinds of structural models of carbons which are graphitizing carbon having a two-dimensional orientation and non-graphitizing carbon having a three-dimensional orientation. Jenkins et al.[23] and Ban et al.[24] pointed out that the essential composition of disordered three-dimensional network structure in non-graphitizing carbons consists of carbon ribbons which get twisted and tangled each other. We focus the difference of the SSA which are produced by the activation of ACF

pristine samples in order to explain the difference of randomness of ACF structures, and propose to adopt the magnitude of SSA as one of the criterions to judge whether one ACF is the graphitizing carbon or non-graphitizing carbon. The magnitude of SSA of a completely two dimensional graphene sheet is 2630 m^2/g which is assumed as a threshold between graphitizing carbons and non-graphitizing carbons. If the value SSA of ACF is smaller than threshold, the structure is decided to be two dimensional-like. The structure of ACF having larger SSA than threshold occurs the production of the multilayers of adsorption molecules because a volume by unit mass of a micropores is larger than that of a slit between graphene sheets. Randomness of the orientation of micrographites, which is the origin of the micrographites, generates the three dimensional structure of ACF. Judging from not only the threshold of SSA but also TEM photographs, it is supposed that ACF1000 is more easily graphitized by heat-teratmnet than ACF3000.

The pore structure of ACF is connected with the micrographite structure and the domain structure of micrographite, and it is important to consider the pore structure of ACF in order to understand the properties of ACF. In addition to the measurement of the micrographite size, the pore size is approximately estimated by measuring TEM photographs at 10 Å to 100 Å which are distributed widely[18]. The difference of the values of SSAs is characterized by the sizes and the distributions of the pores. In Fig. 3, white color area of ACF3000 is larger and more widespread than that of ACF1000. It means that the difference of the magnitude of SSAs directly appears at the degree of the growth of the pore structures. The classification for the surfaces and the pores of the adsorbents

decided by IUPAC at 1972 is shown in Fig. 5[25]. The surface of the adsorbent is sorted out on the outer surface and the inert surface composed by the inert walls of the pores. In the case where size of the pore diameter is larger than 500 Å, it is named "macropore" which plays the role of transport pores in order to admit and diffuse the adsorbate. The pores in the range of 500 to 20 Å are named " micropore". Pores smaller than 8 Å are called "sub-micropore" and/or "ultra-micropore". The adsorption site's model for the foreign molecules is estimated from the results of gas adsorption and the X-ray diffraction which shows structural changes of micro-graphites by gas adsorption, and the micro structure of the micropores is analized[26]. The stacking of graphene sheets consisting of micrographite is disordered, and the distance between the layers of the micrographite is about 3.5 Å which is larger than that of the graphite (~3.35 Å). The introduction of H_2O molecules in ACF makes higher ordered stacking of micrographites, which is caused by the interaction between H_2O molecules and the micrographite. Introduction of N_2 gas also changes the interlayer distance with smaller amount of packing fraction than that of H_2O molecule[16]. The difference of the packing fraction between H_2O molecule and N_2 molecule is expressed by the micro structure of the micropores as shown in Fig. 6. The shape of the micropore of ACF is not of the slit type but of the wedge type[16]. H_2O molecule shows polarity, and is adsorbed to the edge parts of the micrographite wherein surface functional groups showing hydrophobicity exist, resulting in intercalate in the interlayers. However, N_2 molecules is non-polar molecule and adsorbs to the

bottom of the wedge type pore where the larger adsorption energy of N_2 molecules is made by the intermolecure interaction between nitrogens and carbons. So N_2 molecules changes the orientation of the layers easily. Recently, Kaneko et al. had determined the adsorption isotherm of helium on ACFs at 4.2 K[27]. It was found that the micropore volumes estimated by the helium gas adsorption isotherm are greater than those obtained from the nitrogen adsorption isotherm at 77 K by 20~50% [16]. The excess amount with the measurement of micro pore volume by using helium molecules is reflected in the presence of ultra micropores which cannot be assessed by nitrogen molecules. The difference between the amount of adsorbed helium and nitrogen is more significant in the pitch based ACF. The average micropore size determined by the nitrogen adsorption is estimated at 0.8, 1.0 and 0.4 nm for ACF1000, 2000 and 3000, respectively. The excess adsorption amount of helium proves the presence of ultra micropores which makes us presume that the micrographites have the partially closed wedge-shaped pores and/or interstitial cages as shown in Fig. 6.

The surface structure of ACF is characterized with the dangling bond having σ bonding structure. In general, the surface structure of carbons is searched by the thermal desorption[28], the chemical analysis[29], and electron spectroscopy[30]. The edge of a crystallite is covered with the functional groups like oxides of hydrocarbons. The modeled molecular structure of functional groups as the surface oxide is thought to be "cromene" typed structure[31] shown in Fig.7. The carbon atom shows non-polarity. The interaction between the carbon atoms facing to the surface and adsorbents is influenced by dispersion force[32], and the carbon surface

shows hydrophobicity. The result of the adsorption of H_2O molecules labeled by the tritium to the graphite shows that the H_2O molecules selectively adsorb on the parts of ages of micrographites[33], and two or three H_2O molecules per one site of the dangling bond adsorbs on the functional group consisting of activated hydroxide and perfectly desorbs by pumping for 15 hours with heating at 100°C. The proportion of functional groups in the total surface area is estimated at about 5%[34] and non-active surface amounts to 95%. Activated carbons, carbon blacks, and carbon fibers having the micrographite crystals seem to have common surface structures, so it is supposed that the same former surface structure applies to that of ACFs.

The geometrical structure of ACF is understood by the diffraction and numerous experiments of gas adsorptions as mentioned above. However, there are some unknown points about material properties of ACF. For example, gas adsorption of ACF is a reversible reaction which means physisorption. It is a strange and unbelievable phenomenon that the structural change of the micrographite does not cause chemical bonding between surface atoms and adsorbate. The property of ACF is characterized by the surface, the nanoscaled particle, the disordered structure, and the pore structure, and ACF is one of the "coexistent composite" with some kinds of functions which are very interesting.

I-2 Magnetic and Electronic Properties of Carbons

i Two Dimensional Graphite Model

The electronic properties of the micrographite composing ACF structure are based on the two-dimensional graphite model in this thesis, which is caused by ACF structure consisting of micrographite. Stacking of graphene sheets composing micrographite is not regular and unlegitimate along c-axis, and the average interlayer distance is ca. 3.5Å[16] which is larger than twice of van der Waals radius, and the interlayer interaction of micrographite is negligible. Therefore two-dimensional graphite model is enough to explain the electronic state of ACF.

Two-dimensional graphite model is explained as follows. Graphite consists of layered compounds having stacking structure of two dimensional graphene sheets shown in Fig. 8. The bonding length between the nearest two carbon atoms "a" in a graphene sheet is 1.42Å caused by sp^2 hybrid orbital and the magnitude of the resonance integral of π-orbitals between the nearest neighbor carbon atoms.Three dimensional structure of graphite is composed by alternate layer stacking of graphene sheets having different configuration of the unit cell in ab-plane along c-axis. The interlayer distance of graphite is 3.35Å caused by a weak covalent bond whose magnitude of interaction is one tenth in comparison with that of the intra-plane interaction. Therefore the electronic properties of graphite is dominated by π electron in the ab-plane. The theoretical calculation for π-band model of two

dimensional graphite by Wallace[35] and the linear combination of atomic orbitals (LCAO) approximation about polycyclic compounds regarded as graphite by Coulson et al.[36] point out that graphite is the zero gap semiconductor shown in Fig. 9 (a). The two dimensional model of graphite is used in two carbon atoms whose π-electrons fill the first Brillouin zone consisting of a hexagon. The magnitude of density of states is estimated by the following equation;

$$N(E) = 8|E| / 3\pi\gamma_0^2 a^2 \quad (1)$$

where N(E) is the density of states (DOS), E is the energy, and γ_0 is the magnitude of the resonance integral between π-orbitals of the nearest neighbor carbon atoms on a graphene sheet. However, judging from the stacking effect of graphene sheets, we can see three dimensional graphite model having the interlayer interaction of graphite whose electronic state is shown in Fig. 9 (b). π and π^* bands are split by the interlayer interaction, and these bands overlap each other at the peripheries of Fermi energy level, which compose two kinds of Fermi surfaces having the same number of electrons and holes. Therefore graphite is semimetal from the view point of the three dimensional graphite model.

ACF is explained by two dimensional graphite model pointing out that the value of DOS at the Fermi energy level $N(E_F)$ equals 0, however, judging from the conduction behavior of ACF, it is indispensable to consider the electronic state at the peripheries of the Fermi energy level. There is some conflict in this model.

More details and discussions are mentioned in PART IV.

ii Hopping Conduction Mechanism in Non-Crystalline Materials

The crystalline materials have ordered structure whose electrons move as the periodic wave functions. However, the random system and/or the amorphous system as non-crystalline materials have many kinds of random potentials. If the magnitude of the fluctuation of kinetic energy of electrons is smaller than the potential energy, the magnitude of the overlap between the nearest atoms is smaller, and the electrons tend to be trapped at the bottoms of deeper potentials. This phenomenon is called "the localization of electrons" which are activated at higher temperatures, and the hopping conduction occurs in these system. Judging from the ACF structure consisting of an assembly of micrographites, we can ascertain ACF is also composed by random structure with random potential, and it is supposed that hopping conduction between micrographites playing a role of metallic islands is occured by thermal activation process. In this section, the two dimensional random structure like ACF is focused, and the two dimensional variable range hopping mechanism is explained as follows[37].

At the electron localization points in the system, the wave functions of the electrons attenuate in accordance with the function of exp ($-r/\xi$), where ξ is the localization length, and r is the distance from the localizing point of the electrons. The probability of overlap between the wave functions of the adjacent micrographitic domains departed with the length r is in proportion to exp ($-2r/\xi$). Moreover, the occurrence of a hopping event requires the thermal activation which is related to the difference in the potential energies of hopping electrons ΔE. Thus,

the hopping conductivity σ is expressed by the following equations;

$$\sigma = \sigma_0 \exp\left(-2\alpha r - \frac{\Delta E}{kT}\right), \tag{2}$$

where σ_0 is constant. ΔE depends on DOS at Fermi energy level $N(E_F)$ and the dimensionality of the transport system. In the random network system of metallic microdomains having two dimensionality, ΔE is expressed by following equation.

$$\Delta E = \frac{1}{\pi r^2 N(E_F)}. \tag{3}$$

The optimum of hopping length r in order to have the maximum of the hopping probability is estimated from the minimum of the term $-2\alpha r - \frac{1}{kT} \times \frac{1}{\pi r^2 N(E_F)}$,

and in this case r is obtained as equation (4);

$$r = \left(\frac{1}{\pi N(E_F)\alpha kT}\right)^{\frac{1}{3}} \tag{4}$$

Therefore, equation (2) is rewritten by the variable range hopping formula in the temperatures as given by the following equation;

$$\sigma = \sigma_0 \exp\left(\left(-\frac{T_0}{T}\right)^{\frac{1}{3}}\right). \tag{5}$$

Here T_0 is expressed by

$$T_0 = \frac{27}{\xi^2 \pi N(E_F) k}, \tag{6}$$

where k is the Boltzmann constant. Thus the value of DOS at the Fermi energy level $N(E_F)$ in the case of 2D VRH is estimated.

iii Graphitization And σ-Trap Model Of Carbons

It is difficult to analyze the geometrical structure of carbons like ACF directly. However, we can ascertain the geometrical structure indirectly by utilizing heat-treatment. The study of heat-treatment effects of carbons provides very important information in addition to modelling the electronic and the geometrical structure of amorphous carbons which have many kinds of bondings.

Carbons cause structural change by heat-treatment, and their electron states vary drastically. If the pristine structure of some carbon consists of graphitizing carbon, graphitization starts at heat-treatment temperature (H.T.T)=1000~1300°C[38], and the electronic state changes to metallic state at 2800℃. The electronic properties of a soft carbon had been investigated by Morosowski et al. about forty years ago[37], and the change in electron structure going with graphitization process is clarified. The results of H.T.T dependence of the electrical resistivity and Hall coefficient of a soft carbon are shown in Fig. 10[39]. The samples heat-treated below 1000°C show semiconductivity. H.T.T. dependence of the resistivity shows the transition from the insulator to the semiconductor below H.T.T.=1000°C. This is explained by the "σ-trap mechanism[38, 40]" of a soft carbons shown in Fig. 11. On heat-treating carbons, the functional groups are removed from the edge of micrographies, and the unsaturated σ-bondings remain. The π-electrons contained in the carbons are trapped by the unsaturated σ-bondings, and the same number of holes are generated in the valence band, resulting in positive Hall coefficient. The

sample heat-treated above 1000℃ has many more number of electrons trapped by unsaturated σ-bondings than that below 1000℃. The Fermi level moves to the lower energy level of π-band, resulting in the negative carriers. The magnitude of resistivity in the H.T.T. range from 1000°C to 2200°C shows little change. In this temperature range, the generation of impurities like the dangling bonds decreases and the graphitization of crystallite progresses. The number of electrons trapped by the σ-band decreases, and the magnitude of the mean free path of the carriers increase because of enlargement of the size of crystallites. Thus the Fermi level shifts near the top of the π-band, resulting in positive carriers. In the temperature range between H.T.T=2200°C and 3000°C, resistivity decreases again. It means that the upper edge of π band and lower edge of π* band overlap by interplane interaction with ordering of three dimensional stacking, and that supplying the conduction electrons to the π and π* band changes to the negative Hall coefficient.

Thus graphitization of various carbons is explained by the σ-trap model, so that the electronic properties of carbons are described inclusively. Further, the electronic change in ACF1500 (SSA≈1500m^2/g) with heat treatment is also explained by the σ-trap mechanism, which has been proven by the experiments of thermoelectric power of the ACF1500 heat-treated at 1000°C to 2800°C[41]. Consequently, it has been found that ACF1500 is one of the graphitizing carbons[21].

iv ESR Study of Carbons

In this section, ESR studies of graphite and some carbon fibers (CF) are taken up as reference for the ACF study. Graphite and CFs have conduction electrons and/or dangling bonds which are able to be measured as ESR signals, therefore, we are able to get structural and electrical information like the spin density, the magnitude of the magnetic interaction between the spins and so on from the ESR spectra.

The ESR signal of the conduction electron of graphite shown in Fig. 12 had been measured by Wagoner et al. (1960)[42], and is called Dysonian curve[43] which has unsymmetrical line shape. The Dysonian signal has originated from the attenuation of the microwave amplitude and the phase shift which are caused by the high conductivity of the sample. The conductivity of a graphite is σ=2X10^{14} Scm^{-1} (in-plane conductivity), therefore, the microwave for the ESR measurement attenuates by the screening effect of the conduction electrons, and is not able to penetrate from the surface to the inside of graphite, which is called "the skin effect". The magnitude of the skin depth is estimated by $\delta = c/\sqrt{2\pi\omega\sigma}$, where δ is the skin depth of the microwave in the sample, c is the light velocity, ω is the frequency of the microwave, and σ is the conductivity of a sample. The skin depth for the graphite is estimated at $\delta \sim 10^{-4}$ cm. Therefore, the ESR signal of graphite gives information of surface spins because of high conductivity. Further, the graphite shows anisotropy with parallel and perpendicular direction against the

graphite ab-plane, which is expressed by g-values $g_{\parallel}$ and $g_{\perp}$, respectively. $g_{\parallel}$ has no temperature dependence, and the magnitude is $g_{\parallel}$=2.0026 which is similar to the g-value of the free electron. However, the value of $g_{\perp}$=2.0495 at room temperature is larger than that of $g_{\parallel}$, and show the temperature dependence showing the decrease with increasing temperature, which is reflected by the band structure at the Fermi energy level. As mentioned in section **I-2-i**, for the electron structure of graphite, the conduction band and the valence band degenerate at the edges of each bands, and their degenerated level is near by the Fermi energy level, resulting anomalous g-value shift. Thus, the ESR spectrum of graphite gives microscopic properties generated from high conductivity and anisotropy.

Recently, ESR measurement is focused due to the view point of the characterization of properties and the domain structure of CFs which have a lot of possibilities as new industrial materials. Jones and Singer[42, 44] investigate the heat-treatment effect of pitch-based and PAN (polyacrylonitorile)-based CF by ESR method spectra which show drastic change by heat-treatment as shown in Fig.13 (a). The spin density increases with the increase in temperature up to 800°C through the increase of the number of dangling bond spins. And above 800°C, the line width increases with the reduction of the hopping rate of conduction electrons between microcrystals because of the enlargement of the size of a microcrystal by heat treatment. The ESR line shape of PAN-based carbon fibers heat-treated at 3000°C is shown in Fig.13 (b). The type of line shape is similar to the Dysonian type[43] which is assigned by the conduction electron spins of graphite. The g-value of PAN-based CF shows the anisotoropy which means formation of the ordering

of microcrystals in CF by heat-treatment has taken place. The micrographene plane consist of microcrystals which is parallel to the axis of CF, and the vertical orientation on the carbon axis consists of disordered arrangement of the microcristals. Further, they explain the problem of the transverse motional averaging in CF from the ESR line shape and the anisotoropy of the g-value. If they spend their entire spin lifetime within a single domain, the ESR spectrum will be the sum of individual ESR signal from domains of different orientations with respect to the magnetic field. On the other hand, according to another PAN-based CF measured by Robson et al [45], small domain CF is explained as follows. If the transverse domains are so small that a given spin sees essentially all possible crystallite orientations during its life, a time-averaged g-value results $g_{\perp}=(g_{\perp G}+g_{\parallel G})/2$, where $g_{\perp G}$ and $g_{\parallel G}$ are $g_{\perp}$ and $g_{\parallel}$ for graphite. This is to say that the magnitudes of domains of CFs reflect the ESR spectra generated from their conduction electrons.

Thus,the use of ESR measurement is appropriate for understanding the micro structure and properties which are not distinguished by another measurements through the combination of the analysis of the heat-treatment effect with the structural change of CFs. According to the structural similarity between carbons and a graphite, the magnitudes of the conductive domains of carbons are able to be estimated from their ESR line shapes.

I-3 Sample Preparation and Characterization

In present experiments, we have employed pitch-based ACF1000, ACF2000, and ACF3000 whose specific surface areas (SSA) are 1000, 2000, and 3000 m^2/g respectively. The development for the production of CF had been started by Osaka Gas Co., and the development research for the manufacturing process of ACF made from coal tar pitch was carried out by joint development between Osaka Gas Co., Ltd. and Unitika who established AD'ALL Ltd.. They produce ACFs as final products made from specially prepared pitch supplied from Osaka Gas Chemical Co., Ltd..

The production process of pitch based ACFs is shown in Fig. 14 [45]. The technical points for the production of pitch based ACFs is expressed as follows; 1) Preparation of spinnable pitch made from coal tar, 2) Molten spinning of pitch, 3) Infusibility of the pitch fiber, and 4) Activation of the fiber made on infusibility. For process 1, the molecular design of ACF based on the chemical synthesis was considered through the know-how of the infusibility. For process 2, the calculation based on the theory of molten spinning was used for the problem related to the difference of temperature dependence on the viscosity between pitch and raw materials of the synthetic fiber. Infusibility in process 3 is the transformation by heat-treatment of the pitch fiber under the oxidized atmosphere. The infused pitch fiber is able to endure against the activation process. Activation in process 4 is the process for producing innumerable pores by heat-treatment at higher temperature of infused pitch fiber under inert gas atmosphere.

The details of the production of ACF are explained as follows. ACF pristine samples made from spun fiber after the precursors started from petroleum pitch have undergone an antiflammable process at 300°C in air. In the activation process,

the fibers were carbonized at 800 to 1200 °C in the presence of CO_2 or water vapor. In this process, the highly porous structure of ACF was made by depriving carbon atoms from the precursors through oxidization reaction. The magnitude of SSA was measured by adsorption isotherms of N_2 at 77 K and CO_2 at 195 K.

The theoretical carbonization yield of the precursor of ACF is 93%. The chemical formula of ACF is estimated at $[C_{124}H_{80}\ NO]_n$ [46]. The theoretical carbonization yield of pitch based ACF is higher than other ACFs as shown in Table 1.

Basic physical properties are summarized in Table 2 [47], and the distribution of the pore size of ACF is shown in Fig. 15 [48]. These data are measured by the nitrogen gas adsorption method at low temperature by using automatic gas adsorption equipment.

I-4 Object of This Study

ACFs are microporous carbons with huge SSAs ranging from 700 to 3000 m^2/g, and have random structures consisting of an assembly of the micrographites as mentioned in Part I-1. The ACF structure has been mainly investigated by gas adsorptions, along with structural analysis as X-ray diffraction, and the structural model had been added each time until now when the new experimental results were obtained. However, it is difficult to understand the micro structure of ACFs by only these method. In order to understand the micro structure of ACFs, it is necessary to investigate the electronic and magnetic properties of ACFs. In addition, if gas adsorption properties are explained from the view point of variation of the electronic and magnetic properties, further more detailed structures of ACFs and their gases adsorptions states are able to be modeled.

In this thesis, in order to explain the micro structure and the properties generated by the microstructure from the view point of the classification of micro structure, the contents are separated by three parts which are composed of **"Dangling Bonds"** (in Part II), **"Pore Structure"** (in Part III), and **"Micrographite and Network Structure"** (in Part IV).

In Part II, in order to clarify the basal solid state properties and the structure, the magnetic susceptibility and ESR spectra for pitch-based ACF3000 (SSA ~ $3000m^2/g$) are mentioned. In addition, the effects of the presence of oxygen, helium or iodine and of the application of various heat treatments are explained. thus, the Figure of the dangling bond is clarified.

In Part III, a novel microporous structure of ACF3000 is explained from the

view point of magnetic relaxation. It is a new aspect for the estimation in the analysis of the porous structure. In addition, an anomalous spin-lattice relaxation behavior of the dangling bond spins affected by gases adsorption of the various gases is explained. Specifically, helium gas induces a remarkable condensation in ACF, and the existence of ultra micropores in ACF is confirmed.

On the other hand, ACF1000 and ACF2000 with SSA=1000 and 2000 m^2/g are focused in Part IV, and electrical conductivity and magnetic susceptibility have been investigated in order to clarify the relation between the electronic properties and the structure of ACF having a random network of the micrographites. The electrical conductive mechanism and its effect against gas adsorptions are explained, thereby clarifying the electron structure of ACF. The relationship between the density of state of ACF and the value of the orbital diamagnetic susceptibility explain the inner micrographite structure.

Thus, further details of the micro and macro structure of ACF are identified, which are summarized in Part V.

Reference for Part I (Containing Preface)

1. F. Fontana, *Mat. Fis. Soc.* (Ital.), **1**, 679 (1777).
2. Lowitz, *Crell's Chem. Ann.*, **1**, 211 (1786).
3. F. Lipscombe, British Patent, 2887 (1862).
4. J. Stenhous, *Chem. News*, **25**, 239 (1872).
5. J. Hunter, *J. Chem. Soc.*, **18**, 285 (1865).
6. J. Bisscoe and B. E. Warren, *J. Appl. Phys.*, B, 364 (1942).
7. T. Hanawa and J. Kakinoki, *Carbon* , **1**, 403 (1964).
8. H. Hirabayashi and H. Toyoda, in Proceedings of the Fourth Carbon. Conference (Pergamon press, Oxford, 1963) 2, 219.
9. D. F. Baker and R. H. Bragg, *Phys. Rev.*, **B28**, 2219 (1983).
10. J. W. Armstrong, C. Lackson and H. Marsh, *Carbon* , **2**, 239 (1964).
11. D. Robson, F. Y. I. Assabghy, and D. J. E. Ingram, *J. Phys. D: Appl. Phys*, **4**, 1426 (1971).
12. M. Z. Tahar, M. S. Dresselhaus and M. Endo, *Carbon* , **24**, 67 (1986).
13. A. A. Bright and L. S. Singer, *Carbon*, **17**, 59, (1979).
14. K. Kuriyama and Dresselhaus, *J. Mater. Res.*, **6**, 104 (1991).
15. A. A. Bright, *Phys. Rev.*, **B20**, 5142 (1979).
16. K. Kaneko, C. Ishii, M. Ruike, and H. Kuwabara, *Carbon*, **30**, 1075 (1991).
17. M. S. Dresselhaus, A. W. P. Fung, A. M. Rao, S. L. di Vittorio, K. Kuriyama, G. Dresselhaus, and M. Endo, *Carbon* , **30**, 1065 (1992).
18. M. Endo, K. Oshida, S. L. di Vittorio, M. S. Dresselhaus and M. Shindo, International Symp. on Fractal and Physically Adsorption Molecular States,

Chiba, Japan, May 14-15, (1992).

19. K. Kaneko, private communications.

20. M. Endo, private communications.

21. R. E. Frankline, *Proc. Roy. Soc.* (London), **A209**, 196 (1951).

22. S. Otani, *Carbon* (in Japanese), **61**, 60 (1970).

23. G. M. Jenkins, K. Kawamura, and L. L. Ban, *Proc. Roy. Soc.* (London), **A327**, 501 (1972).

24. L. L. Ban, D. Crawford, and H. Marsh, *J. Appl. Cryst.*, **8**, 415 (1975).

25. IUPAC-Manual of Symbols and Terminology for Physicochemical Quantities and Units, Butterworths, London (1972).

26. T. Suzuki, M. Kasu, and K. Kaneko; *Chem. Phys. Lett.* (in press).

27. H. Kuwabara, T. Suzuki, and K. kaneko, J. Chem. Soc. Faraday Trans. 87, 1915 (1991).

28. R. L. Zapp, and A. M. Gessler, *Rubber Age*, **74**, 234 (1953).

29. V. A. Graten, and D. E. Weiss, *Australian J. Chem.*, **10**, 309 (1957).

30. Y. Nakayama, F. Soed and A. Ichitani, *Carbon*, **28**, 21 (1990).

31. S. Ogiwara, KAITEI TANSO ZAIRYOU NYUMON (in Japanese), p188, THE CARBON SOCIETY OF JAPAN (1984).

32. M. M. Dubinin and P. L. Walker Jr., (ed), Chemistry and Physics of *Carbon*, **2**, 51, Marcel Dekker (1966).

33. G. L. Montet, Proc. 5th Conf. on Carbon, 1961, Pergammon Press, **I**, 116 (1962).

34. D. Rivin, J. Aron and I. Medalia, *Rubber Chem. Technol.*, **41**, 330 (1968).

35. P. R. Wallance, *Phys. Rev.*, **71**, 662 (1947).

36. Coulson and R. Taylor, *Proc. Phys. Soc.*, **65**, 815 (1952).

37. N. F. Mott and E. A. Davis, "Electronic Process In Non-Crystalline Materials",

38. S. Mrosowski and A. Chabarski, *Phys. Rev.*, **104**, 74 (1956)

39. E. A. Kmetko, *J. Chem. Phys.* **21**, 2152 (1953)

40. T. Tsuzuku, *TANSO*, **163**, 163 (1994).

41. T. Enoki, K. Inukai, K. Suzuki, M. Endo, and N. Shindo, private communication.

42. G. Wagonen, *Phys. Rev.*, **118**, 647 (1960).

43. F. J. Dyson, *Phys. Rev.*, **98**, 349 (1955).

44. J. B. Jones and L. Singer, *Carbon*, **20**, 379 (1982).

45. D. Robson, F. Y. Iassabghy and D. J. E. Ingman, *J. Phys. D: Sppl. Phys.* **4**, 1426, (1971).

46. N. Shindo, K. Tai and Y. Matsumura, Chemical engineering, **32**, 28 (1987).

47. K. Tai, K. Nakai and N. Shindo, SENIKIKAIGAKKAISHI (in Japanese), **41**, 356 (1988).

48. K. Tai and M. Kibe, NENRYOU OYOBI NENNSHOU (in Japanese), **57**, 161 (1990).

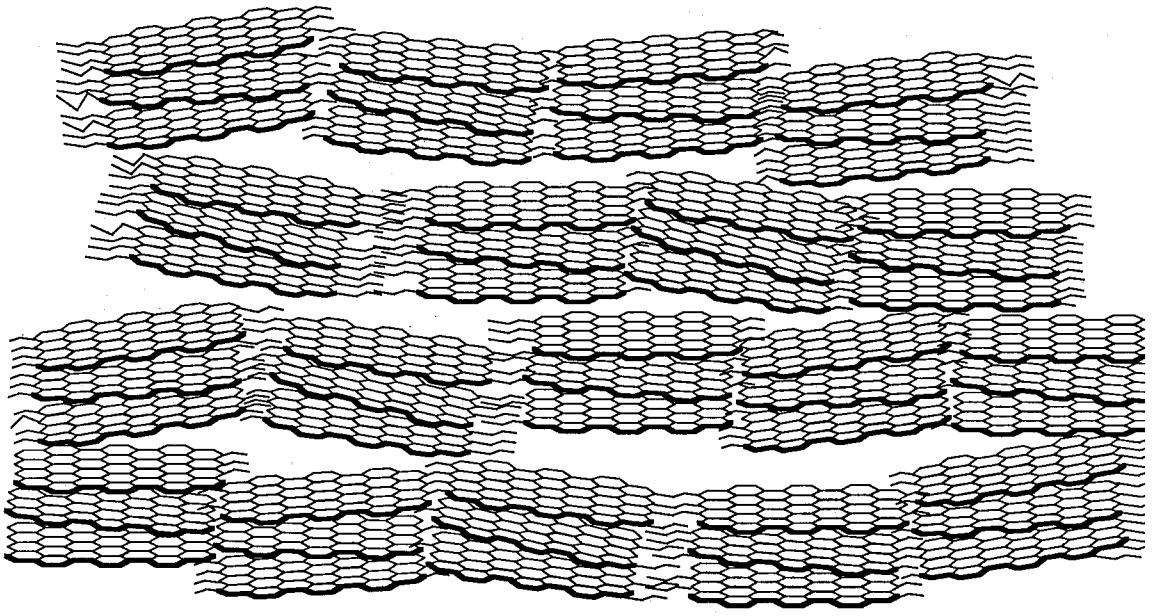

Fig. 1 The model structure of activated carbon fiber.

(a)

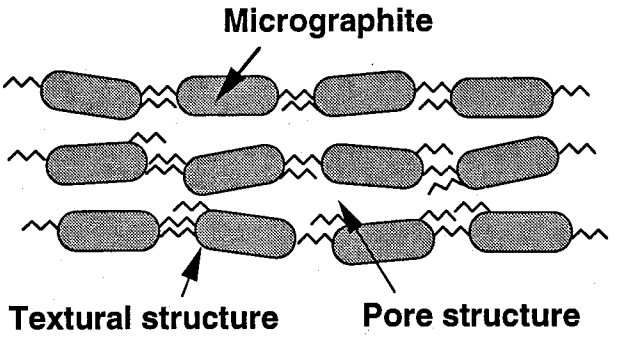

(b)

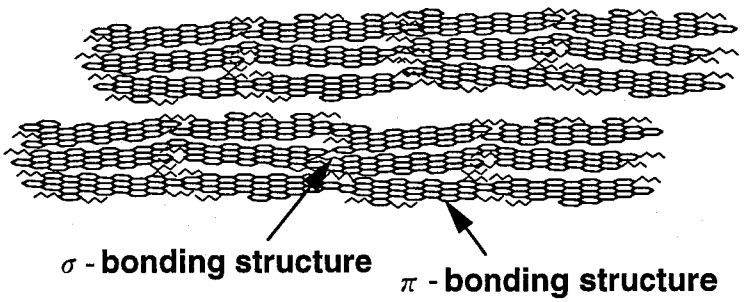

(c)

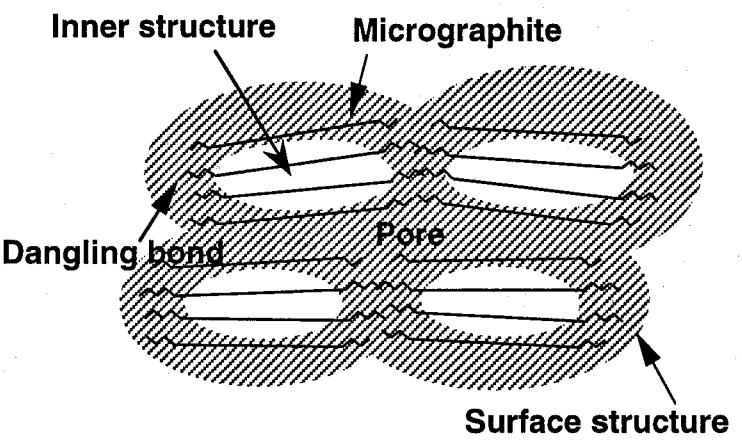

Fig. 2 The classification of the geometrical structure of ACF.
(a) Textural structure and pore structure.
(b) π-bonding structure and σ-bonding structure of textural structure.
(c) Inner structure and Surface structure.

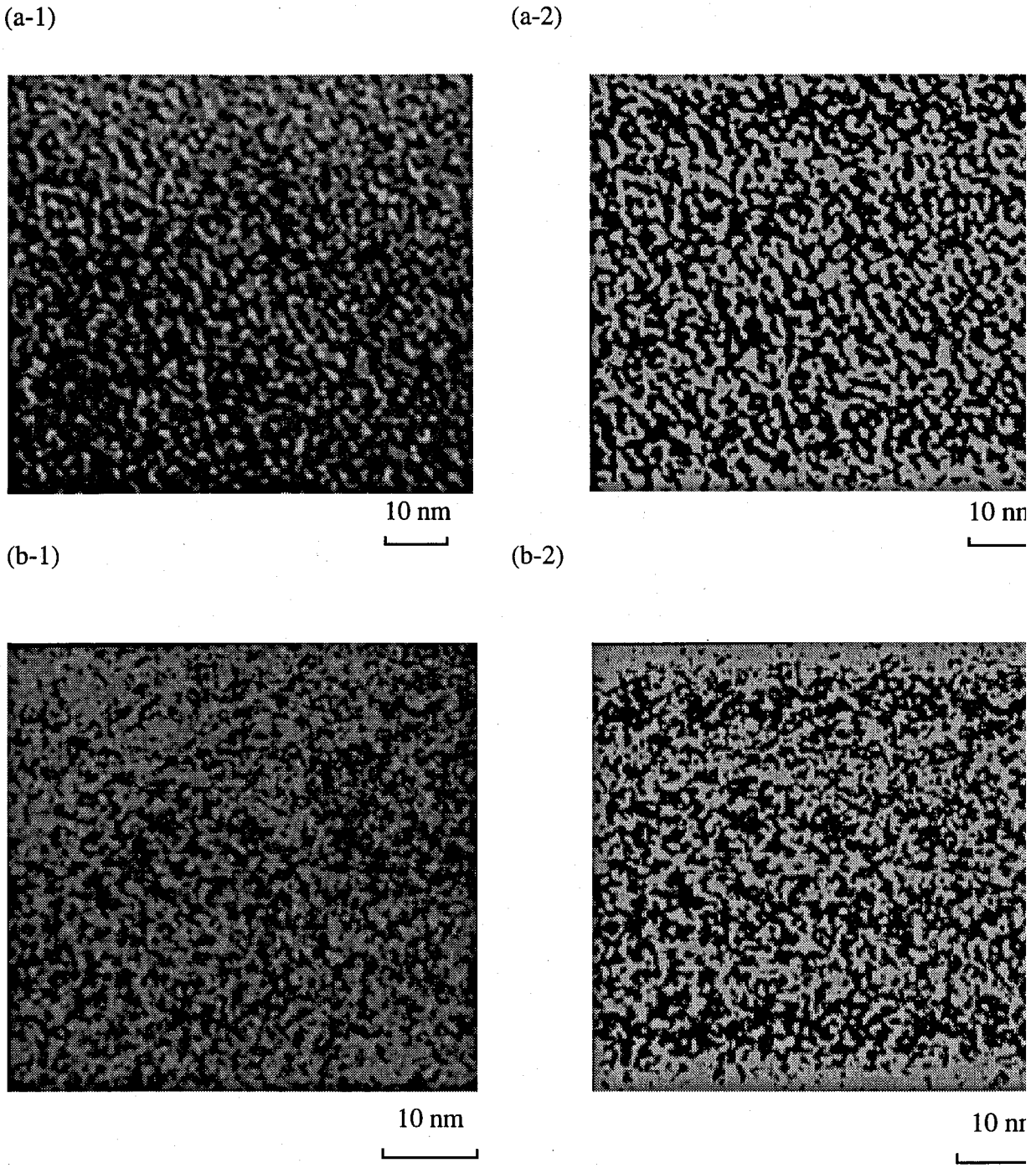

Fig. 3 TEM photographs of ACF1000 (a-1) and ACF3000 (b-1), and the digitized TEM images for ACF1000 (a-2) and ACF3000 (b-2) by Endo at 1992. (Ref. 20)

(a)

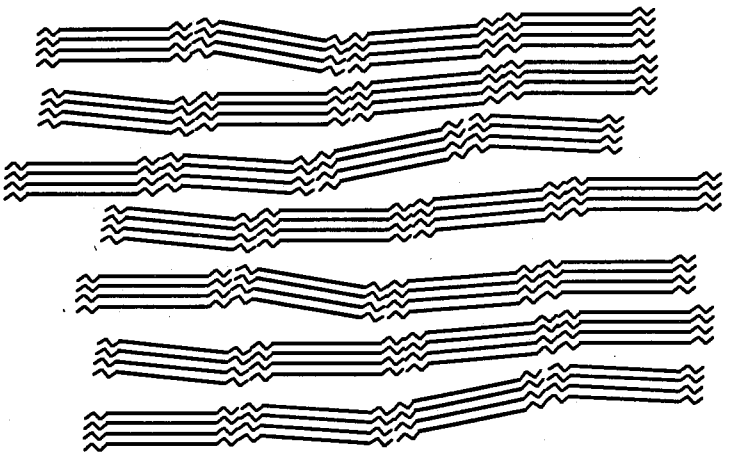

(b)

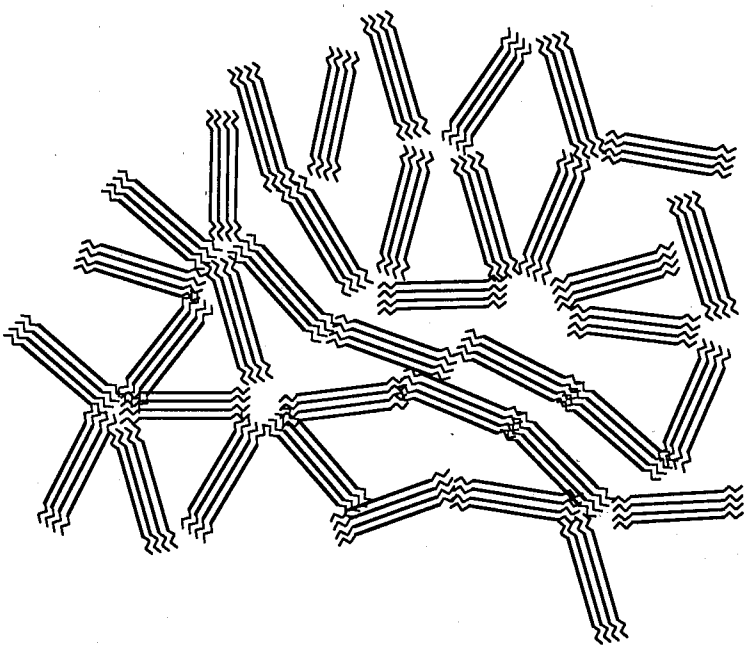

Fig. 4 Franklin model for the microstructures of (a) graphitizing carbons and (b) the non-graphitizing carbons. (Ref. 20 and 21)

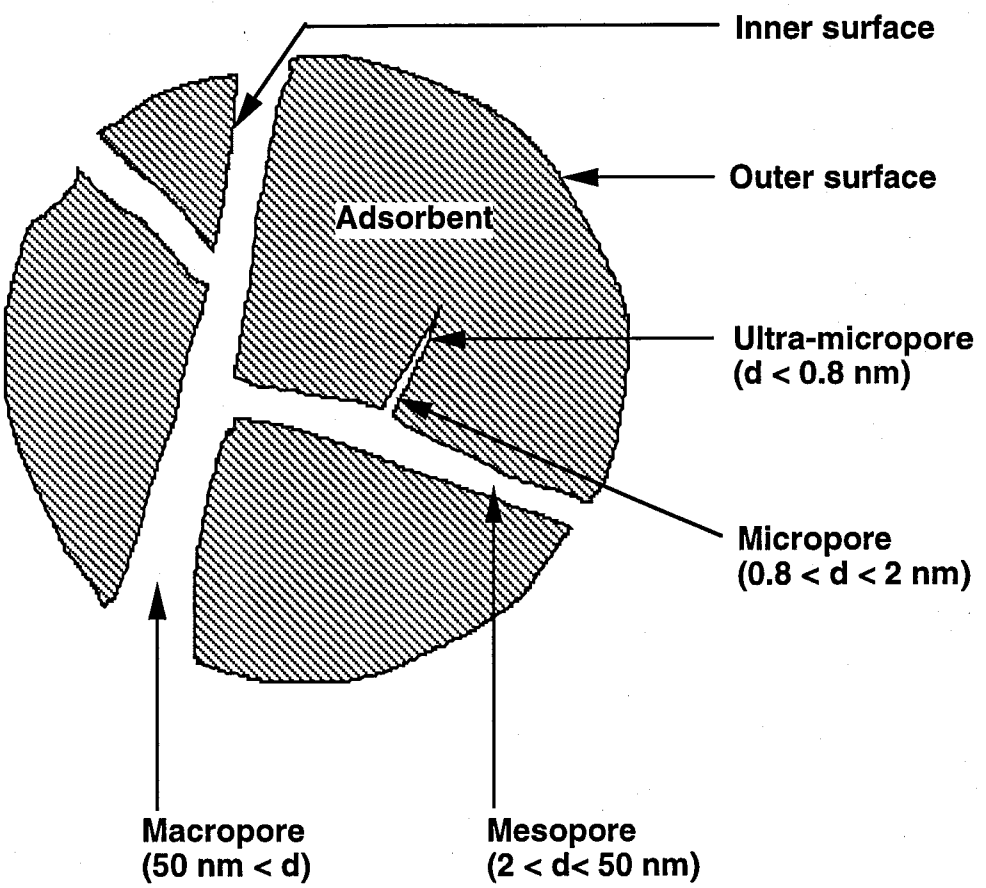

Fig. 5 The classification for the surfaces and the pores of the adsorbents. Symbole "d" shows the diameter.
[IUPAC-Manual of Symbols and Terminology for Pysicochemical Quantities and Units (1972), (Ref. 24)]

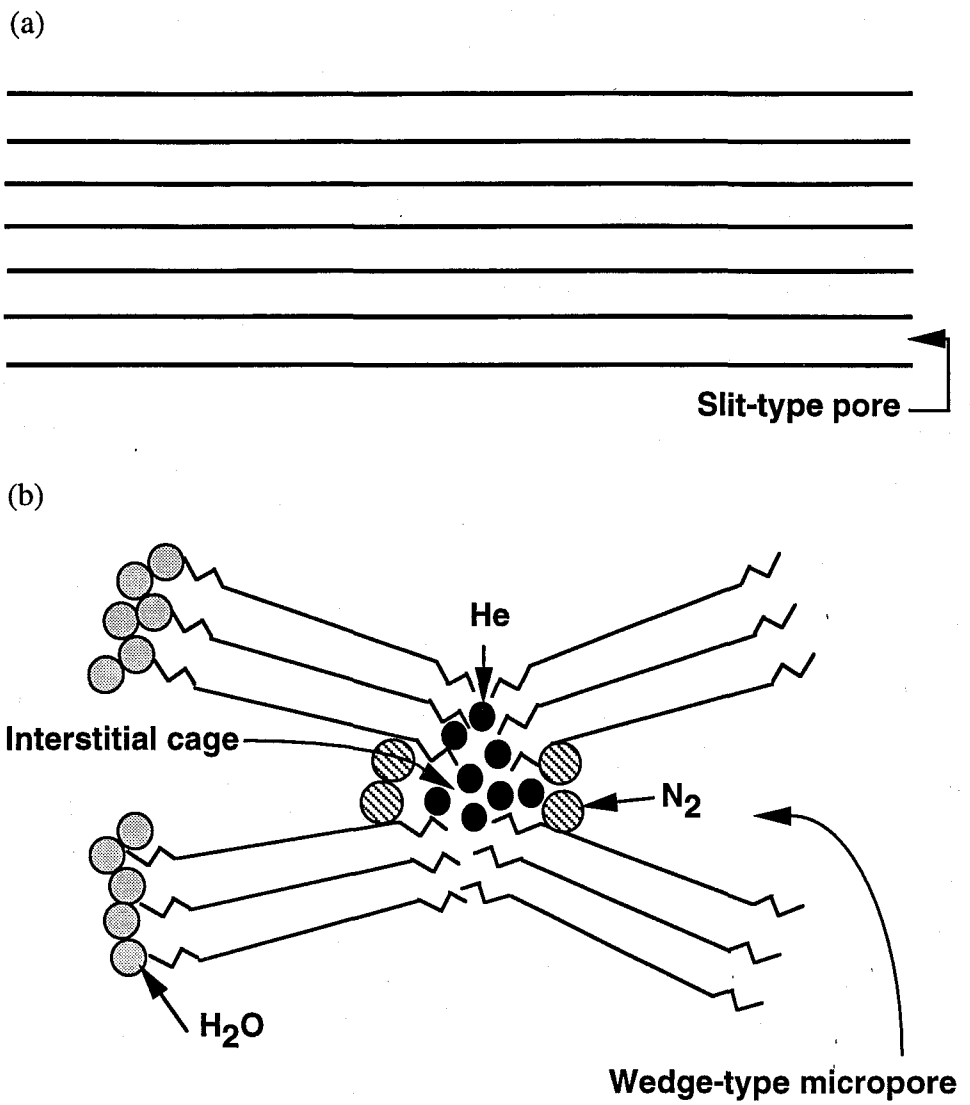

Fig. 6 The pore types and the model of the gas adsorption site of ACF. (Ref. 15) (a)The slit-typed pore shown in the inter layer compounds like graphite. (b)The wedge-type micro pore shown in ACF.

(a) Phenil group

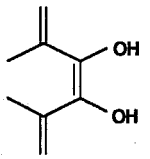

(b) Carbonyl group, quinone group

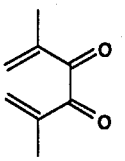

(c) Carboxyle group

(d) Absorute carboxyle group

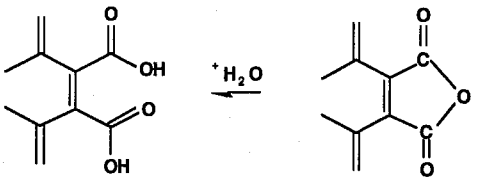

(e) γ-Lactoyl group

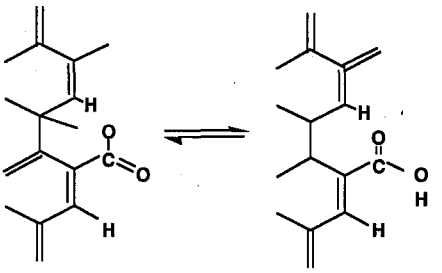

(f) δ-Lactoyl group

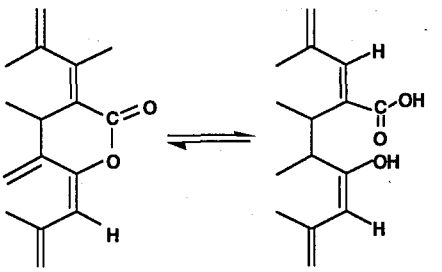

Fig. 7 The structural model of surface oxides on carbons. (Ref. 29.)

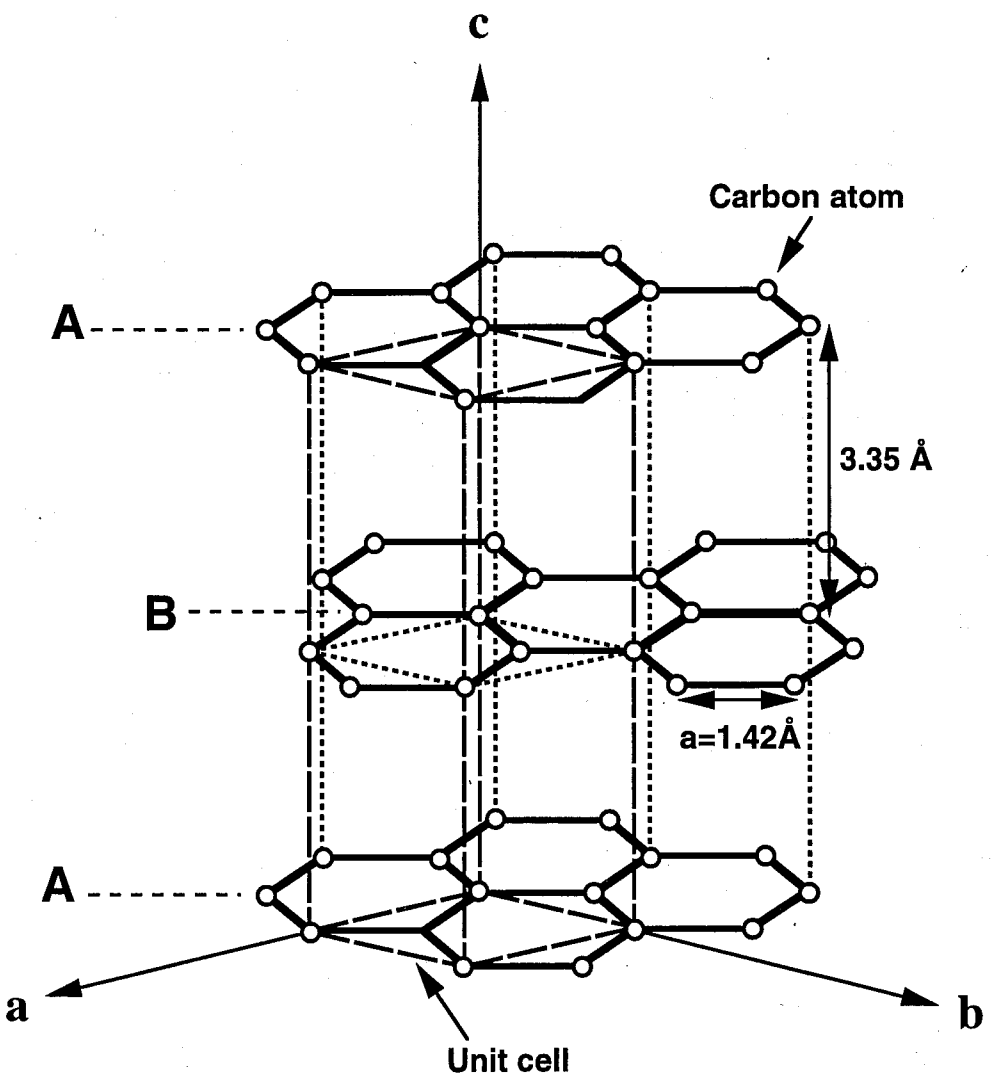

Fig. 8 The crystal structure of a graphite. A rhombohedron drawn by the dash lines indicates a unit cell containing two A-type carbon atoms amd two B-typecarbon atoms.

(a)

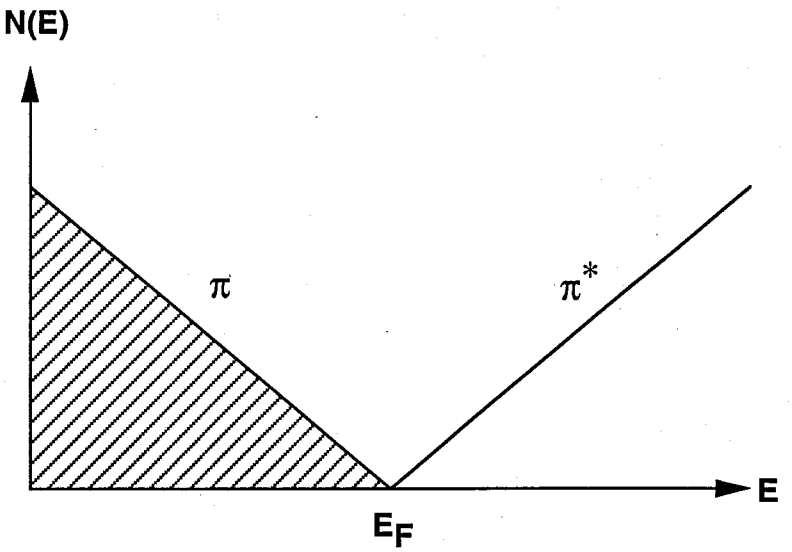

(b)

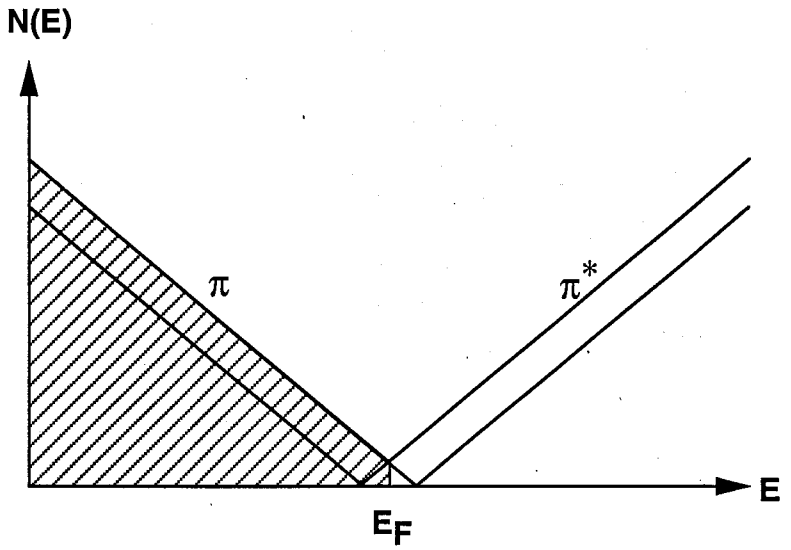

Fig. 9 The electronic structure model for (a) a graphene and (b) a graphite.

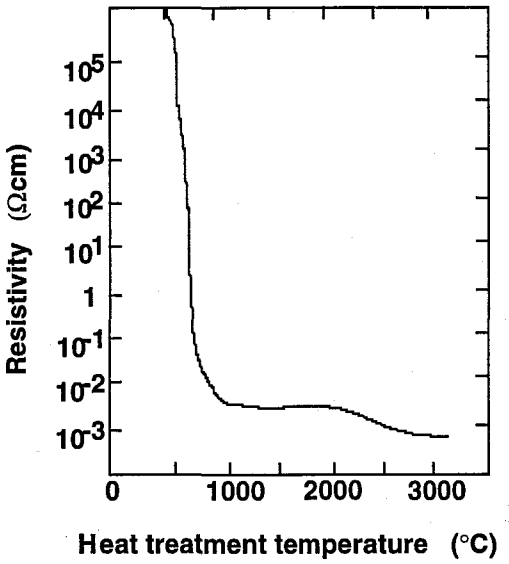

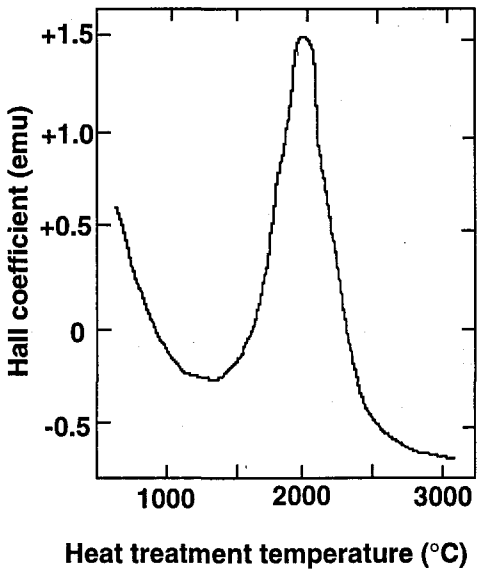

Fig. 10 (a) Electrical resistivity of a soft carbon at room temperature as a function of heat-treatment temperature, and (b) Hall coefficient for a soft carbon at room temperature as a function of heat-treatment temperature. (Ref. 37)

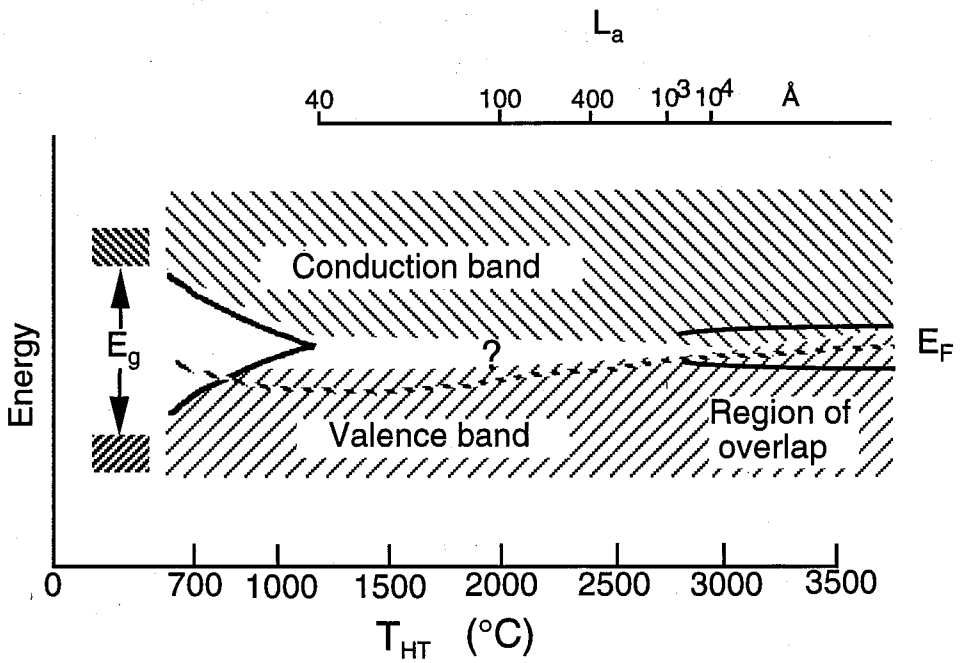

Fig. 11 A sketch of a simple band model proposed by Morozowski as a functiono heat-treatment temperature for the σ-trap model to qualitatively explain the electrical resistivity and Hall coefficient. The in-plane crystallite size L_a for bulk heat-treated carbons is indicated. Room temperature data are from Morozowski for bulk carbons (full line) and from Robson et al. for PAN fibers (dotted line). (Ref. 37) The dotted line denotes the Fermi energy level (E_F) The band model where the electron state is marked by "?" indicates that E_F moves from the valence band (for $T_{HT} \geqq$ 1500°C) to the conduction band (for $T_{HT} \leqq$ 1500°C), and means tha uncertainty of the band structure.

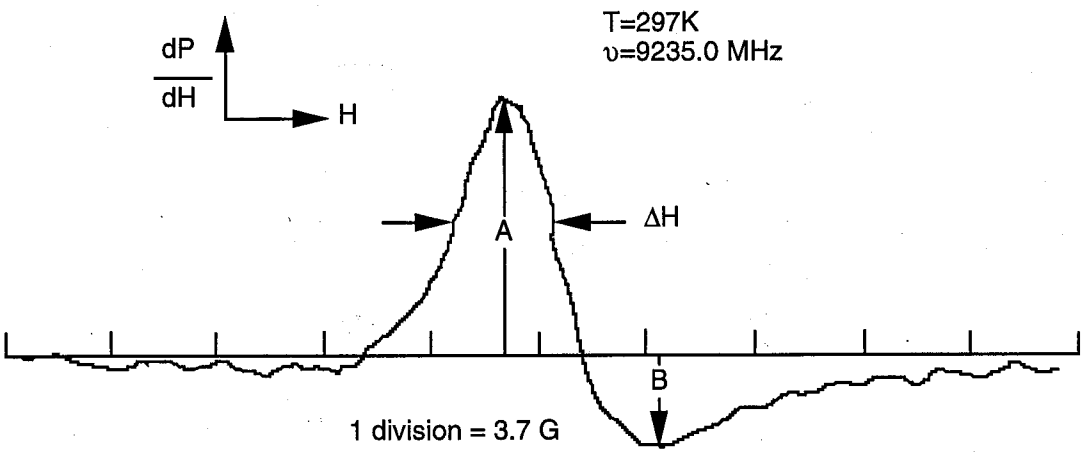

Fig. 12 ESR spectrum of graphite. (Ref. 40)

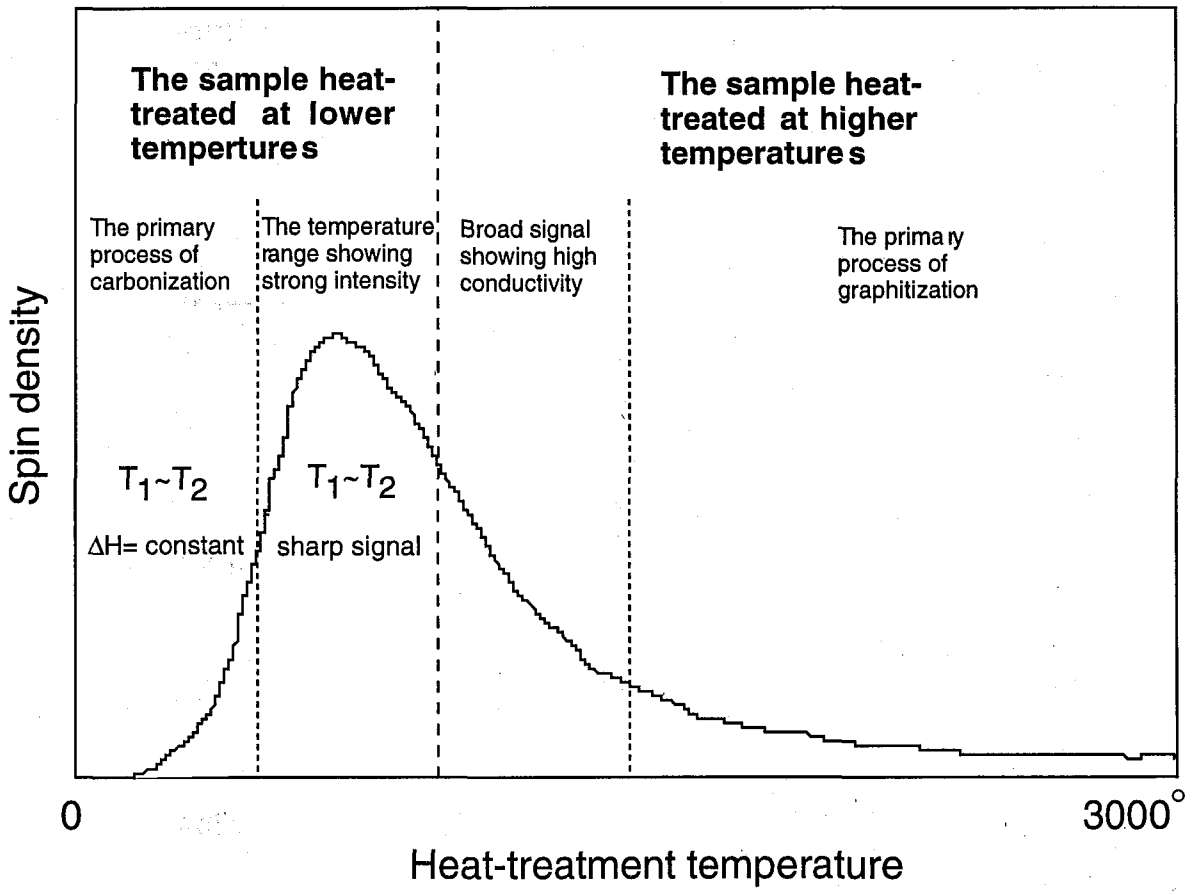

Fig. 13 (a) The relationship between heat treatment temperature for the preparation of CFs and the ESR signal intensity. (Ref. 43)

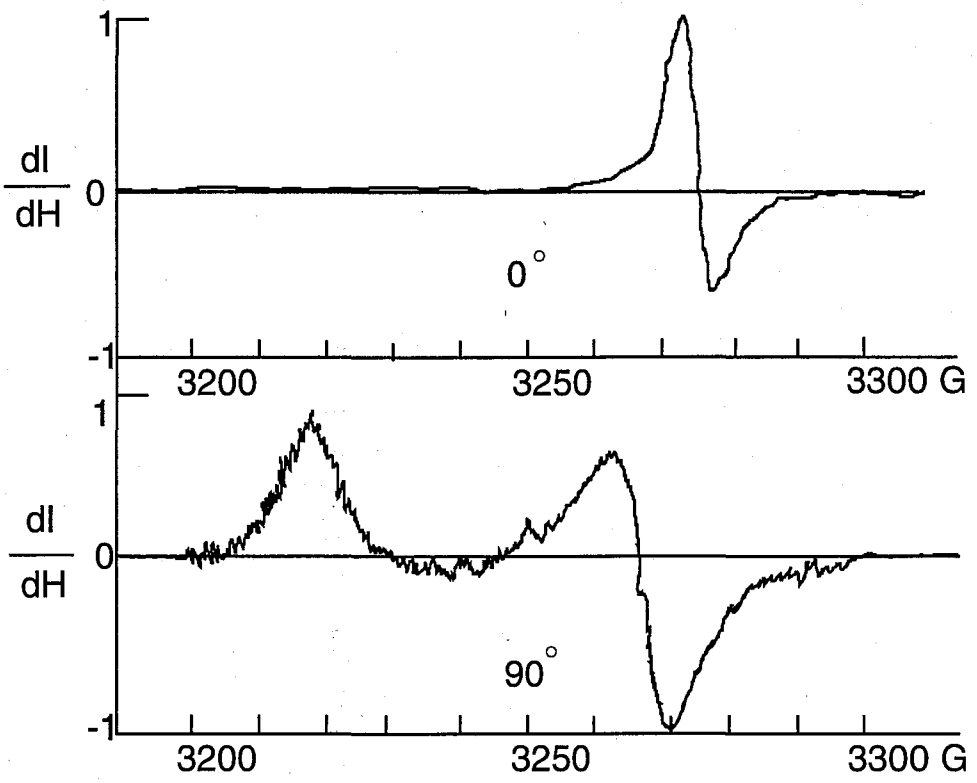

Fig. 13 (b) Normalized experimental ESR spectra of PAN based CF withthe fiber at 0 and 90° to the magnetic field. Areas under the corresponding line shapes are equal. Signal-to-noiseratio of 90° spectrum was very poor due toextreme anisotropy broadening. (Ref. 42)

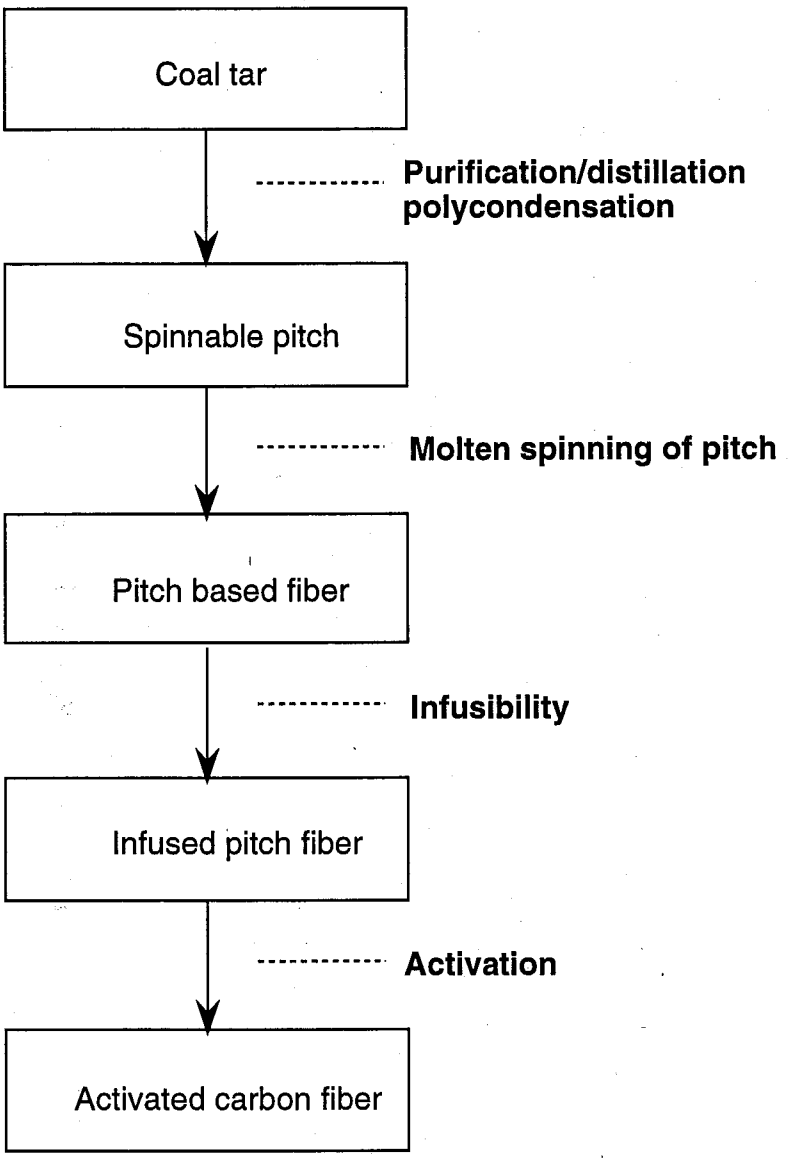

Fig. 14 The flow chart of the production process for pitch based ACF.

Table 1 The theoretical carbonization yields of ACFs. (Ref. 46)

Base raw materials	Chemical formula	Theoretical carbonization yield [%]
Cellulose	$[C_6H_{10}O_3]_n$	44.4
PAN	$[C_3NH_3]_n$	67.9
Phenol	$[C_{63}H_{55}O_{11}]_n$	76.6
Pitch	$[C_{124}H_{80}NO]_n$	93.1

Table 2 Basic physical properties of pitch based ACF. (Ref. 47)

		ACF1000	ACF1500	ACF2000
SSA	(m^2/g)	1000	1500	2000
Pore radius	(Å)	8	9	9
Pore volume	(ml/g)	0.5	0.8	1.1
Acetone adsorption	(wt%)	20	33	45
Iodine adsorption	(mg/g)	1300	1500	1800
Modulus of elasticity	(kg/mm^2)	700	500	350

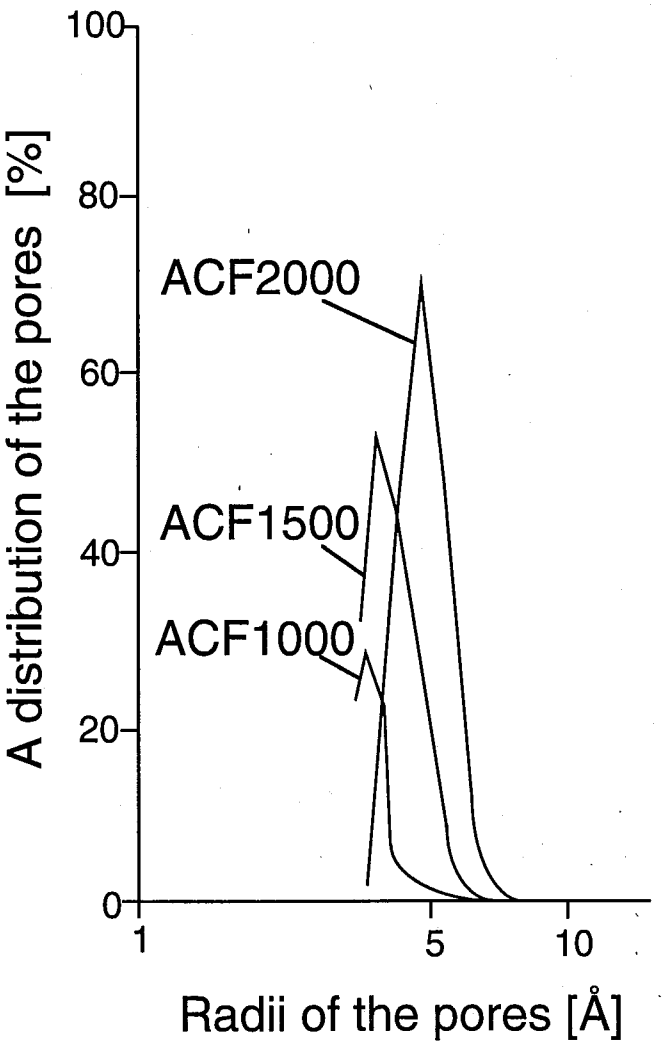

Fig. 15 A distribution of the poresfor pitch based ACF. (Ref. 14)

Part II

Dangling Bond

II-1 Introduction

The dangling bonds which are indispensable when explaining the properties of materials having random and/ or amorphous structure are worth of notice for the study of the properties of ACFs. In particular, ACF3000 with SSA ~ 3000 m^2/g has a lot of micropores, and consists of a more disordered structure than other ACFs with SSA ~ 1000 to 2000 m^2/g, resulting in a lot of dangling bonds which give the spins.

Concerning the spin centers of carbons, usually, two kinds of structural models as the spin centers are considerable as shown in Fig. 1. One is an unpaired electron within a broken σ-bond generated by severing of the σ-bonding such as C-C or C-H[1]. In the case of that the spin species are the broken σ-bonds, the spin centers are localized at the peripheries of crystallites or on the functional groups. Another model is an unpaired π-electron spin center like the π-electron free radical observed in aromatic rings delocalized in the crystallite[2]. These spin center models were found by investigating the heat-treatment effects of the ESR spectra observed in carbons, activated carbons, and another kinds of organic compounds. Every carbon shows the maximum spin concentration under the heat-treatment at 600°C, which were explained by the spin models mentioned above[3]. Thinking from the σ-electron model, heat-treatment above 600°C results in the recombination of broken σ-bonds going with the growth of the crystallite, and the frequency of the recombination of σ-bonds is larger than that of the generation of σ-bonding,

resulting in the decrease of unpaired electrons. According to the π-electron model, unpaired π-electrons are not generated until the crystallite's size enlarges to a certain extent by heat-treatment. In addition, at the same time, the generation of unpaired π-electrons makes electron pairs, resulting in the decrease of spin concentration.

The spins contained in carbons composed by hydrocarbons are sensitive not only to the heat-treatment but also to the gas adsorption. Introducing of oxygen gas to carbons causes the change of the intensity and the linewidth of the ESR spectrum[4]. These phenomenon is reversible between before and after introducing the oxygen gas, and the evacuation of oxygen gas regenerates the previous state. Two cases to explain the reversible oxygen adsorption effects of the ESR spectra are proposed as follows[5, 6]. One is the case that peak-to-peak line width increases with decreasing the peak-to-peak height by increasing of the oxygen gas pressure, resulting in the constant of the intensity. And another case is that the constant line width and the decrease of the peak-to-peak height originates from the decrease of the intensity by the increasing of the oxygen gas pressure. The former shows the enlargement of the spin-spin relaxation rate, and the latter shows the disappearance of the spins with the weak chemisorption of the oxygen gas.

As mentioned in the following section, the ESR spectrum of ACF3000 indicating localized dangling bonds is sensitive to heat-treatment and gas adsorption, though the ESR signals of dangling bonds are not obtained in other ACFs[7]. In short, only ACF3000 is able to give electronic information of dangling bond spins by the ESR method. For this reason, ACF3000 has been chosen as the

sample in order to investigate dangling bond spins.

In order to investigate the properties of dangling bond spins, the ESR method and the measurements of magnetic susceptibility are utilized. Their results of pristine ACF3000 are compared to those of gas adsorbed samples and heat-treated samples, and the characters of dangling bonds are summarized from the view points of gas adsorption effects and heat-treatment effects.

II-2 Experiments

Every sample preparation is carried by the evacuation below 10^{-5} Torr for 12 hours at room temperature. One sample is used for one series of experiments of gas adsorption effect and/or heat-treatment effect, because of avoiding the sample dependence.

The sample preparation for the gas adsorption effects is as follows. The oxygen pressure dependence of the ESR signals was observed by varying the oxygen gas pressure every 10 Torr up to 90 Torr, after pumping. The sample introduced 10 Torr nitrogen gas was also prepared. Iodine doping was made by exposing samples to iodine vapor at room temperature for 2 hours after evacuation. The sample preparation for the heat treatment effects is as follows. The sample for the ESR spectra is heated by every 50 °C up to 700 °C for one hour with pumping. The samples used for the magnetic susceptibility measurements were heat-treated at several temperatures from 200 °C to 800 °C under a vacuum of 10^{-5} Torr for 8 hours after the evacuation at room temperature for 3 hours. The sample for the mass spectra was pumped in advance for 2 hours below 10^{-5} Torr by using 10 mg

ACF3000 because of removing moisture.

The ESR measurements have been carried out in the X-band region at a frequency υ~9.4 GHz by using the microwave power of 1 mW where there is no saturation effects, and the g-values are calibrated by α, α-diphenyl-β-picryl hydrazyl (DPPH). The sample mass in the ESR tube for every sample was adjusted on the order of 0.5 mg because of the adjustment of the Q-value. All measurements are carried at room temperature. The magnetic susceptibilities of heat-treated samples were measured by an automatic magnetic pendulum between 4K and 300K. The thermal desorption for the mass spectra is carried out every 10 °C upto 770 °C with the heating speed of 10°C / min.

II-3 Results and Discussion

ESR spectra of ACF3000 is shown in Fig. 2 for the sample in air and in vacuum. ACF3000 pristine sample gives a broad ESR signal with a line width $\Delta H \approx 800G$ and the g-value $g \approx 2.05$ in ambient atmosphere. However the evacuation of an ESR sample tube generates a narrow signal with $\Delta H \approx 40G$ and $g \approx 1.99$ superposed upon the broad signal whose line shape and the g-value hardly change before and after the evacuation. The change in these ESR spectra is reversible between adsorption and desorption of air. The spin concentration of the narrow signal is estimated at 10^{19}/g which is the same order as other carbon materials [8,9].

In order to find out the source of the narrow signal, the oxygen gas and the nitrogen gas are introduced in the sample, because the change in the narrow signal

between adsorption and desorption of air is supposed to mean that the oxygen gas or the nitrogen gas being of the components of air causes the change in the narrow signal. The profiles of the ESR signal are shown in Fig. 3 for the sample with different O_2 pressures. The oxygen gas pressure dependence of peak-to-peak height and line width of the narrow signal are shown in Fig. 4. The intensity of the narrow signal does not change with the increase of pressure, while the line width is drastically broadened by the dipole-dipole interaction between paramagnetic spins of oxygen molecules and spins observed in the narrow signal. However, the broad signal is not affected by the oxygen gas. The line shape becomes the same as the spectrum in the ambient atmosphere by the introduction of 90 Torr oxygen gas. The introduction of nitrogen gas does not change either the narrow signal or the broad signal shown in Fig. 5. According to the experimental results which indicate a delicate effect caused by oxygen gas on the narrow signal, the narrow signal is assigned to dangling bond spins located around the peripheries of micro-pores.

In order to confirm the assignment of the narrow signal to dangling bond spins by other experiment and clarify the assignment of the broad signal, the ESR spectrum of iodine doped sample is measured. Iodine doping modifies both the narrow signal and the broad one shown in Fig. 6. The narrow signal disappears completely, while the intensity of the broad signal is reduced by about one order of magnitude. This finding suggests that the formation of the bonds between dangling bonds and iodine atoms brings about the extinction of the magnetic moments at the dangling bonds. The decrease in the broad signal is related to the increase of the skin effect due to high conductivity achieved by charge transfer between ACF3000 and iodine, since the introduction of iodine also affects the Q-value of an ESR

cavity, suggesting an enhancement of the electrical conduction. From these results, the narrow signal and the broad signal are respectively assigned to isolated dangling bond spins at the peripheries of the micrographites and conduction π-electrons with the mixing of dangling bonds electrons directly connected to the π-system.

On the relation between a distribution of dangling bond spins and the ACF structure, the dangling bond spin state is modeled through the interpretation of ESR spectrum of ACF3000. The magnitudes of the line width for both the narrow signal and the broad signal are about 10 to 100 times larger than that of ordinary carbons assigned to be dangling bond spins and the conduction π-electron spins[4,7]. To check the ESR line shape, the ratio $\Delta H_{hw} / \Delta H_{pp}$ is calculated, where ΔH_{hw} and ΔH_{pp} are a half-height linewidth of the differential peak and a peak-to-peak linewidth of an ESR spectrum, respectively. Purely Gaussian and Lorentzian line shapes give the values 1.92 and 2.40, respectively[10]. In the case of ACF3000, the ratio shows 2.2 for the narrow signal and 2.3 for the broad signal, which are nearly Lorentzian type line shape. Consequently, it is supposed that exchange interaction works for both the broad and narrow signals. From the estimation of dangling bond spin concentration assigned to the narrow signal, the mean distance between the dangling bond spins is calculated at 40 Å which is too distant to realize exchange interaction. Therefore, it is suggested that the distribution of the dangling bond spins is inhomogeneous. The analysis of the line shape shows Lorentzian features in the whole oxygen pressure range investigated, suggesting the pressure of exchange interaction between oxygen spins and

dangling bond spins. Here, in order to extract information on the correlation between the adsorption state of oxygen molecules and the behavior of the narrow ESR signal, we investigate adsorption isotherm of oxygen molecules. From the analysis of the isotherm explained in Part III and the density of ACF3000 (~1.7g/cm^3), the mean value occupied by an oxygen molecule is estimated at ca. 82000 Å^3, which corresponds to the mean distance of ca. 30 Å between oxygen molecules. This is comparable to the mean distance between the dangling bond spins obtained the spin concentration of ~10^{19} /g. If we assume that the adsorbed oxygen molecules are distributed homogeneously in micropores whose peripheries have attached dangling bond spins, the average distance is deduced to be ca. 30 Å, which corresponds to the dipolar width of ΔH_{dip} ~ 1G taking into account the relation $\Delta H_{dip} \sim \mu_{O_2} \cdot \mu_d / r^3$ where μ_{O_2} and μ_d are the magnetic momentous of oxygen molecule and dangling bond. Contrary to this, the increase of the linewidth is one order of magnitude larger than that estimated here. Moreover, the line shape having Lorentzian features indicated the presence of exchange interaction between the oxygen spin and the dangling bond spin, while the ESR saturation curve under oxygen gas, which will be presented in Part III, shows the behavior of a homogeneous spin system, suggesting evidence on the presence of the exchange interaction. In addition, the adsorption isotherm of oxygen molecules has a different trend from that of other gaseous materials which are considered to be accommodated as physisorbed species. Consequently, it is concluded that the absorbed oxygen molecules are distributed inhomogeneously and attached to the dangling bond sites through weak chemisorption.

Next, the reflection of the heat-treatment on the structure and magnetic properties of the dangling bonds is analyzed by examining the heat-treatment effects of ACF3000. Figure 7 shows ESR spectra of an ACF3000 sample heat-treated at various temperatures. The heat-treatment temperature dependence of the peak-to-peak height and line width of the narrow signal are shown in Fig. 8 . In the temperature range above 100°C, the narrow signal shows the decrease of the peak-to-peak height and the broadening of the peak-to-peak line-width with increasing heat-treatment temperature. Finally it almost disappears about 350 °C. The height of the broad signal starts decreasing and the line shape is deformed above 400 °C. The Q-value of the ESR cavity is also depressed at the same time. This means that heat-treatment makes the electronic properties more conductive. Then the observation of signals above 700 °C becomes very difficult because of the decreasing Q-value.

The results of magnetic susceptibilities of heat-treated samples at 200 °C to 800 °C are shown in Fig. 9. The absolute values of the susceptibilities increase with increasing heat-treatment temperature. Every susceptibility obeys the Curie law at low temperatures, while the other component with a weak temperature dependence is emphasized above about 40K. The observed susceptibilities of ACFs χ_{obs} consist of four kinds of components;

$$\chi_{obs} = \chi_C + \chi_T + \chi_{core} + \chi_{orb} \qquad [1]$$

where χ_C is the Curie term, χ_T is a weak temperature dependent spin paramagnetic term, χ_{core} is the Pascal diamagnetic term and χ_{orb} is the orbital diamagnetic term. The magnitude of the diamagnetic component which consists of χ_{core} and χ_{orb} is

given by $-0.8X10^{-6}$ emu/g, from the measurements of the diamagnetic susceptibility by Kaneko et al.[11]. Table 1 presents the heat-treatment temperature dependence of χ_{obs}, χ_C, and χ_T.

For the spin concentration of χ_C, it is estimated at 2.8×10^{19}/g for the non heat-treated sample. Comparing the magnitudes of their spin concentrations estimated in χ_C with those in the ESR intensity, the spin species given by χ_C correspond to the spins originating from the ESR narrow signal. The dangling bond spin concentration N_C increases with increasing heat-treatment temperature. Remarkable enhancements of N_C are shown below H.T.T = 200°C and above H.T.T = 600°C, and the increase of N_C between 200°C and 600°C is very weak. The increase in χ_C means that new dangling bonds are generated by the heat-treatment, taking into account the experimental results of mass spectroscopy which are discussed in the next paragraph.

We discuss the results of the enhancement of the spin paramagnetic components χ_T. The increase of χ_{obs} with increasing of heat-treatment temperature is mainly based on the increase of spin density of dangling bond spins, and this phenomenon is mainly appears in the component of χ_C. However, not only χ_C but also χ_T increases by heat-treatment above 600°C, which contributes to an enhancement of χ_{obs}. According to the ESR spectra above H.T.T.=400°C, both line shapes of the narrow signal and the broad signal changes. They mean that the structure and the electron state of the micrographite is modified, which is

supported by the more shallow Q-dip of heat-treated sample, meaning higher conductivity than that of the pristine sample. There are two possibilities concerning the cause of the enhancement of χ_T with heat-treatment: (1) the generation of dangling bond spins directly connected to the micrographite having strong interactions with π-conduction electrons on the micrographites; and (2) the enhancement of the Pauli paramagnetism with increasing of the density of state at Fermi energy level. For (1), the weak temperature dependent χ_T is considered to be reflected in the π-conduction electron spins observed by the broad ESR signal. It is considered that χ_{orb} is not changed by the present heat-treatments, since heat-treatment below 1300 °C is not effective for the graphitization of ACF[12]. Therefore, the increase in χ_{obs} in the high temperature range is ascribed mainly to the enhancement of the spin paramagnetic components χ_T. This implies that the decomposition of functional groups generates dangling bond spins which are directly connected to the micrographites and have strong interactions with conduction electrons on the micrographites. For (2), it is supposed that one of the causes of the increase of χ_T by a heat-treatment is an enhancement of Pauli paramagnetic susceptibility (χ_{Pauli}) with increasing the conductivity. And assuming the existence of the density of state (DOS) at Fermi energy level (E_F) for ACF3000, the temperature dependence of χ_T shown at higher temperature means the temperature dependence of DOS in the case of $E_F \approx kT$, and χ_{Pauli} shows the temperature dependence. By Fujita et al.[14], the results of their theoretical

calculation indicates that the edge structure of the micrographite influences DOS at Fermi energy level. According to the mass spectra, it is supposed that the edge structure of micrographites changes by heat-treatment above H.T.T.=800°C, and these results support the interpretation of enhancement of χ_{Pauli} by heat-treatment above H.T.T.=800°C.

The mass spectra support the analysis of the ESR spectra and the magnetic susceptibilities of the heat-treated samples, and inform the molecular structures of the functional groups and the dangling bonds. The mass spectra for ACF3000 are measured to characterize the thermal desorption and decomposition processes up to 800 °C as shown in Fig. 10. They give structural information related to functional groups attached to a network of the micrographites. We observed anomalous changes in the mass spectra at about 150 °C and 650 °C in the process. Species with mass numbers 17 and 18 are desorbed in the temperature range below 200 °C, which are expected to correspond to OH and H_2O, respectively, associated with adsorbed gaseous materials H_2O in ACF. The decrease of the peak-to-peak height and the increase of the line width of the narrow ESR signal shown in the temperature range between 100°C and 200°C (see Fig. 8) are imaged as follows. The dangling bond spins at the peripheries of micropores are bared by the desorption of H_2O adsorbed in micropores with heat-treatment around 150°C as indicated in mass spectra, and the dipole-dipole interaction between the nearest neighbor dangling bond spins works more effectively due to the induced structural deformation. In short, it is supposed that the change of ESR narrow signal at 150°C is generated by the structural change through the desorption of H_2O and CO_2 gases adsorbed in micropores. Small angle scattering of x-ray diffraction of

ACF indicates the peak-shift at lower angle by the water desorption from ACF, and Kaneko et al. points out the structural change of the micrographites and the micropores[13]. Above 400 °C, the mass number 28 has the largest intensity of all the mass numbers observed in this measurement. The behavior of the spectrum of mass number 28 is able to be interpreted as follows. The bondings of the hydrocarbons and functional groups as the surface oxides at the peripheries of micrographites are broken by heat-treatment above 400°C, resulting in removing of C_2H_4 and CO. According to the ESR spectra showing asymmetric line shapes and the reduced Q-dip above H.T.T.=400°C mentioned in Fig. 7, the desorption of the molecules with mass number 28 causes the structural change of micrographites, resulting in the change of the electrical properties of ACF. The heat-treatment modifies the disordered structure of micrographites and makes the structure more regular, giving rise to an enhancement in electrical conductivity, although the temperature range in the present experiment is too low for graphitization. It is expected that new dangling bonds are made after the decomposition process of functional groups above 400 °C and the number of dangling bond spins become enhanced.

Finally, we comments on the graphitization of ACF. The graphitization process of Carbon fibers occurs in the temperature range between 1300°C and 3000°C, usually. However, the present result on the behavior of dangling bond spins proves that the precursor process for the graphitization already starts below H.T.T=1300°C.

II-4 Summary

The properties of the dangling bonds are investigated in pitch-based ACF3000. ESR spectra and magnetic susceptibility show the presence of two kinds of spins which are isolated dangling bond spins and π-conducttion electron spins in micrographites. The dangling bond is reactive to the gas adsorption and the heat treatment, and their effects to the dangling bond are sensitively reflected in the magnetic properties. The oxygen molecule is selectively adsorbed at the peripheries of the dangling bonds. The iodine molecule attacks not only the dangling bond but also the π-electrons, resulting in the change of the electronic structure of ACF3000. Namely, chemical are generated between the dangling bonds and the introduced iodine atoms, and the charge transfer from the π-electronic system to iodine atoms strongly enhances conductive nature of ACF. The heat treatment up to 800 °C is mainly effective to the change in the boundary structure of micrographite as the increase of the number of the dangling bonds, which is supported by mass spectra between room temperature and 800 °C. In addition, in this temperature range, graphitzation does not start apparently. However, the precursor for the graphitization process already starts in this temperature range.

Reference for Part II

1. H. Alamatsu, S. Morozowski, and D. Wobschall, Proc. Third Carbon Conference, Pewrgamon, 135 (1959).
2. J. Ubersfeld, and E. Erb, Proc. Third Carbon Conference, Pergamon, 103 (1959).
3. D. J. E. Ingram and J. E. Bennett, Phil. Mag., **45**, 545 (1954).
4. J. W. Armstrong, C. Jackson, and H. Marsh, Carbon **2**, 239 (1964).
5. D. E. G. Austen, D. J. E. Ingram, and J. G. Tapley, Trans. Farad. Soc., **54**, 400 (1958).
6. D. J. E. Ingram, Proc. Third Carbon Conference, Pergamon, 93 (1959).
7. K. Kuriyama, TANSO (in Japanese), **155**, 282, (1992).
8. M. S. Dresselhaus, A. W. P. Fung, A. M. Rao, S. L. di Vittorio, K. Kuriyama, G. Dresselhaus, and M. Endo, Carbon **30**, 1065 (1992).
9. A. Nakayama, K Suzuki, T. Enoki, S. L. di Vittorio, M. S. Dresselhaus, K. Koga, M. Endo, and N. Shindo, Synthetic Metals, **55-57**, 3736(1993).
10. K. Tanaka, T. Koike, T. Yamabe, J. Yamauchi, Y. Deguchi and S. Yata, Phys. Rev. **B35**, 8368, (1987).
11. K. Kaneko, Y Yamaguchi, C. Ishii, S. Ozeki, S. Hagiwara, and T. Suzuki, Chem. Phys. Lett. **176**, 75 (1991).
12. T. Enoki, K. Inukai, K. Sugihara, M. Endo, and N. Shindo, private communication.
13. T. Suzuki and K. Kaneko, Carbon, 26 (1988) 734.
14. M. Fujita, Wakabayashi and K. Nakada, private communication.

(a)

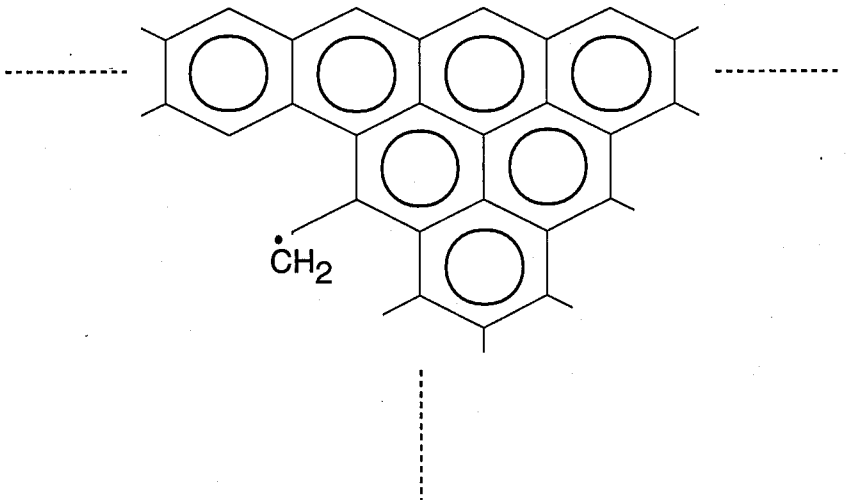

(b)

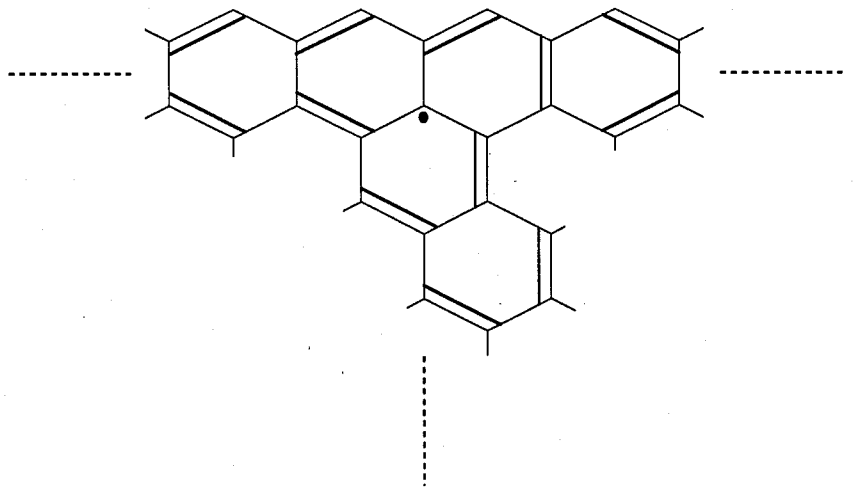

Fig. 1 The structural models of the spin centers. (a) The dangling bond model based on an unpaireed electron within a broken σ-bonds. (b) An unpaired π-electron spin center model like the π-electron free radical observed in aromatic rings delocalized in the crystallite.

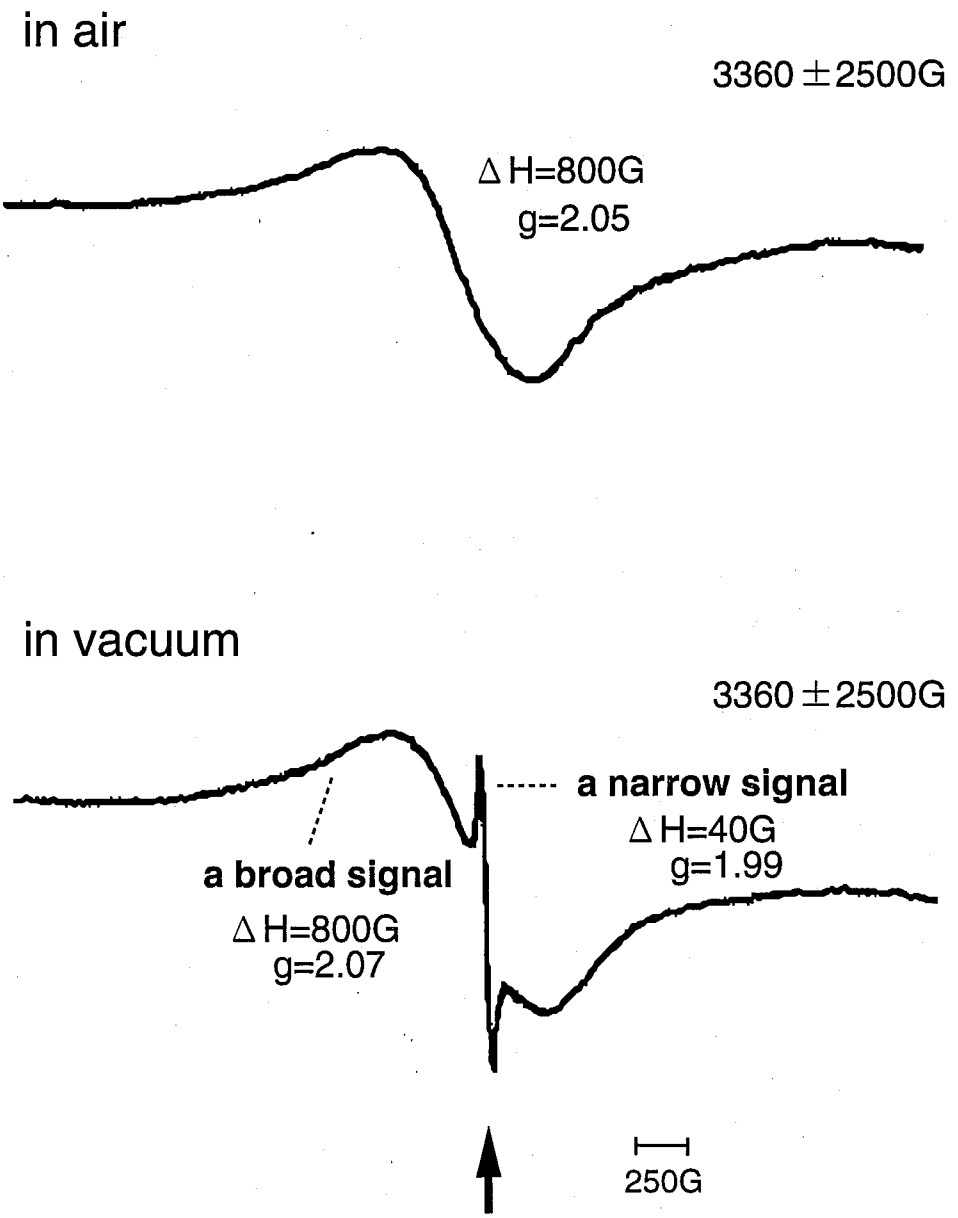

Fig. 2 ESR spectra of ACF3000 measured (a) in air and (b) in vacuum at room temperature. The arrow shows the position of g=2.00.

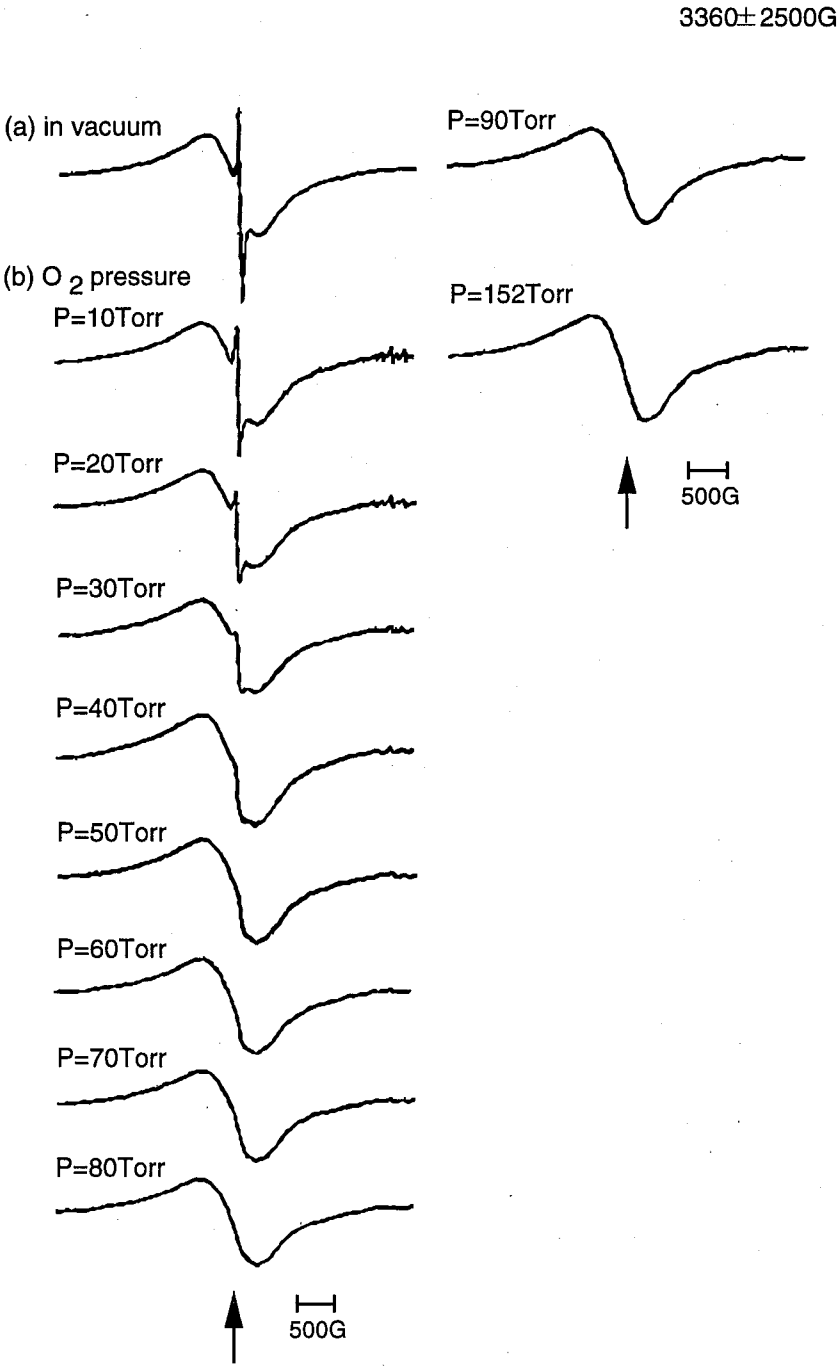

Fig. 3 ESR spectra of ACF3000 at room temperature, (a) in vacuum (b) in oxygen gas atmosphere (oxygen pressures are 10, 20, 30, 40, 50, 60, 70, 80, 90, and 152 Torr). The arrows show the position of g=2.00.

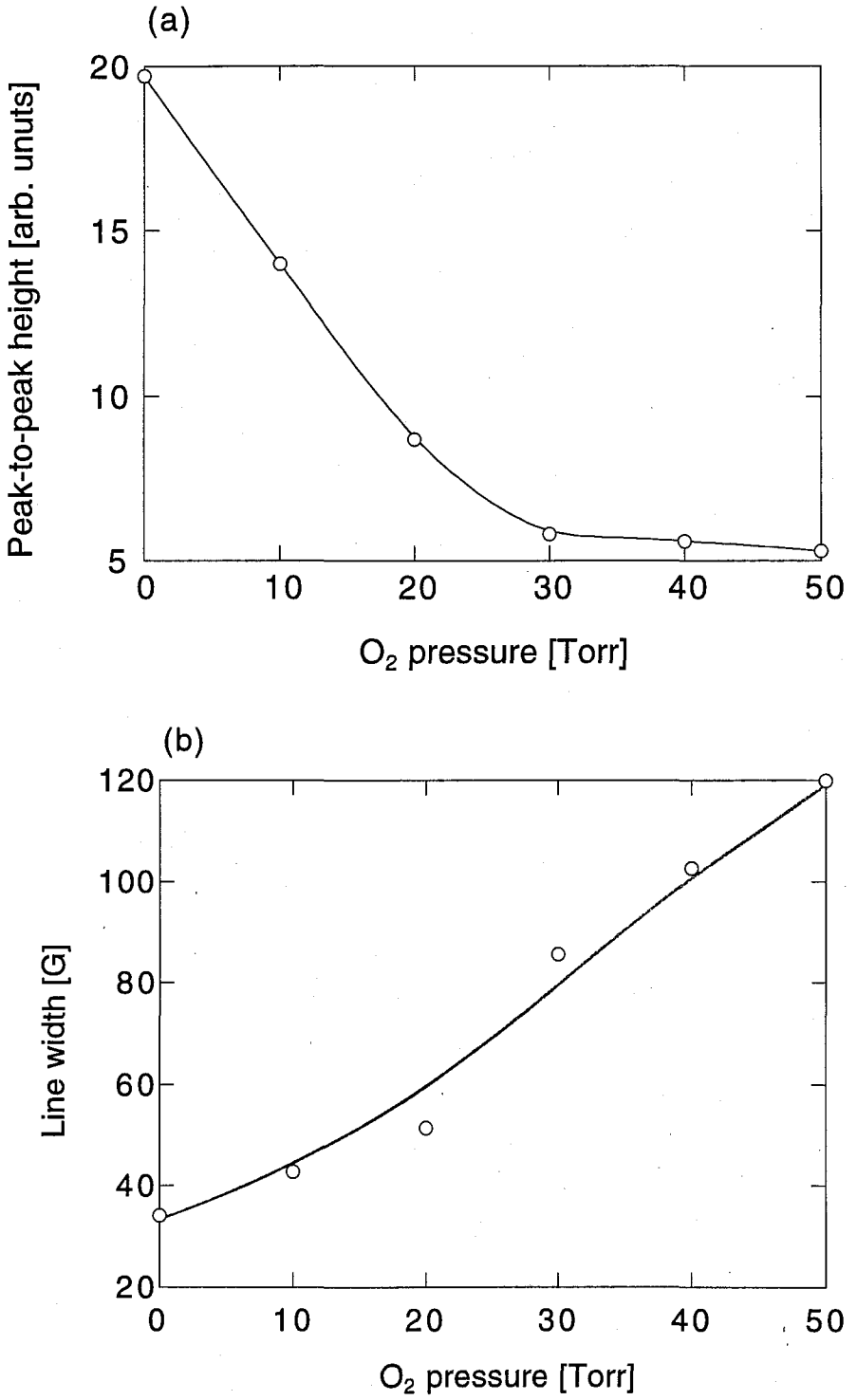

Fig. 4 Change in the narrow signal through introduction of oxygen gas at room temperature. (a) the peak-to-peak height vs. O_2 pressure. (b) the peak-to-peak line width vs. O_2 pressure.

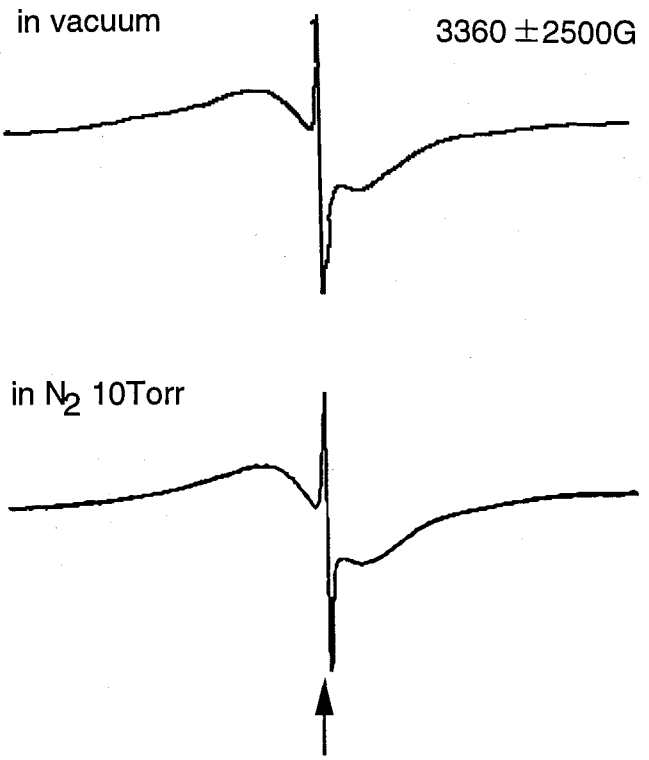

Fig. 5 ESR spectum of ACF3000 in 10Torr nitrogen gas at room temperature. The ESR spectrum of evacuated sample is also shown for comparison. The arrow shows the position of g=2.00.

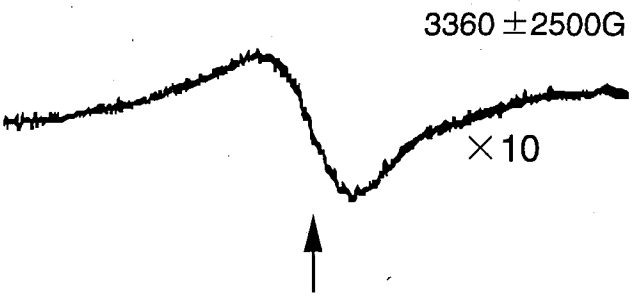

Fig. 6 ESR spectrum of iodine doped ACF3000 at room temperature. The arrow shows the position of g=2.00. The ESR spectrum of the sample with no iodine is already shown in Fig 5. The height of this spectrum is scaled up ten times comparing with Fig. 5.

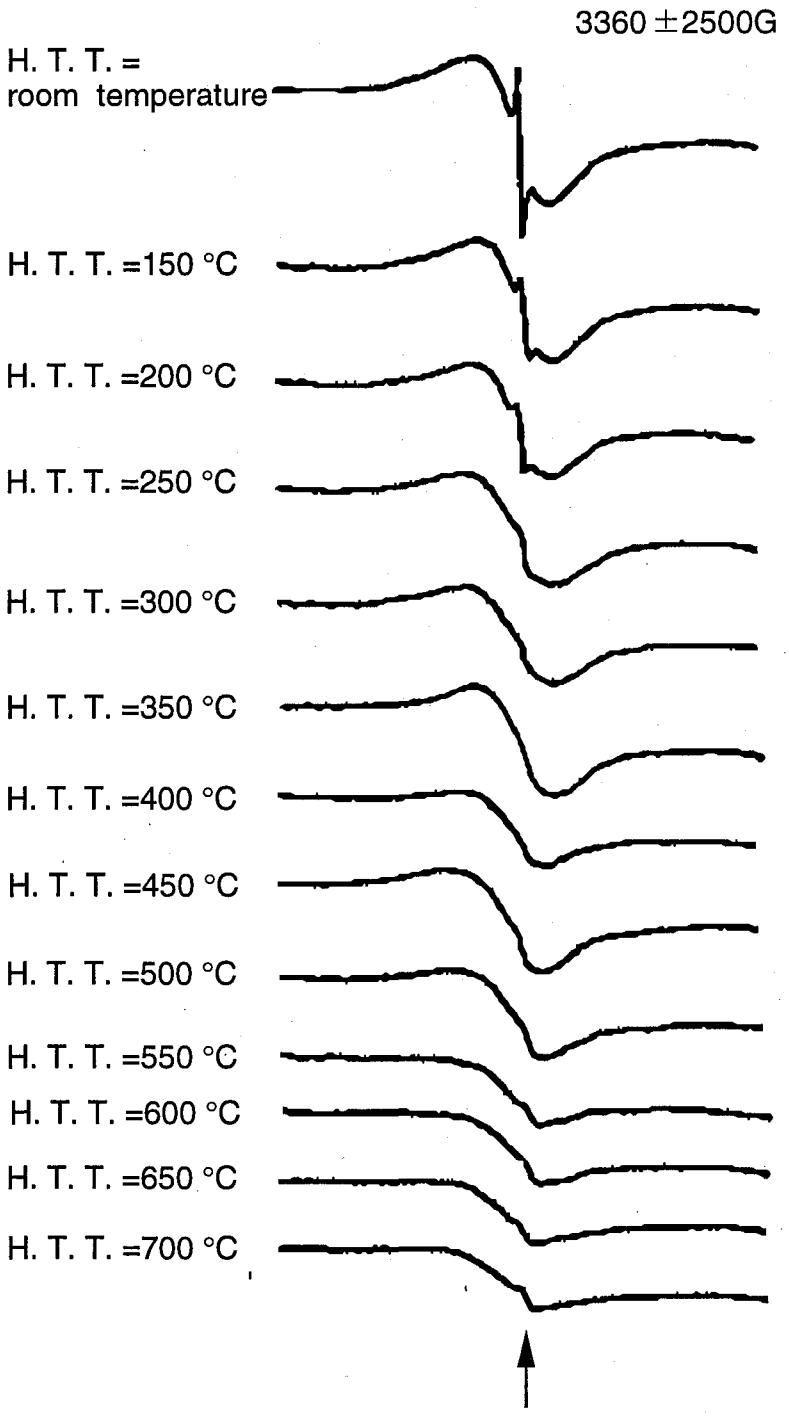

Fig. 7 ESR spectra of ACF3000 heat-treated at room temperature to 700°C. Every spectrum is measured at room temperature. The arrow shows the position of g=2.00.

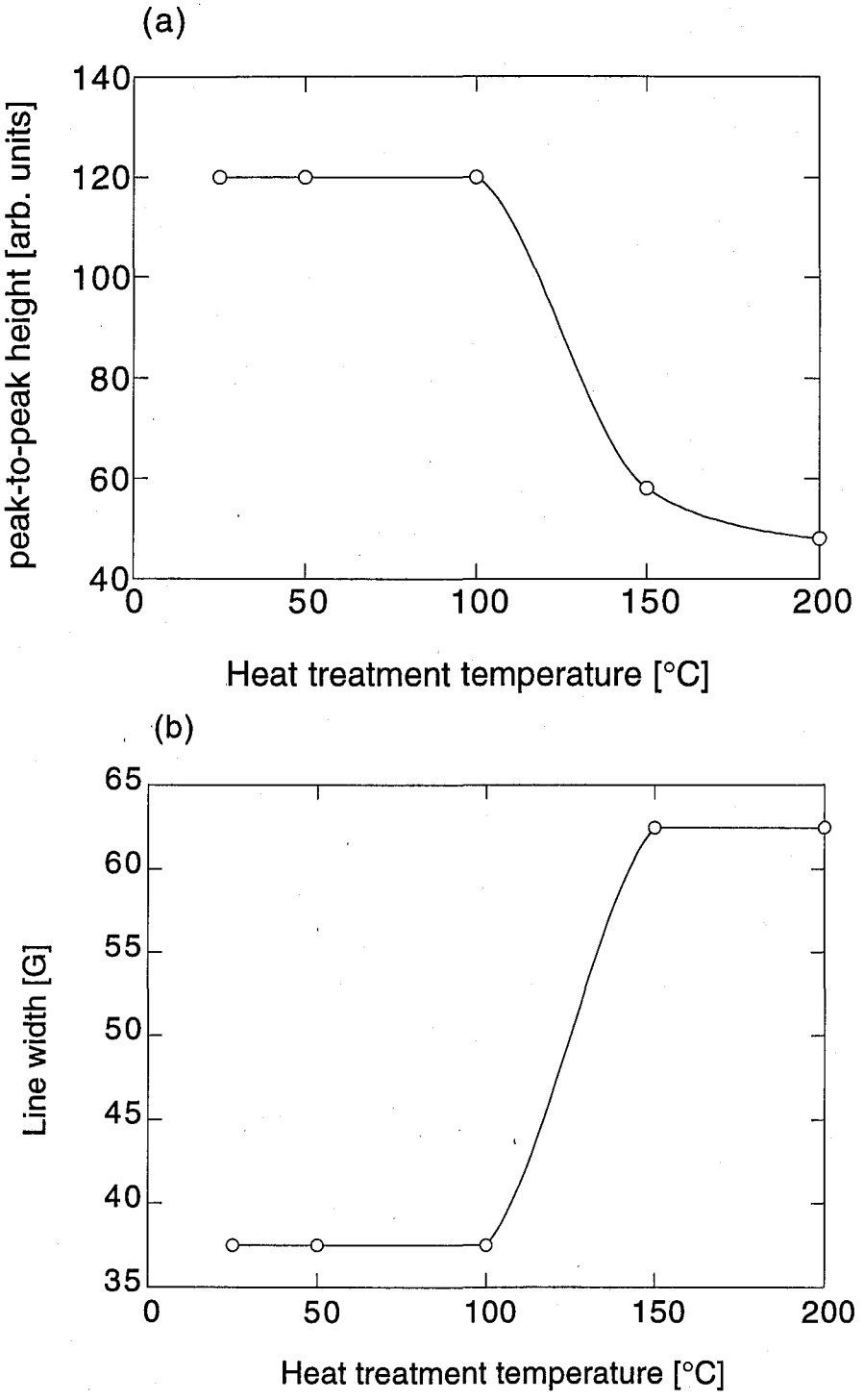

Fig. 8 Changes in the narrow signal through heat treatment. (a) The peak-to-peak height vs. heat treatment temperature. (b) The peak-to-peak line width vs. heat treatment temperature.

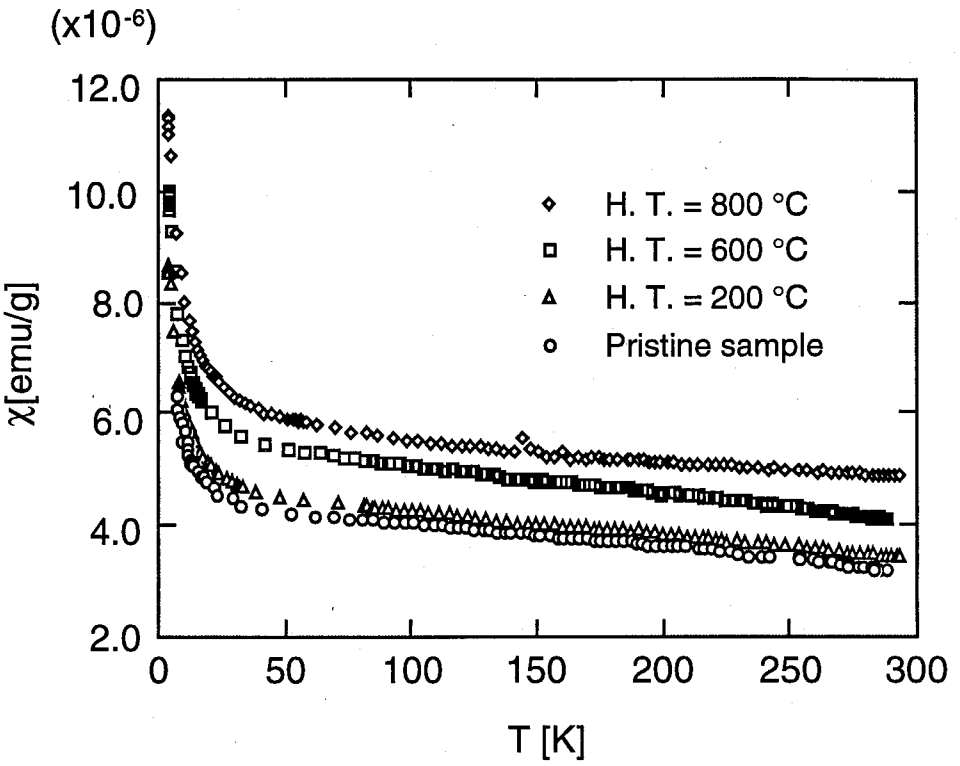

Fig. 9 Magnetic susceptibilities of ACF3000 heat-treated at 200 °C to 800 °C.

Table 1. Magnetic susceptibilities at room temperature and their analysis of ACF3000 heat-treated at 200, 600 and 800°C.

Heat-treatment temperature (°C)	χ_{obs}(emu/g・Oe)	χ_C(emu/g・Oe)	θ(K)	N_C(/g)	χ_T(emu/g・Oe)
r.t.	3.2×10^{-6}	6.1×10^{-8}	-0.1	2.8×10^{19}	3.9×10^{-6}
200	3.4×10^{-6}	7.9×10^{-8}	-0.7	3.7×10^{19}	4.2×10^{-6}
600	4.1×10^{-6}	8.7×10^{-8}	-0.6	4.0×10^{19}	4.9×10^{-6}
800	4.9×10^{-6}	1.0×10^{-7}	-0.4	4.9×10^{19}	4.6×10^{-6}

θ is Weiss temperature for χ_C, N_C is spin concentration for χ_C, and χ_T is the weakly temperature dependent spin susceptibility appearing at high temperatures.

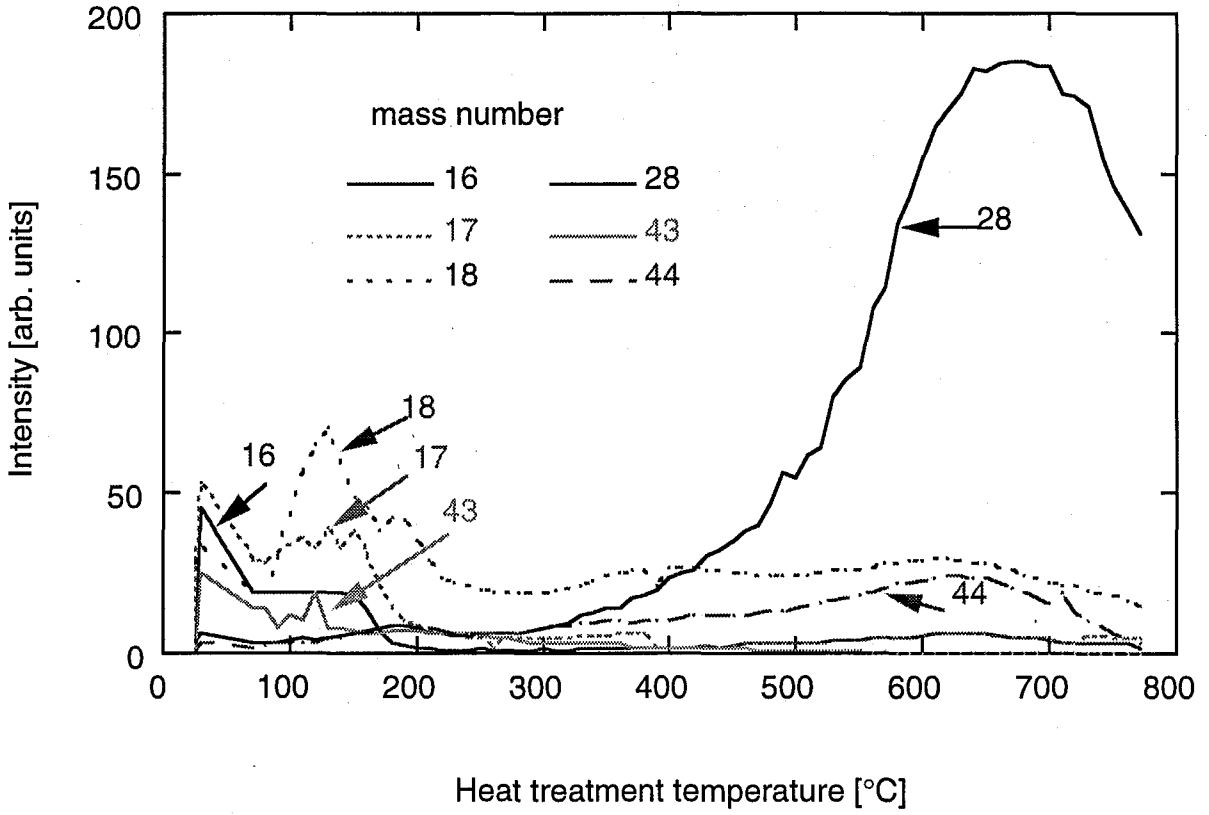

Fig. 10 Mass spectra of ACF3000 measured by thermal desorption.

Part III

Pore Structure

III-1 Introduction

There are many kinds of porous carbon materials which adsorb large amounts of gases. ACFs exhibit superior molecular adsorption properties associated with their microporous structure, which give rise to large SSAs. Assuming that the adsorbed molecules cover both surfaces of a single graphite sheet, SSA is estimated at 2630m^2/g [1] which is the theoretically achieved upper limit. However, the magnitude of SSA~3000 m^2/g of ACF exceeds SSA~2630 m^2/g. This implies that adsorbed gaseous molecules form a condensed state in the micropores. The micropore is provided by an assembly of many micrographites comprising disordered stacks of three to four graphene sheets with a dimension of ca. 20 Å X 20 Å. The micropore size is estimated to be about 10 Å [2]. Although ACFs are solids, they are sensitive to any gases, because they have a lot of micropores and more than 40% of carbon atoms constituting ACF face to the surface [3].

The ESR technique provides useful tool for the investigation of the microstructure of carbon materials[4-6]. According to the ESR and magnetic susceptibility measurement, ACF3000 has ca.~10^{19}/g dangling bond spins at the peripheries of the micrographite. They are electronically localized from the micrographites, because the ESR signal of these dangling bond spins with the line width of 40 G is independent of another one of the conduction electron spins with line width of 800 G generated from the micrographite. The ESR signal of the dangling bond spins is found to be easily modified by the presence of adsorbed oxygen gas for ACFs which was discussed in Part II [7,8]. This suggests that the

dangling bond spins can be used effectively to probe the detailed micropore structure. This section demonstrates that the presence of ultra micropores in ACF3000 is confirmed not only by the adsorption isotherm but also by the ESR measurement which shows anomalous spin-lattice relaxation behavior induced by helium gas. In addition, it is clarified that the gases adsorbed at room temperature form the condensed state in the micropores and the ultra micropores.

III-2 Experiments

In this experiment, pitch-based ACF3000 was employed, and He, Ne, Ar, H_2, N_2, and O_2 gases were used as the guest gases. The sample preparation is carried out as follows. For the gas adsorption isotherm measurements, ACF sample was preliminary evacuated below 10^{-5} Torr at room temperature for 12 hour in advance. The same sample was used for all the ESR measurements with different gases, because of avoiding the sample dependence of ACF, In the series of the ESR measurements, the sample used in a measurement with a kind of gas was evacuated before it was used for the next measurement with the different gas. In the ESR observation, we focus on the narrow signal with the line width of 40 G assigned to the dangling bond spins in order to investigate the spin-lattice relaxation of dangling bonds in relation to the adsorption of various gases. The microwave power dependence of ESR spectra was measured up to 200 mW in X-band region at room temperature for the estimation of the spin-lattice relaxation time with each gases. To estimate the magnitude of the effective pressure of adsorbed gases inside pores, the adsorption isotherms were investigated at room

temperature by the gravimetric method. The gravimetric adsorption apparatus is shown in Fig. 1. The amount of adsorption is determined after degassing of the adsorbent up to 10^{-5} Torr at room temperature, and the measurement is carried till the gas adsorption attains to the equilibration state. Using this equipment, we can measure the weight uptake with the resolution of 0.001mg.

III-3 Results

The saturation curves, which give the microwave power (q) dependence of the ESR intensity (I), are shown in Fig. 2 for ACF3000 adsorbing 10Torr of He, Ne, Ar, H_2, N_2, and O_2 gases. The evacuated sample shows a deviation from the linear I vs. $\sqrt{q}$ relation above 1mW. In the weak microwave power region , the I vs. $\sqrt{q}$ plots for 10Torr pressure of various gases and vacuum show a similar behavior. However, with increasing q the ESR intensities except that for helium gas are saturated and decrease with further increase of q.The curve has a long tail on the high power side after passing through a maximum point of the intensity. This feature suggests that the saturation of the intensity takes place above 1 mW, and that the saturation curve behaves as an inhomogeneous spin system except that for oxygen gas. All samples adsorbing gases show a much larger microwave power for the saturation than that of the evacuation sample. Particularly, the sample with 10 Torr helium gas does not show any saturation up to 200 mW which is the upper microwave power limit of the ESR spectrometer. The oxygen gas introduced-sample shows a different ESR saturation curve from the sample with other gases. This saturation curve is characterized by a homogeneous spin

system which shows a steep drop of intensity on the higher power side of the intensity peak[9]. Figure 3 illustrates the I vs $\sqrt{q}$ plots for the sample with various He pressures taken at room temperature. The plots show less saturated behavior on the increase of He pressure. The sample with 10 Torr helium gas does not show any saturation up to 200 mW which is the maximum power available for ESR machine.

The adsorption isotherms of He, Ar, N_2, and O_2 gases are investigated at room temperature, whose results are used for the estimation of the effective pressures of adsorbed gases inside pores. Here, we show how to estimate the effective pressure, and then exhibit the behavior of effective pressure for the investigated gases. In the gas adsorption experiments, the gas introduced in the pores is condensed, resulting in a big difference between atmospheric pressure outside ACF (apparent pressure) and effective pressure inside pores (P_{eff}). Assuming that the gas behaves as identical gas in the micropores, P_{eff} in micropores is calculated on the basis of the equation of state for ideal gas. The total volume of the micropores in ACF (V_{pore}) is expressed by the difference between the volume of ACF (V_{ACF}) and that of the total micrographite entity ACF (V_g)[6],

$$V_{pore} = V_{ACF} - V_g = \frac{M_{ACF}}{d_{ACF}} + \frac{M_{ACF}}{d_g}, \qquad [1]$$

where M_{ACF} is the mass of ACF used in this measurement, and d_{ACF} is density of ACF (d_{ACF}=1.7 g/cm^3). For the density of the total micrographite entity, we employ the density of regular graphite d_g=2.25 g/cm^3. Then the effective pressure

P_{eff} in micropores is approximated by using the equation of gas state as follows;

$$P_{eff} = \left(\frac{m_{ad}}{M_{ad}} \right) \frac{RT}{V_{pore}}, \qquad [2]$$

where m_{ad} and M_{ad} are the observed weight uptake and molecular weight for the introduced gas, respectively. The effective pressures inside the micropores are shown in Fig. 4 as a function of the apparent pressures of several gases. On introducing 10 Torr helium gas into ACF, the effective pressure becomes 80atm, which is the tremendous enhancement, that is 6000 times larger than the apparent pressure. The adsorption of other gases yields effective pressure in micropores that are two orders of magnitudes smaller than that of helium. The large condensation of helium gas at room temperature is the exceptional feature in the gas adsorption in microporous materials that has never been found, and this finding suggests that a novel molecular sieve effect is expected in helium-ACF system.

III-4 Discussion

The spin-lattice relaxation time T_1 is analyzed for the samples adsorbing the gases from the results of the ESR saturation measurements. T_1 is obtained from the saturation method by using T_1 of 1,1'-diphenyl-2-picrylhydrazyl (DPPH) as the reference materials as follows [10].

$$T_1 = \left[\frac{q_{DPPH(0.75)}}{q_{(0.75)}} \right] \times \frac{T_{1,\,DPPH}^{\,2}}{T_2}, \qquad [3]$$

where $q_{DPPH(0.75)}$ and $q_{(0.75)}$ denote the magnitudes of microwave power at which

the intensities (I) for DPPH and ACF become $0.75 \times I_{max}$, respectively. $T_{1,DPPH}$ and T_1 are the spin-lattice relaxation times for DPPH and ACF, respectively, and the value of $T_{1,DPPH}=6 \times 10^{-9}$ sec is employed[10]. T_2 is estimated from peak-to-peak line width of the corresponding ESR signal. The values of T_1 estimated from eq.[1] are listed in Table 1 for the samples with several different kinds of gases used in the experiment. In addition, the spin lattice relaxation rates of the helium introduced-sample are estimated and figured out as the function of the helium gas pressures as shown in Fig. 5. These results clarify that the gas adsorption governs the spin-lattice relaxation mechanism of the dangling bond spins in micropores. Notably, the helium gas has an exceptionally strong effect on the spin-lattice relaxation rate.

What kind of mechanism is responsible for anomalously enhanced spin-lattice relaxation process in the sample with helium gas? To clarify the mechanism is the main theme of this section. Before doing this, we briefly discuss the feature of the other gases.

As already mentioned above, the sample adsorbing 10 Torr H_2, N_2, and Ar gas show almost identical saturation behavior at room temperature. The relaxation rate of these sample are larger than that of the evacuated sample, although they are considerably smaller than that of the sample with helium gas. The increase of gas pressure from 10Torr to 760 Torr gives little change in ESR saturation behavior for the samples with Ar and/or N_2 gases. This suggests that the introduced gases are almost saturated in the micropores above 10Torr, while the oxygen gas introduced-sample shows a different ESR saturation curve from the sample with other gases. This saturation curve is characterized by a homogeneous spin system

which shows a steep drop of intensity on the higher power side of the intensity peak[10]. The difference of the saturation curve between the oxygen gas-introducing sample and the sample with other gases comes from the different in the gas adsorption state in ACF, and that oxygen molecules are weakly chemisorbed on the dangling bond spins[7]. Since the behavior of the adsorption of each gas in ACF is expected to be reflected in the spin-lattice relaxation rate, ESR provides a complementary information on the adsorbed state in ACF to the results obtained from other experiments.

What is the factor in gas adsorption in ACF? It is known that gaseous materials having larger polarizability are more stabilized with larger enthalpy of adsorption. The magnitude of enthalpy of adsorption in ordinary gas adsorption systems varies on the order of $He < Ne < H_2 < O_2 < Ar < N_2$ [11]. This suggests that helium is least stabilized in micropores among the gases investigated, in disagreement with the present experimental findings. In other words, the trend related to the enthalpy of adsorption is not applicable to the helium adsorption in ACF micropores. Next, we compare the molecular size of the introduced gases which is expected to play an important role in the adsorption in the micropore. Table I shows the comparison of the molecular size. Comparing the molecular size to the trend in the gas adsorption observed in the present experiment, only the smallest size helium shows the exceptionally large condensation in the micropores. These experimental results provide evidence of the presence of ultra micropores which can accommodate only helium atoms with the smallest diameter of 2.57 Å[12], and the dangling bond spins are considered to be found mainly in the ultra micropores [2]. Considering the

reflection of the effective pressure to gas adsorption of ACF, the existence of ultra micropores could be a significant feature in the gas adsorption in ACF. Taking into account the anomalous large condensation of helium, the strong enhancement in the spin-lattice relaxation rate is considered to originate from the collisional process between helium atoms and dangling bond spins.

Next, we discuss the spin-lattice relaxation mechanism with the helium collisional process in order to clarify the strong enhancement in the spin-lattice relaxation rate in helium adsorbing ACF. In an ordinary graphite system, the spin-lattice relaxation takes place through the phonon process where the acoustic phonons with the sound velocity of 2×10^6 cm/sec[13] assist the relaxation from the spin system to the heat reservior. As mentioned in Part 1, ACF consists of the network of micrographitic domains with the dimension of La^2 = ca. 20 $Å^2$. Therefore, the finite size effect of the micrographitic domains makes the phonon dispersion be discrete with the energy separation of $\hbar(2\pi/L_a)v_s$~240K, resulting in the appearance of the activation energy in the phonon excitation process. Therefore, the phonon assisted spin-lattice relaxation mechanism becomes ineffective in ACF. This means that the helium collisional process can contribute to the spin-lattice relaxation process. Here, we analyses the enhancement in the spin-lattice relaxation rate in helium adsorbing ACF on the basis of the theory developed by Sugihara[14]. Interaction between a dangling bond electron and electrons of a helium atoms is expressed in terms of the electric dipole-dipole interaction;

$$V(r, r_1, r_2, R) = \frac{e^2}{R^3} \sum_{i=1}^{2} \left\{ r \cdot r_i - \frac{3(R \cdot r)(R \cdot r_i)}{R^2} \right\}, \qquad [4]$$

where r is the coordinate of the dangling bond electron; r_1, r_2 the coordinates of the electrons of a He atom; and R vector connecting the helium atom and the carbon atom related to the dangling bond (see Fig. 5(a)). The wave functions of the dangling bond and the π-electron shown in Fig. 5(b) are given by eqs.[5] and[6], respectively,

$$\phi^{(g)} = \frac{1}{\sqrt{3}} \left\{ \psi_{2s} + \sqrt{2}\, \psi_{2px'} \right\}, \qquad [5]$$

$$\phi^{(e)} = \psi_{2pz'}. \qquad [6]$$

The presence of the spin-orbit interaction induces a slight admixture of the opposite spin-state in the dangling bond spin states, resulting in the modification of the wave functions as given in the following equations,

$$\phi_{\uparrow} = \phi_{\uparrow}^{(g)} + \varepsilon \cos 2\theta \phi_{\downarrow}^{(e)}, \qquad [7]$$

$$\phi_{\downarrow} = \phi_{\downarrow}^{(g)} + \varepsilon \cos 2\theta \phi_{\uparrow}^{(e)}, \qquad [8]$$

where $\uparrow$ and $\downarrow$ denote the spin states for up and down spins, respectively, and

$$\varepsilon = \frac{1}{\sqrt{6}} \frac{\bar{\lambda}}{\Delta}. \qquad [9]$$

Δ is the energy difference between $\phi^{(g)}$ and $\phi^{(e)}$, and $\bar{\lambda}$ is the mean value of the spin-orbit coupling for carbon 2p-state.

The spin-lattice relaxation rate, which is related to the transition probability in the spin flip process of the dangling bond spin, is given by the effective spin

reversal Hamiltonian H_{eff} involving the electronic states of the dangling bond and the helium electrons which interact to each other through the electric dipole-dipole interaction,

$$\langle \uparrow, g|H_{\mathrm{eff}}|\downarrow, g\rangle$$

$$= \sum_{\lambda=\uparrow,\downarrow} \sum_{j} \left\langle \phi_{\downarrow}, \varphi_j^{(g)} | V | \phi_{\lambda}, \varphi_j^{(e)} \right\rangle \left\langle \phi_{\lambda}, \varphi_j^{(e)} | V | \phi_{\downarrow}, \varphi_j^{(g)} \right\rangle (E_{\uparrow j} - E_{\downarrow j})^{-1}, \qquad [10]$$

where $\varphi^{(g)}$ and $\varphi_j^{(e)}$ are the ground state ^1S and the excited state ^1P for a helium atom;

$$\varphi^{(g)}(r_1, r_2) = \varphi_{1s}(r_1)\varphi_{1s}(r_2)\chi(S=0), \qquad [11]$$

$$\varphi_j^{(e)}(r_1, r_2) = \frac{1}{\sqrt{2}}\left[\varphi_{1s}(r_1)\varphi_{2pj}(r_2) + \varphi_{2pj}(r_1)\varphi_{1s}(r_2)\right]\chi(S=0), \qquad [12]$$

j=x, y, z and $\chi(S=0)$ is the spin singlet state,

$$E_{\downarrow j} - E_{\uparrow g} \approx E(^1P) - E(^1S) \equiv \Delta E \approx 21 \text{ eV}. \qquad [13]$$

Using eqs. [4]-[13], the spin-lattice relaxation rate is expressed by the following equation;

$$\frac{1}{T_1} = 2 \times \frac{2\pi}{\hbar} \sum_{K, K'} \left|\langle \uparrow, K|H_{\mathrm{eff}}(R)|\downarrow, K'\rangle\right|^2 f_K \delta(E_{K\uparrow} - E_{K'\downarrow}) W, \qquad [14]$$

where K denotes the momentum of a helium atom, f_k the Boltzmann distribution function and W the probability of the $p_{z'}$-state being vacant. $E_{K\uparrow(\downarrow)}$, f_k, and the wave function Φ_K are given by

$$E_{K\uparrow(\downarrow)} = E_K \mp \mu_B H,\ E_K = \frac{\hbar^2}{2M} K^2,\ \Phi_K = \frac{1}{\sqrt{2}} e^{iK\vec{R}},$$

$$f_K = Ae^{-E_K/k_B T},\ A = 8n\left(\frac{\pi\hbar^2}{2Mk_B T}\right)^{3/2},\ \text{n: number density of He atoms.} \qquad [15]$$

After the calculation is carried out, the explicit expression of the spin-lattice relaxation is obtained as follows.

$$\frac{1}{T_1} = \frac{6.05}{9\sqrt{2\pi}\,\hbar^4} nM^{\frac{3}{2}} \left(\frac{p}{\Delta E}\right) \frac{(e^2 IJ)}{R_0^6} \sqrt{k_B T}\, W. \qquad [16]$$

where n, M and R_0 are the number density, the mass of a helium atom and the minimum distance at which a helium atom approaches to a dangling bond, respectively. p is the factor given by $p = \bar{\lambda}/\Delta$. *I* denotes an integral associated with helium atom and *J* corresponds to the dangling bond electron expressed by following equations,

$$I = \int \varphi_{1s}(r) z \varphi_{2p_z}(r) dr,\ J = \int \psi_{2s}(r) x \psi_{2p_x}(r) dr, \qquad [17]$$

where $\varphi_{1s}(r)$, $\varphi_{2p_z}(r)$ are the wave function for 1s and $2p_z$ states for a helium atom, and $\psi_{2p_x}(r)$ are π-electron wave function of the dangling bond spin. We have no definite information on the electronic structure of the functional groups, which give rise to the dangling bond spins.Then the 2s and 2p-states corresponding to carbon atom are employed to obtain *J* and p. To estimate eq. [16], the following value are

employed;

$n=1.85\times10^{21}$ /cm^3 (for P_{eff}=10Torr), $M=6.7\times10^{-24}$ g,

ΔE=21eV, T=300K, $p=4\times10^{-3}$,

$IJ=0.52a_0^2$ (a_0 is Bohr radius),

R=3Å, W≈0.2. [18]

Then we obtained the value of the spin-lattice relaxation rate at P_{eff}=10Torr and T=300K, $T_1^{-1}\approx10^6$ sec^{-1}, which is in good agreement with the observed value for the sample adsorbing 10Torr helium gas. The above discussion suggests that the helium atoms with the smallest diameter (2.57Å) accommodated in the ultra micropores effectively work to enhance the spin-lattice relaxation in the dangling bond spin system through the helium collisional process.

III-5 Summary

Using the dangling bond spins as a testing probe, the ESR spin-lattice relaxation rates T_1^{-1} is investigated for ACF3000 in the presence of the He, Ne, Ar, H_2, N_2, and O_2 gases in order to clarify the pore structure and the properties originating from the pores, and the mechanism for the anomalously enhanced spin-lattice relaxation process in the sample with He gas is discussed by using the results of gas adsorption isotherms. T_1^{-1} s are almost identical among ACFs adsorbing foreign gases with different molecular weight and size except helium and oxygen. The finding that the T_1^{-1}s for diatomic molecules are identical to those for inert gas

atoms suggests that the internal degrees of freedom such as rotations and vibrations do not participate in the acceleration of T_1^{-1}. In the case of oxygen adsorption, the ESR saturation curve behaves as a homogeneous spin system, different from the behavior of the curves in other gases. This suggests that the adsorbed oxygen molecules form weak covalent bonds to the dangling bonds in micropores.

In particular, helium gas is found to cause a marked enhancement in the spin-lattice relaxation rate. In addition, extraordinarily strong condensation of helium gas occurs in the pore even at room temperature. This anomalous phenomenon proves the novelty of the structure of micropores in ACF having ultra micropores, which can accommodate only smallest diameter helium atoms. The extraordinarily strong condensation of helium gas in the ultra micropores has never been reported before and are prodigious from the point of physysorption phenomena in microporous materials. Anomalous helium-gas-induced spin-lattice relaxation is explained by the collision of the helium gas governed by electric dipole-dipole interaction which was discovered for the first time as a new spin-lattice relaxation mechanism. This is realized by the remarkably large helium gas condensation at room temperature in microporous materials.

Reference For Part III

1. Kaneko, Solid State Physics (in Japanese) **27**, 403 (1992).
2. M. Endo, K. Oshida, S. L. di Vittorio, M. S. Dresselhaus and M. Shiraishi, International Symp. on Fractal and Physically Adsorption Molecular State, Chiba, Japan, May 14-15, (1992).
3. K. Kaneko and C. Ishii, private communication.
4. S. Morozowski, J. Low Temp. Phys. **35**, 231 (1979).
5. G. Wagnoer, Phys. Rev. **118**, 647 (1960).
6. J. W. Armstrong, C. Jackson, and H. Marsh, Carbon **12**, 239 (1964).
7. A. Nakayama, K. Suzuki, T. Enoki, S. L. di Vittorio, M. S. Dresselhaus, M. Endo, and N. Shindo, Synth. Met. **57**, 3736 (1992).
8. S. L. di Vittorio, A. Nakayama, T. Enoki, M. S. Dresselhaus, M. Endo, and N. Shindo, J. Mater. Res. **8**, 2282 (1993).
9. H. Kuwabara, T. Suzuki, and K. Kaneko, J. Chem. Soc. Faraday Trans. **87**, 1915 (1991).
10. L. S. Singer and J. Kommaudeur, J. Chem. Phys. **34,** 133 (1961).
11. R. M. Barrer in "Zeolites: Science and Technology", edited by F. Ramoa Riberio, Alirio E. Rodrigues, L. Deane Rollmann, and Claude Naccache (Martinus Nijhoff Publishers, The Netherlands, 1984), p 227.
12. J. O. Hirschselder, C. S. Curtiss, and B. B. Bird, "Molecular theory of gases and liquids" (J. Wiley, New York, 1954).
13. K. Sugihara, J. Phys. Soci. Jap. **53**, 393, (1984).
14. K. Sugihara, A. Nakayama, and T. Enoki, J. Phys. Soci. Jap. **64**, 2614, (1995).

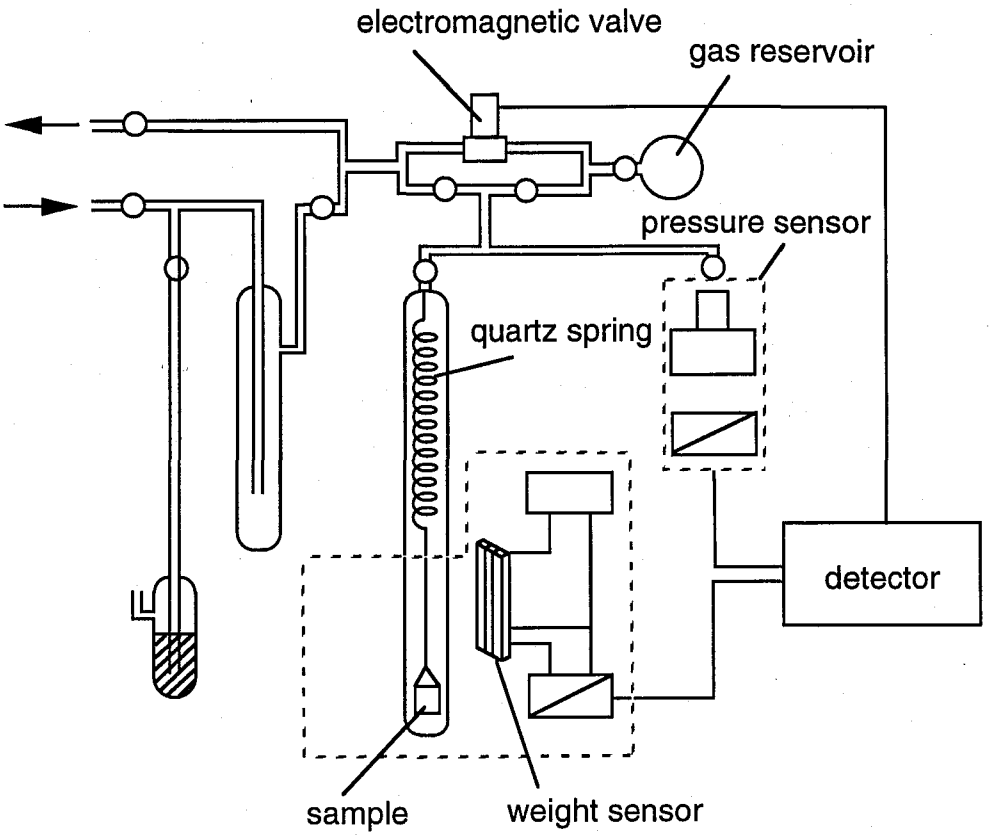

Fig. 1 Schematic diagram of the gravimetric adsorption apparattus.

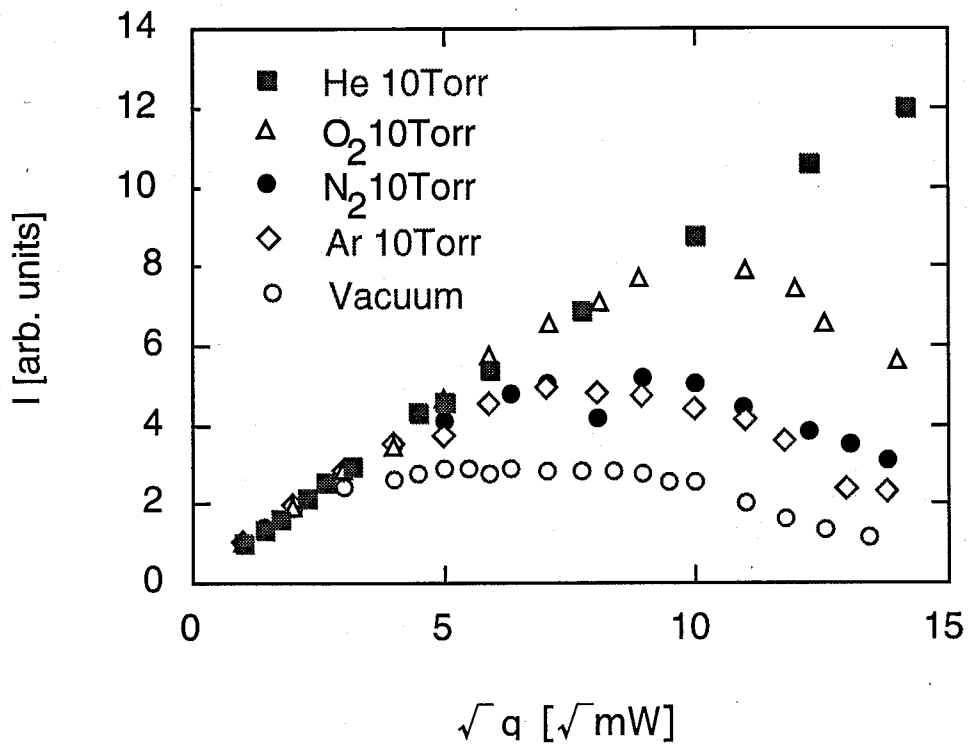

Fig. 2. The microwave power (q) dependence of the ESR intensity (I) under presence of gaseous materials at room temperature. The behavior of the sample with H_2or Ne is almost identical to that with N_2 or Ar.

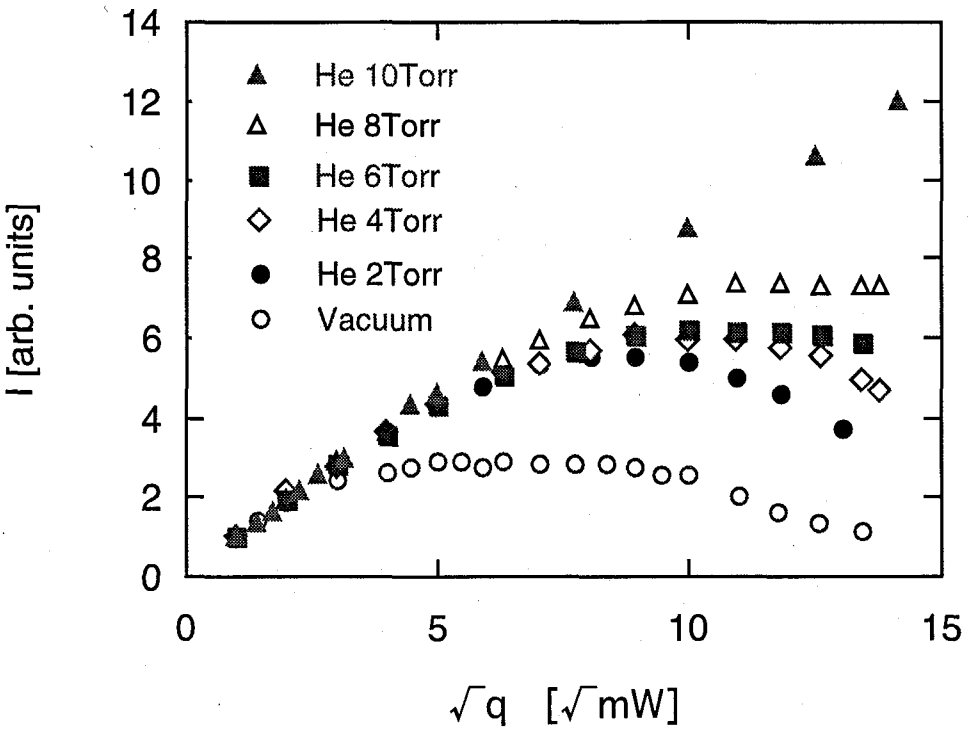

Fig. 3. The microwave power (q) dependence of the ESR intensity (I) under the presence of helium gas to10 Torr at room temperature.

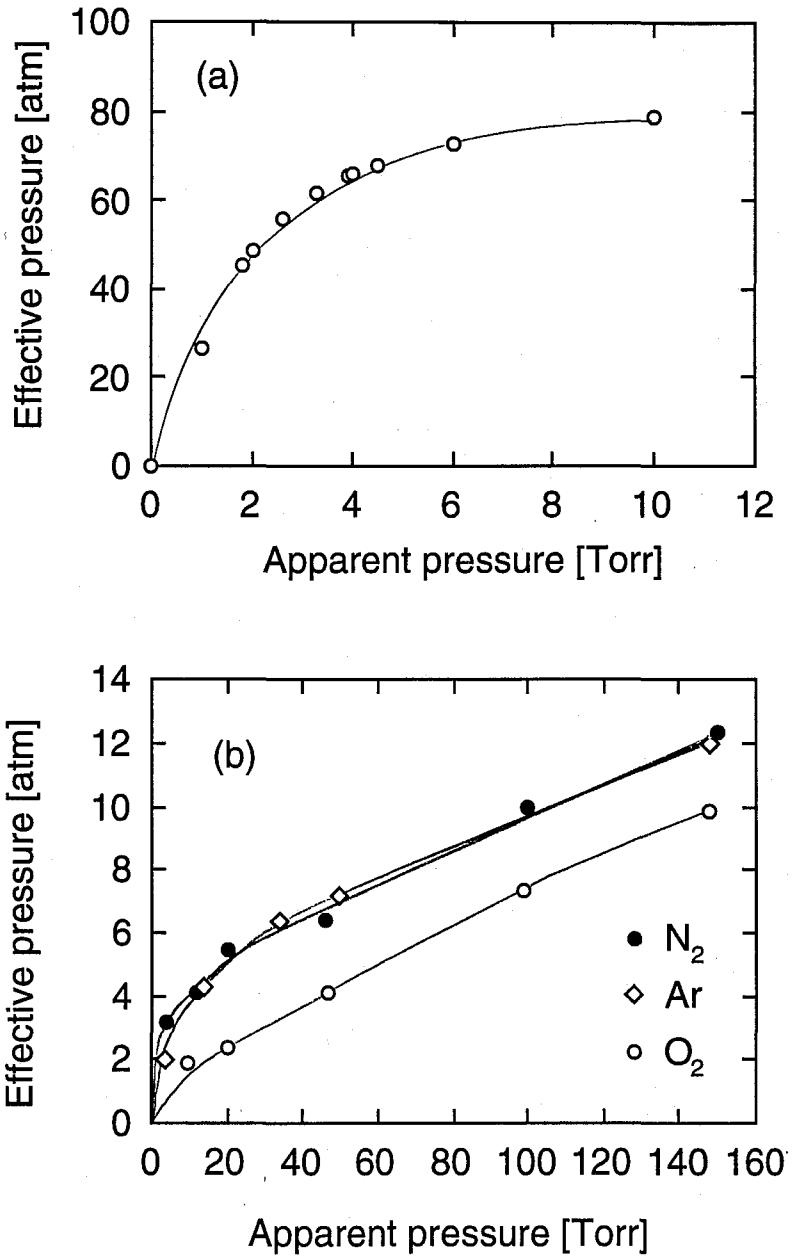

Fig. 4. The effective pressure in the micropores as a function of apparent pressure for (a) He, and (b) N_2, O_2, and Ar. The solid lines are guides for the eyes.

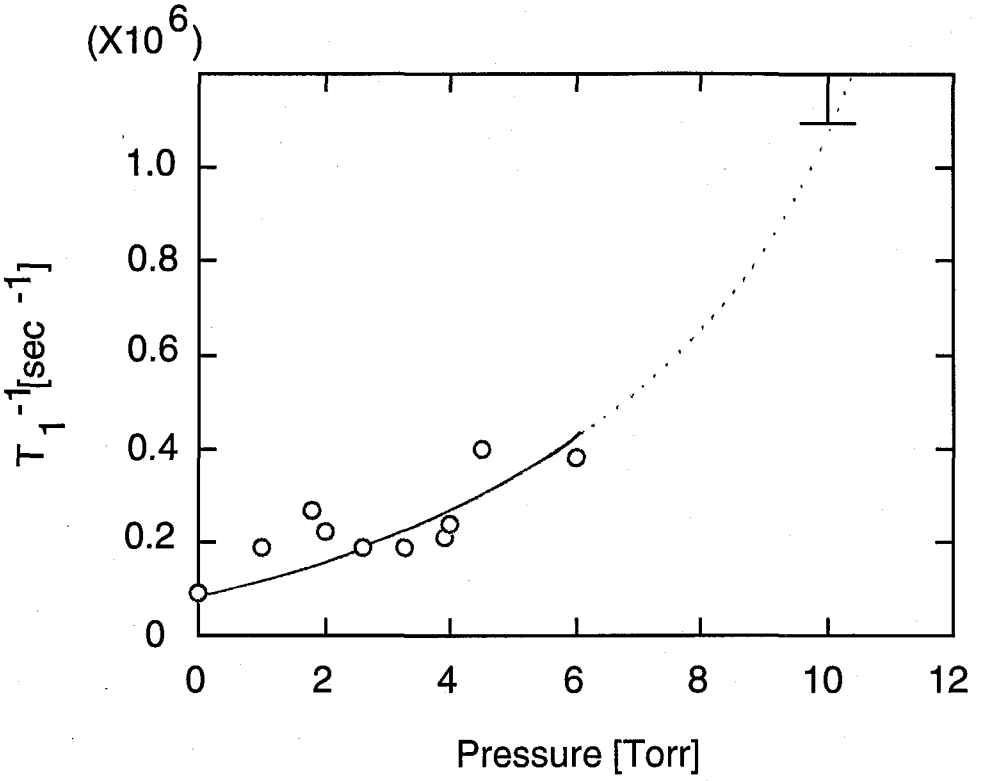

Fig. 5. The plot of spin-lattice relaxation rate T_1^{-1} vs. helium pressure for the dangling bond ESR signal. The sample witth 10 Torr helium gas does not show any saturation up to 200 mW which is the maximum power of the ESR machine, so that the lower limit for T_1^{-1} was estimated by assuming that the saturation occurs at 200 mW, and was illustrated as "$\perp$" in this graph. The solid line is a guide for the eye.

Adsorbed gases	The atomic and molecular sizes	The effective pressure in the pore	The apparent pressure of adsorbed gas	T_1
	[Å]	[Torr]	[atm]	[sec]
He	2.576	2	48.5	5×10^{-6}
		4	66.1	4×10^{-6}
		6	72.8	3×10^{-6}
		10	78.9	$<10^{-6}$
Ne	3.418	10	-	6×10^{-6}
Ar	2.789	10	3.3	6×10^{-6}
		760	-	3×10^{-6}
H_2	2.968	10	-	6×10^{-6}
N_2	3.681	10	4.2	5×10^{-6}
		760	-	2×10^{-6}
O_2	3.433	10	1.9	$<2\times10^{-6}$
vac.				2×10^{-5}

Table 1 The atomic and molecular sizes of the adsorbed gases, The spin-lattice relaxation rate T_1 of the dangling bond spins in the gas adsorbed ACF3000, and the effective pressure of the adsorbed gases in the pores

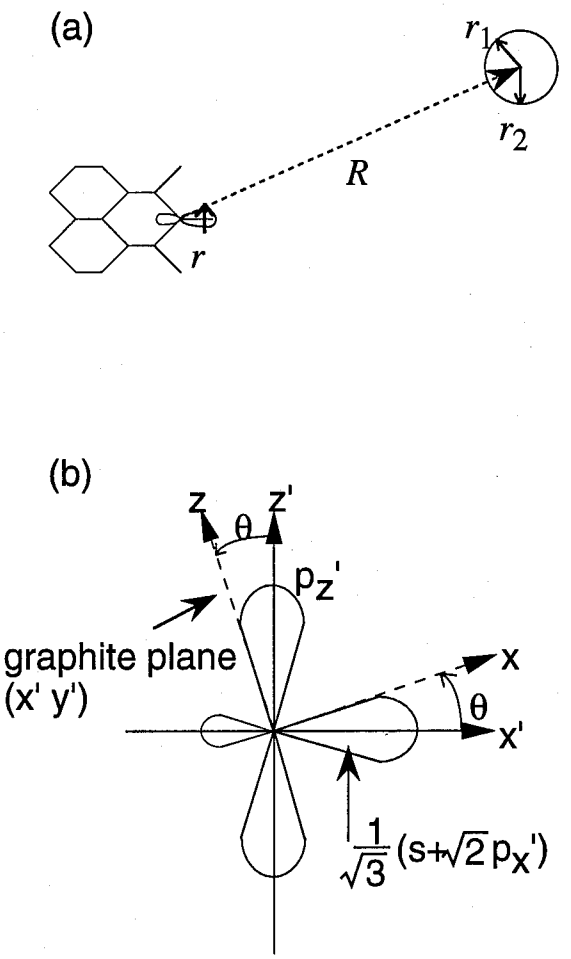

Fig. 5 (a) The model of the dangling bond attacked by a helium atom. The arrow denotes the dangling bond spin. r is the coordinate of the dangling bond electron, r_1 and r_2 the coordinates of the electrons of a helium atom, R the vector connecting a helium atom and the carbon atom related to the dangling bonds.
(b) (x', y') represents the graphitic plane and z'-axis is parellel to magnetic field. (x', y')-plane is the same as (x, y)-plane. A π-orbital and a dangling bond orbital of carbon atom are represented by $p_{Z'}$ and $(1/\sqrt{3})(s+\sqrt{2}p_{x'})$, respectively.

Part IV

Micrographite and Network Structure

IV-1 Introduction

Recently, various studies have been carried out to obtain information on the ACF network structure in relation to the origin of their magnetic and electronic properties. X-ray diffraction [1], Raman spectra [2], transmission electron micropore observations [3] and gas adsorption [4] were investigated. Kaneko et al. modeled the ACF structure which is an assembly of many micrographites forming disordered stacks of three to four graphene sheets with a dimension of ca. $20 \times 20 Å^2$ [5]. The transport properties provide information on the electronic structure related to the network of micrographitic domains. The resistivity, whose magnitude at room temperature ranges $2 \times 10^{-3} \Omega m$ [6] and on the same order for phenol-based carbon fibers [7], is explained in terms of two dimensional variable range hopping (2D VRH) related to disordered structural network of metallic micro-graphitic domains. The heat-treatment of ACFs at high temperatures1300 - 2800 °C reduces the magnitude of randomness in the structure and induces a strong modification of the electronic structure [8] which is explained by "the σ-trap mechanism" proposed by Morozowski [9] mentioned in details in Part II. The functional groups are removed from the marginal regions of the micrographites on heat-treating the samples, resulting in the generation of σ-type dangling bonds. In this process, conduction π-electrons are trapped by unsaturated σ-bondings, and consequently the same number of holes are generated in the valence π-band. Thus, the number of carriers at the Fermi level changes with heat-treatment, and the magnitude of the mean free

path of carriers increases with enlargement of the size of crystallites above heat-treatment temperatures of 2800 °C.

ACF structure consists of the network of the micrographites governing the electronic and magnetic properties, so that the edge structure of micrographite is supposed to give an electronically important role[10]. ESR and the magnetic susceptibility measurements are helpful in understanding the micro structure at the peripheries of the micrographite. In particular, the combination of ESR and gas adsorption measurement provides information on the interaction between the introduced gaseous molecule and the dangling bond spin, and the structural modification of the micropores generated by gas uptake[11]. The investigation of the dangling bond spin ESR signal under oxygen atmosphere reveals the formation of weak bounding between oxygen molecules and dangling bond spins in the micropores.

As mentioned above, recent works have been devoted to the understanding of the solid state properties of ACFs related to the disordered microporous network structure. However, there is little knowledge about the structure of the micrographitic domain itself, and the effect of gas adsorption on the solid state properties has not been well understood. Furthermore, the role of the network structure in a micrographite has not been proved from the view point of electronic and magnetic properties of ACF.

In this section, the network structure governing conduction mechanism of ACF is discussed through the experimental results of electrical conductivity. Furthermore, details of micrographites composing the network structure is estimated from the results of magnetic susceptibility and electrical conductivity.

IV-2 Experiemnts

In current experiments, we employed pitch-based ACF with SSA=1000 and 2000 m^2/g (ACF1000 and ACF2000).

Electrical conductivities for ACF1000 and ACF2000 were measured by the direct current four-prove method from 30 K to 285 K. Four electrical contacts were achieved by sandwiching an ACF fiber between four grafoil pieces and a quartz plate having four electrodes of evaporated gold films. In order to determine the absolute value of the electrical conductivity σ, scannning electron microscopy (SEM) was used for the measurement of the fiber diameters. Gas adsorption effects for electrical conductivities were investigated for oxygen gas and nitrogen gas which were introduced into the sample of ACF1000. The specially designed cell shown in Fig. 1 was used for the measurement of electrical conductivity in the atmosphere of nitrogen gas or oxygen gas. The sample was heated at 200 °C and ~10^{-5} Torr before introducing gas into the cell. 700 Torr nitrogen gas or oxygen gas was introduced at room temperature.

The magnetic susceptibilities were measured in temperature ranging from 4 K to 300 K using an automatic magnetic pendulum in the applied field H=1 T.

IV-3 Results

Temperature dependences of electrical conductivities σ are shown in Fig.2 (a) for ACF1000 and ACF2000 in the whole observed temperature range. The

temperature dependences of conductivities show semiconductive behavior with similar characteristics between ACF1000 and ACF2000. Discontinuous changes in the plots observed above ca. 150 K are associated with changes in contact resistance at the interface between sample and electrodes which were generated by thermal contraction. The absolute values of conductivities of both ACF1000 and ACF2000 at room temperature are estimated at 4.5 and 7.5 Scm^{-1}, respectively, by using fiber diameters obtained from SEM results as shown in the photograph of Fig. 3. The fiber diameters are estimated at 18 μm for both ACF1000 and ACF2000 samples. The SEM photographs show that the cross sections of the fibers are rather regular rounds having a smooth surface.

Figure 2 (b) shows the plots of $\ln(\sigma/\sigma_{r.t.})$ vs $T^{-1/3}$ below ca. 80 K for ACF1000 and ACF2000. According to the result shown in Fig. 2 (b), the conductivity obeys $\exp\left\{-(T_0/T)^{1/3}\right\}$ dependence at low temperatures below 80K where T_0 is estimated at 2.0×10^4 K for both ACF1000 and ACF2000. Figure 2 (c) shows $\ln\sigma$ vs 1/T plot above 180 K, which suggests that conductivity is dominated by the thermal activation process $\exp(-\Delta E/kT)$ in the higher temperature range. From the results shown in Fig. 2 (c), ΔE is estimated at 60 to 80 meV on average for 3 samples for both ACF1000 and ACF2000, which is in semi-quantitative agreement with the activation energy ΔE~44 meV obtained by the ESR measurement of ACF3000 having SSA=3000 m^2/g[12]. The analysis of temperature dependence of conductivities will be carried out in relation to the electronic state in "**Discussion**".

In order to investigate the influence of gas adsorption on the transport property

of ACF, time dependence of the resistivities of ACF1000 is measured under oxygen gas or nitrogen gas atmosphere at room temperature. In Fig. 4, time dependences of the variation rates of the resistivities are plotted before and after the introduction of 700 Torr nitrogen or oxygen gas at room temperature. The introduction of nitrogen gas makes the resistivity increase by less than 1 % in 200 min. The increase is saturated in about 50 min. Meanwhile, for oxygen gas, a steep resistivity increase is observed in the first 10 min and the total resistivity increase reaches ca. 3.5% for 200 min. The details about the adsorption states of these gases are mentioned in "**Discussion**".

The temperature dependence of magnetic susceptibilities of ACF1000 and ACF2000 are shown in Fig. 5. The susceptibilities for both ACF1000 and ACF2000 show diamagnetic behavior at high temperatures above about 20-30 K while they obey the Curie-Weiss law at low temperatures similar to the behavior of ACF3000[11]. The observed magnetic susceptibility of ACF χ_{obs} consists of the following components,

$$\chi_{obs}=\chi_C+\chi_{Pauli}+\chi_{orb}+\chi_{core}, \quad [1]$$

where χ_C is the Curie-Weiss component of localized spins, χ_{Pauli} is the Pauli paramagnetic component for conduction electrons, χ_{orb} is orbital diamagnetic component, and χ_{core} is the Pascal diamagnetic component. The observed magnetic susceptibility χ_{obs} below 40 K gives the Curie-Weiss component χ_C having localized spin concentrations $N_C=2.2\times10^{19}$ /g and $N_C=3.3\times10^{19}$ /g in the antiferromagnetic molecular field of Weiss temperature θ=-0.6 K and θ=-1.3 K

for ACF1000 and ACF2000, respectively, as summarized in Table 1. The component of χ_C is thought to be caused by the dangling bond spins being at the peripheries of the micrographitic domains. The obtained spin concentrations are about the same to spin concentration of ACF3000[11]. This suggests that the dangling bond spin concentration does not depend on the value of SSA among ACF1000, ACF2000, and ACF3000 samples. The core contributions χ_{core} are estimated at $\chi_{core} = -5.6 \times 10^{-7}$ emu/g for both ACF1000 and ACF2000 on the basis of the composition $[C_{124}H_{80}NO]_n$[13] using Pascal rule. For the analysis of the Pascal diamagnetism, we assume the mean structure of ACF, which is described in terms of the aromatic part having 36 benzene rings and the remaining aliphatic bridging part, taking into account the composition and the micrographitic domain size of ACF. The contributions of χ_{Pauli} and χ_{orb} will be estimated in the next section, as summarized in Table 1.

IV-4 Discussion

We extracted information on the electronic structure of ACF from the analysis of the conductivity. The density of states (DOS) at the Fermi level $N(E_F)$ in the case of 2D VRH is estimated as follows. Judging from the random structure of ACF composed of an assembly of micrographites, it is assumed that the electrons are localized on metallic micrographites, and the hopping conduction occurs between micrographites by thermal activation process. Around the marginal region

of the micrographites, the wave functions of the electrons attenuate in accordance with the function of exp(-r/ξ), where ξ is the localization length, so that the overlap between the wave functions of the adjacent micrographitic domains is in proportion to exp(-2r/ξ). Moreover, the occurrence of a hopping event requires the thermal activation which is related to the difference in the potential energies of hopping electrons ΔE between the adjacent micrographitic domains. Thus, the hopping conductivity σ is expressed by the following equation;

$$\sigma = \sigma_0 \exp\left(-2\alpha r - \frac{\Delta E}{kT}\right), \tag{2}$$

where σ_0 is constant[14]. ΔE depends on DOS at the Fermi energy level $N(E_F)$ and the dimensionality of the transport system of ACF. In the random network system of metallic microdomains having two dimensionality, conductivity expressed in eq.(2) is rewritten by the variable range hopping formula as given by the following equation;

$$\sigma = \sigma_0 \exp\left(\left(-\frac{T_0}{T}\right)^{\frac{1}{3}}\right). \tag{3}$$

Here T_0 is expressed by

$$T_0 = \frac{27}{\xi^2 \pi N(E_F) k}, \tag{4}$$

where k is the Boltzmann constant. As shown in "**Results**", the manner of temperature dependence observed below 50K is explained in terms of the two-

dimensional variable range hopping (2D VRH)[14], taking into account the two dimensionality of the micrographite network structure of ACF. The in-plane size of a micrographite L_a in ACF is estimated at L_a~25 Å from Raman spectra[1, 3]. The range where electrons enable to move coherently on ACF is limited within a micrographite domain which is regarded as a metallic island as shown in FIG. 6, and the conduction electrons are scattered at the boundaries of micrographites. Therefore, if we assume ξ to be the in-plane size of a micrographite ξ~25 Å, DOS is estimated at $N(E_F) = 8 \times 10^{17}$ $eV^{-1}m^{-2}$ for both ACF1000 and ACF2000. This suggests that ACF1000 and ACF2000 have almost the similar electronic structure, taking into account the similar behavior of magnetic susceptibilities for both samples which will be mentioned later. The presence of the finite density of state a E_F implies that the impurity band is located around E_F, since the intrinsic band structure of graphite is explained in terms of the zero gap semiconducter with no density of states at E_F as shown in Fig. 7.

Now, we discuss the relation between the micrographite network structure and the two-dimensionality in the electron transport observed in the present experiment. In general, there are two kinds of micrographitic carbons; one is graphitizing carbon with two dimensional orientation of micrographites, and the other is nongraphitizing carbon with random orientation of micrographites proposed by Flankline[15]. In the case of ACF, according to the X-ray diffraction analyses[1] and Raman spectra[2], it has been found that ACF consists of an assembly of 2D-micrographites. The result of the diamagnetic susceptibility suggests that the ACF sample heat-treated at 1500 K to 3000 K is well

graphitized[5], with two dimensionally preferred orientations of micrographites. Judging from the structural information, ACF is classified to be in the former category, and it is supposed that the micrographites are linked to each other by the σ-bondings extending to the two dimensional directions, and that the micrographite network has the disordered structure having two dimensionality to some extent. So, it is reasonable that the VRH mechanism observed below 50 K is explained on the basis of two dimensionality of the micrographite network structure. And the electrons hop between micrographites in two dimensional directions through the σ-bonding bridges which give the overlap of the wave functions between adjacent micrographites.

Next we discuss the relationship between gas adsorption and a conduction mechanism for ACF. Non-active nitrogen gas is known to induce the structural change in the micrographite of ACF[16]. In the case of nitrogen gas adsorption at 165 K, the interlayer distance between graphitic sheets decreases by 6% when nitrogen gas is introduced, even though the amount of nitrogen gas is less than 5% of the saturated amount[16]. The change of the interlayer distance of the micrographite is explained by the relation between the structure of ACF and the adsorption site of the nitrogen molecules. The micropore of ACF is characterized by the wedge-type pore, so that nitrogen molecules can easily enter into the wedge-type pore through a wide-open entrance at the side surface of the micrographite as shown in Fig. 8 (a). Adsorption of nitrogen gas changes the micropore shape from the wedge-type to the slit-type which causes a slight expansion of the ACF network structure. The conductive pass connected between micrographites existing

before nitrogen gas adsorption are cut by reorientation of the micrographites after nitrogen gas adsorption. Therefore, the change in stacking structure affects the network structure between the micrographites, and results in an increase in resistivity by nitrogen uptake. In the case of adsorption of oxygen gas, the adsorption site is supposed to be different from that of nitrogen gas. According to the ESR spectra assigned to the dangling bond spins existing at the peripheries of micrographites[11], the change in the ESR signal by introducing oxygen gas suggests the formation of weak covalent bonds between the dangling bonds and oxygen molecules. Namely, in the case of oxygen gas adsorption, the ESR saturation curve behaves as a homogeneous spin system, different from the behavior of curves in nitrogen gas showing trends for inhomogeneous spin system[17]. In addition, the adsorption isotherm for oxygen at room temperature has different behavior patterns from that of inert gases including nitrogen gas, which reveals evidence for the formation of weak chemical bondings. The adsorption of water vapor is informative in the explanation of oxygen gas adsorption to ACF[16], since the adsorption manner of water molecule is supposed to be similar to that of oxygen molecule, from the trend of chemical activity. Water molecule is gradually introduced into the parts in which the functional groups are located, and the structural change in micrographite is not induced until water molecules are adsorbed in the interlayer space of micrographites, thus changing the orientation of micrographites. Therefore, the steep change of resistivity at the beginning of adsorption is considered to be associated with the formation of weak covalent bonds with oxygen, which induces not only the charge transfer between oxygen molecules and micrographite but also the structural change. The structural change

model is summarized in Fig. 8.

Finally, we analyze the electronic structure from the results of magnetic susceptibilities and conductivities, and attempt to obtain information on the geometrical structure of micrographites itself. The values of χ_{Pauli} for both ACF1000 and ACF2000 are calculated at 1.1×10^{-7} emu/g from $\chi_{Pauli} = 2\mu_B{}^2N(E_F)$ by using $N(E_F)$ whose values are obtained from the variable range hopping conductivity. After subtracting the values of χ_C, χ_{Pauli} and χ_{core} from the observed susceptibility χ_{obs}, we obtain the contributions of χ_{orb} for the samples having randomly oriented micrographite planes; -3.9×10^{-7} emu/g for ACF1000 and -3.5×10^{-7} emu/g for ACF2000. The value of the orbital susceptibility $\chi_{orb//}$ in the field applied perpendicular to the graphitic plane is obtained to be -1.2×10^{-6} and -1.1×10^{-6} emu/g for ACF1000 and ACF2000, respectively, by multiplying by 3, since the graphitic microdomains are randomly oriented. The observed absolute values of $\chi_{//orb}$ for ACF1000 and ACF2000 are one order of magnitude smaller than the value ($\chi_{//orb}=-8 \times 10^{-6}$ emu/g) for graphite having the infinitely extended planar structure of condensed polycyclic aromatic hydrocarbon[18]. The component $\chi_{//orb}$ for graphite originates from the delocalized π-electrons on the infinite graphite plane. Therefore, the fact that ACF has smaller orbital diamagnetism than graphite proves that the micrographitic domain in ACF has a finite size. Subsequently, the magnitude of $\chi_{//orb}$ of ACF is compared to other

condensed polycyclic aromatic hydrocarbons having finites size and graphite fine particles. The magnitude of the orbital diamagnetic susceptibility for graphite fine particles having a domain size of 50 Å is reported to be -0.5×10^{-6} emu/g[19] which is not so different from that of ACF, despite the fact that the grain size of these fine-particles is larger than that of ACF. It means that in spite of the entangled appearance of ACF fibers, the micrograhpites of ACF are well graphitized in comparison with the grain of graphite fine-particles. Here, we compare the estimated value of the orbital diamagnetic susceptibility with that of condensed aromatic hydrocarbons consisting of N benzene rings, in order to get information on the structure of the micrographitic domains. The relation between the number of benzene rings N and the value of $\chi_{//orb}$ for polycyclic aromatic compounds is shown in FIG. 9 after the data in literatures[19]. From the $\chi_{//orb}$ vs N plot, we obtain the empirical relation expressed by the following equation;

$$\log|\chi_{orb}| = -4.7 - 15 \times \frac{1}{N}. \quad (5)$$

Using eq. (5), the magnitude of $\chi_{//orb}$ for condensed polycyclic aromatic compound with N=36, which is considered to correspond to the average structure of the micrographite in ACF, $\chi_{//orb}$ is expected to be -8.0×10^{-6} emu/g which is about eight times larger than the experimental results for ACF1000 and ACF2000 as shown in Table 1. The cause for the difference between them is thought to be as follows. The deviation from the expected value of $\chi_{//orb}$ for model polycyclic aromatic compounds implies the presence of a distortion and/or defects in the

micrographite which depresses the effective size of the π-electronic system in the micrographite. Again, by use of eq. (5) the number of benzene rings N which corresponds to the observed value of $\chi_{//orb}$ is estimated at N=12 and N=11 for the effective sizes of the π-electronic systems in ACF1000 and ACF2000, respectively. The magnitude of $\chi_{//orb}$ is correlated to the degree of the delocalization of π-electrons in the graphite sheet, indicating the extent of the plane structure. Therefore, the experimental finding reveals that the graphene sheet of ACF is deformed with some degree of nonplanarity caused by defects and distortions of in-plane structure. Analogous observation is reported in carbon ribbons. $\chi_{//orb}$ of a polyacrylonitrile-based carbon fiber (PAN-CF) and benzene derived carbon fiber (BDF)[21] is explained by the folded ribbon model, that is the micro-folded layer structure, proposed by McClure and Hickman[22]. ACF does not have periodically folded graphene sheets like carbon ribbons, however, according to the present results, the micrographite in ACF has nonplanar structure with defects like crators on the moon surface. We have two possible reasons why the micrographite has a nonplanar structure. One is that the degenerate π-electronic structure of graphite is solved due to the presence of defects. Another is that the presence of functional groups attached to graphitic microdomains causes steric hindrance, resulting in the generation of nonplanarity in graphitic micro domains.

IV-5 Summery

Transport and magnetic properties of pitch-based ACF1000 and ACF2000 with

SSA~1000 and 2000 m^2/g are investigated in order to get information on the micrographite network structure and the internal structure of the mocrographitic domain having the size of ca. 20 Å. The temperature dependence of conductivities for both ACF1000 and ACF2000 are described in terms of the two-dimensional variable range hopping mechanism, whose behaviors are extrapolated to the ordinary thermally activation hopping conduction with the activation energy E_a=60 ~ 80 meV in the higher temperature range. The dimensionality of the transport properties of ACF is supposed to be caused by the specific network structure of micrographitic domains which are linked to each other through bridges composed of σ-bonding carbons. Assuming that the localization length is regarded to be equal to the domain size, the densities of states at the Fermi energy level are estimated at $N(E_F)\sim10^{18}\ eV^{-1}m^{-2}$ for both ACF1000 and ACF2000.

Introduced nitrogen gas or oxygen gas changes the electrical conductivity, which is caused by a change in the micrographite network structure. In addition to the structural modification by the introduced gas, oxygen affects the electronic structure of ACF through the formation of weak chemical bonding between dangling bonds and oxygen molecules.

The magnetic susceptibilities for both ACF1000 and ACF2000 show the Curie-Weiss temperature dependent susceptibility below 40 K, which suggests the presence of $10^{19}/g$ localized magnetic moments associated with dangling bond spins attached to the peripheries of micrographite. The orbital diamagnetic susceptibilities $\chi_{//orb}$ of ACF1000 and ACF2000 were estimated at -1.2×10^{-7} emu/g and -1.1×10^{-7} emu/g, respectively, which are about one order of

magnitude as small as that expected for the condenced polycyclic aromatic hydrocarbons having the same number of benzene rings to the average number of benzene rings of ACF1000 and 2000. This proves that the graphene sheet of ACF is deformed with some degree of nonplanarity caused by defects and distortions of the in-plane structure.

Reference For Part IV

1) K. Kaneko, S. Ozeki, T. Suzuki, and K. Kakei, "Characterization of Porous Solid II," pp429, F. Rodriguez -Reiniso et al. (Editor), Elservier Science Publishers B. V., Amsterdam (1991).

2) T. Suzuki, K. Kaneko, *Carbon* **26**, 734 (1988).

3) A. M. Rao, A. W. P. Fung, M. S. Dresselhaus, and M. Endo, *J. Mater. Res.* **7**, 1788 (1992).

4) M. Endo, K. Oshida, S. L. di Vittorio, M. S. Dresselhasus, and M. Shiraishi, International Symp. on Fractal and Physically Adsorbed Molecular States, Chiba, Japan, May, 14-15 (1992).

5) K. Kakei, C. Ishii, M. Ruike, H. Kuwabara, and K. Kaneko, *Carbon* **130**, 1075(1992).

6) K. Kuriyama, *TANSO* **155**, 282 (1992) (in Japanese).

7) S. K. di Vittorio, M. S. Dresselhaus, M. Endo, J-P. Issi, L. Piraux, and V. Bayot, *J. Mater. Res.* **6**, 778 (1991).

8) T. Enoki, K. Inukai, K. Suzuki, M. Endo, and N. Shindo, private communication.

9) S. Morozowski, *Phys. Rev.* **85**, 609 (1952).

10) A. Nakayama, K. Suzuki, T. Enoki, S. L. di Vittorio, M. S. Dresselhaus, K.Koga, M. Endo, and N. Shindo, *Synthetic Metals,* **55-57**, 3736 (1993).

11) A. Nakayama, K. Suzuki, T. Enoki, M. Endo, and N. Shindo, private communication.

12) N. Shindo, K. Tai, and Y. Matsumura, *Chem. Eng.* **28**, 1 (1987).

13) N.Mott, *in Conduction in non-crystalline material* (Clarendon Press, Oxford 1987).

14) R. E. Frankline, *Proc. Roy, Soc.* (London), A209, 196 (1951).

15) K. Kaneko, *Solid State Physics* (Japan), 27, 403 (1992).

16) A. Nakayama, T. Enoki, K. Suzuki, C. Ishii, K. Kaneko, M. Endo, and N.Shindo, *Solid State Commun.* **93**, 323 (1995).

17) D. B. Fishbach, *Phys. Rev.* **123**, 1613 (1961).

18) D. E. Soule, C. W. Nezbeda, A. W. Czanderna, *Rev. Sci. Instr.* **35**, 150 (1964).

19) R. McWeeny, *Proc. Phys. Soc.* **A 65**, 839 (1952).

20) K. Matsubara, K. Kawamura, T. Tsuzuku, *Japanese J. Appl. Phys.* **25**, 1016 (1986).

21) J. W. McClure and B. B. Hickman, *Carbon* **20**, 373 (1982).

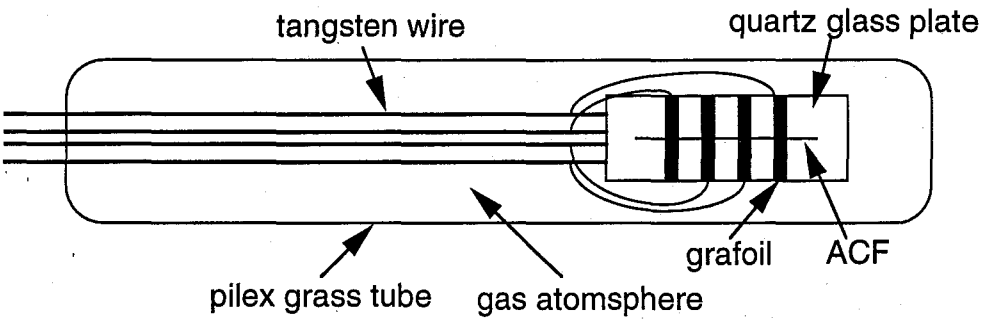

Fig. 1. The glass cell for the measurement of electrical conductivities for the gas adsorbing sample.

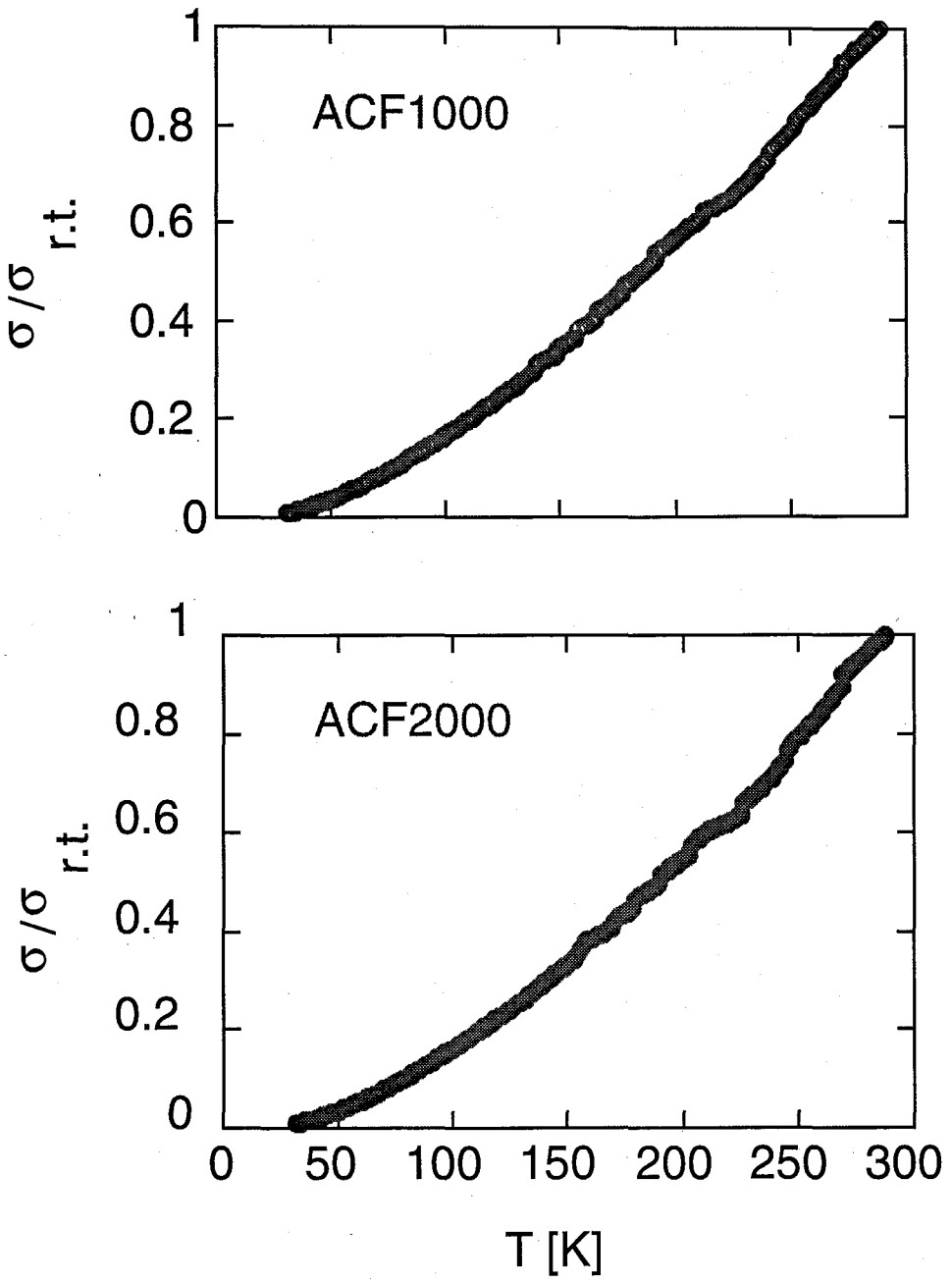

Fig. 2(a) The temperature dependence of the conductivity for ACF1000 and ACF2000.

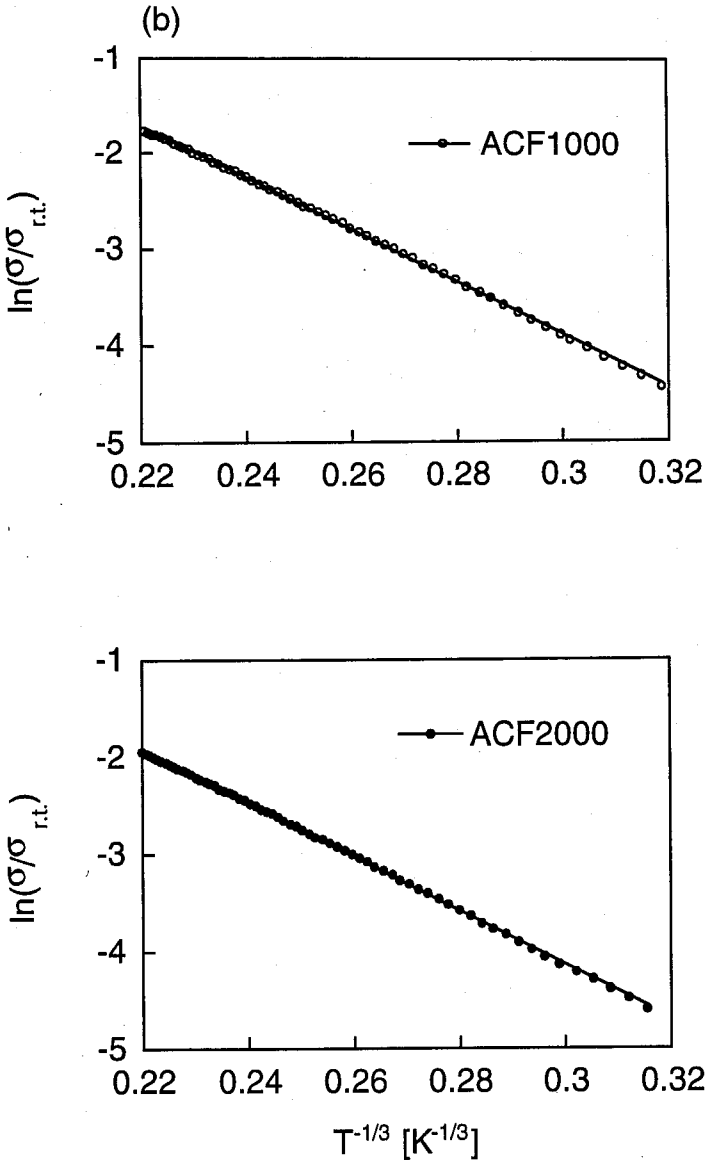

Fig. 2 (b). Plots of $\ln(\sigma/\sigma_{r.t.})$ vs $T^{-1/3}$ in the low temperature range below about 80K.

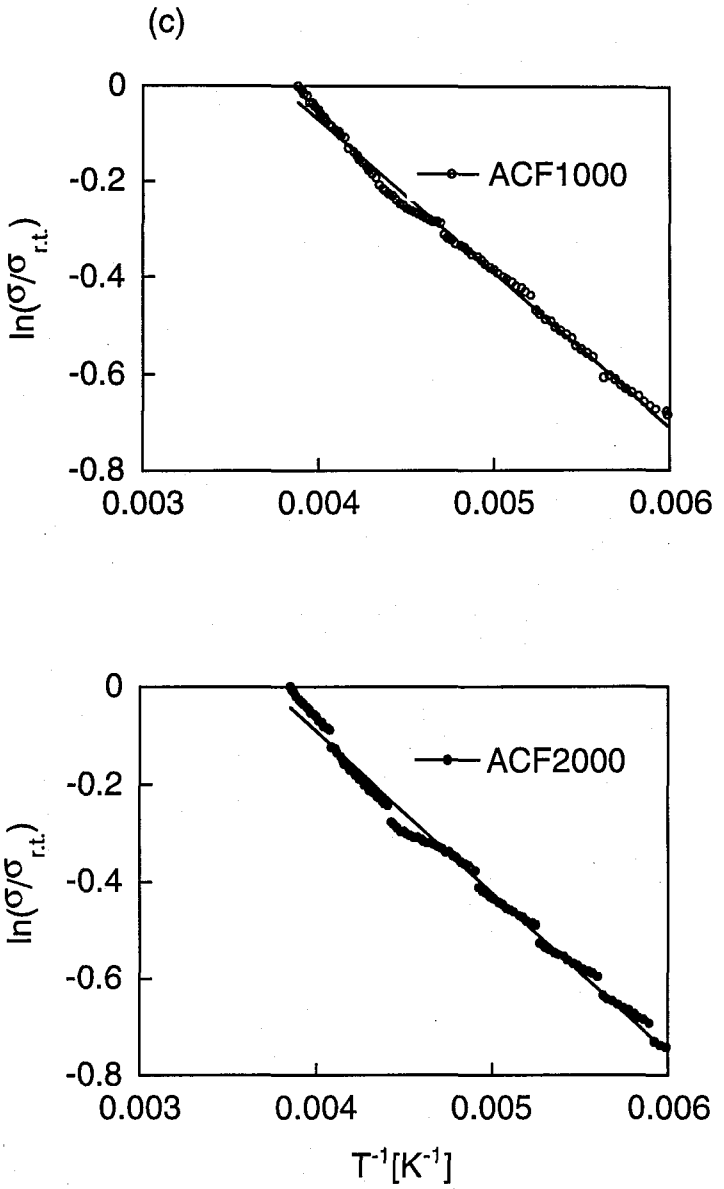

Fig. 2 (c) Plots of ln ($\sigma/\sigma_{r.t.}$) vs T^{-1} in the high temperature range above about 180K. Discontinuous changes in the plots obtained above ca. 150K are associated with the changes in contact resistance at the interface between the sample and the electrodes which were generated by thermal contraction.

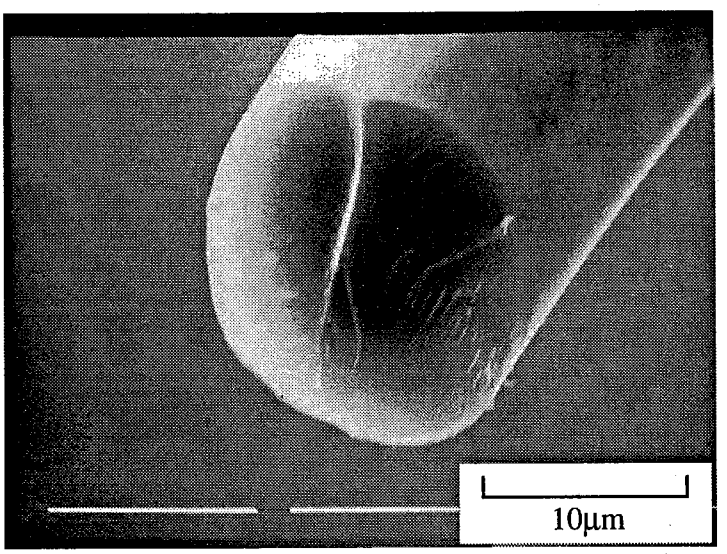

Fig. 3. Scanning electron microscopy (SEM) photograph of the cross section of pitch based ACF1000 (m^2/g).

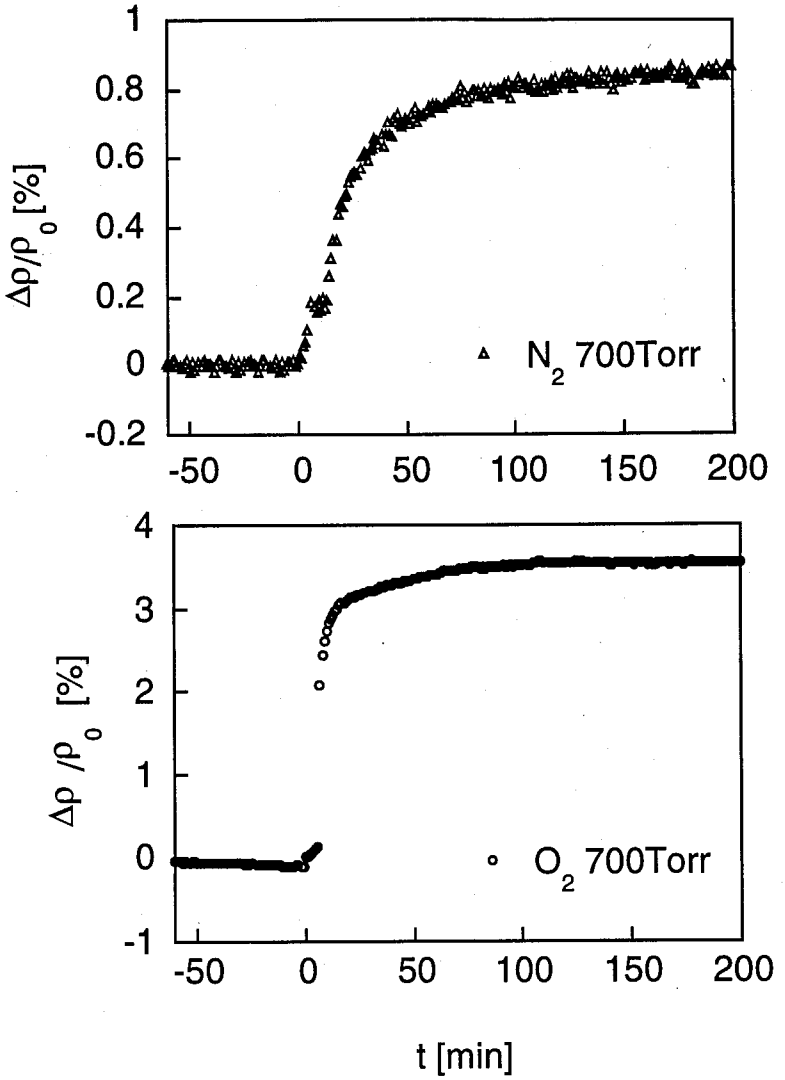

Fig. 4 Time dependence of the variation rate of the resistivity for ACF1000 adsorbing 700Torr N_2 gas (△) and 700 Torr O_2 gas (○) at room temperature. The vertical axis represents the percentage of the variation rate of the resistivity ρ. ρ_0 is the value of the resistivity at t=0 which shows the starting point of the gas adsorption.

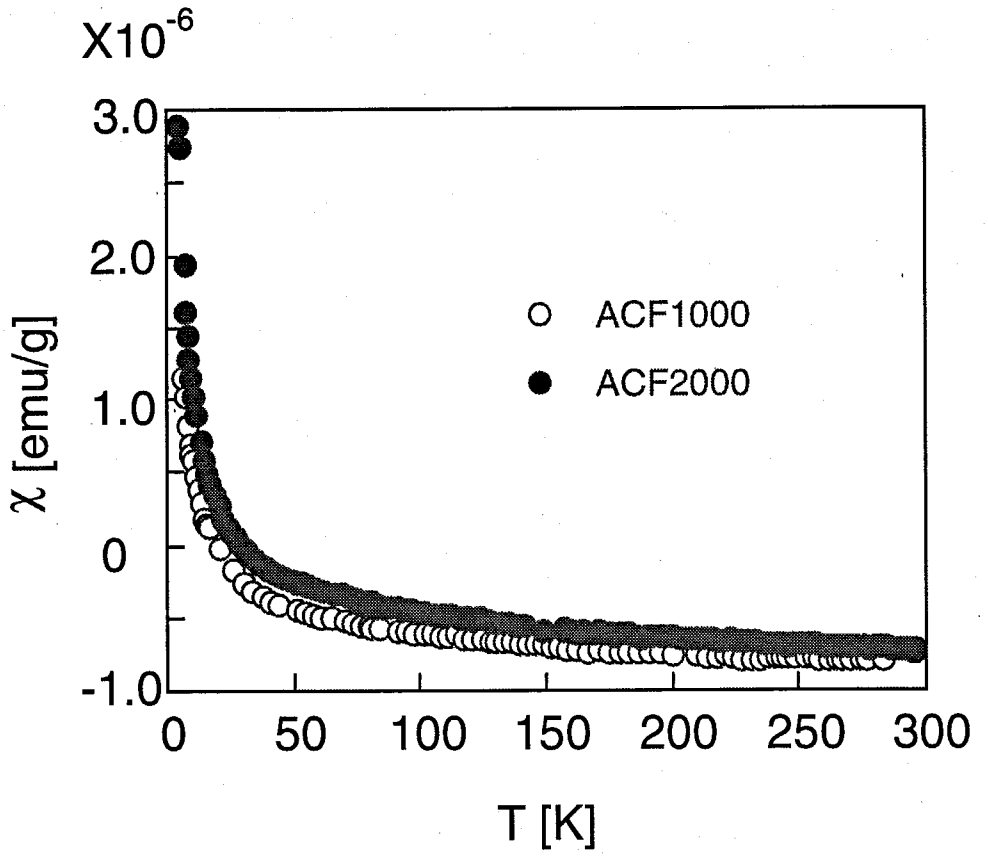

Fig. 5 Temperature dependence of magnetic susceptibility for ACF1000 (○) and ACF2000 (●).

Table 1. Contributions of Curie-Weiss spin-paramagnetism χ_C, core diamagnetism χ_{core}, Pauli-paramagnetism χ_{Pauli} and orbital diamagnetism $\chi_{//orb}$ to the observed magnetic susceptibility χ_{obs} measured at room temperature, where $\chi_{//orb}$ is the orbital susceptibility in the field perpendicular to the graphitic plane. N_C and θ are the localized spin concentration and the Weiss temperature, respectively, in the Curie-Weiss susceptibility.

Sample	χ_{obs} (emu/g)	χ_C (emu/g)	θ (K)	N_C (/g)	χ_{core} (emu/g)	χ_{Pauli} (emu/g)	$\chi_{//orb}$ (emu/g)
ACF1000	-7.9×10^{-7}	4.9×10^{-8}	-0.6	2.2×10^{19}	-5.6×10^{-7}	1.1×10^{-7}	-1.2×10^{-6}
ACF2000	-7.3×10^{-7}	6.8×10^{-8}	-1.3	3.3×10^{19}	-5.6×10^{-7}	1.1×10^{-7}	-1.1×10^{-6}

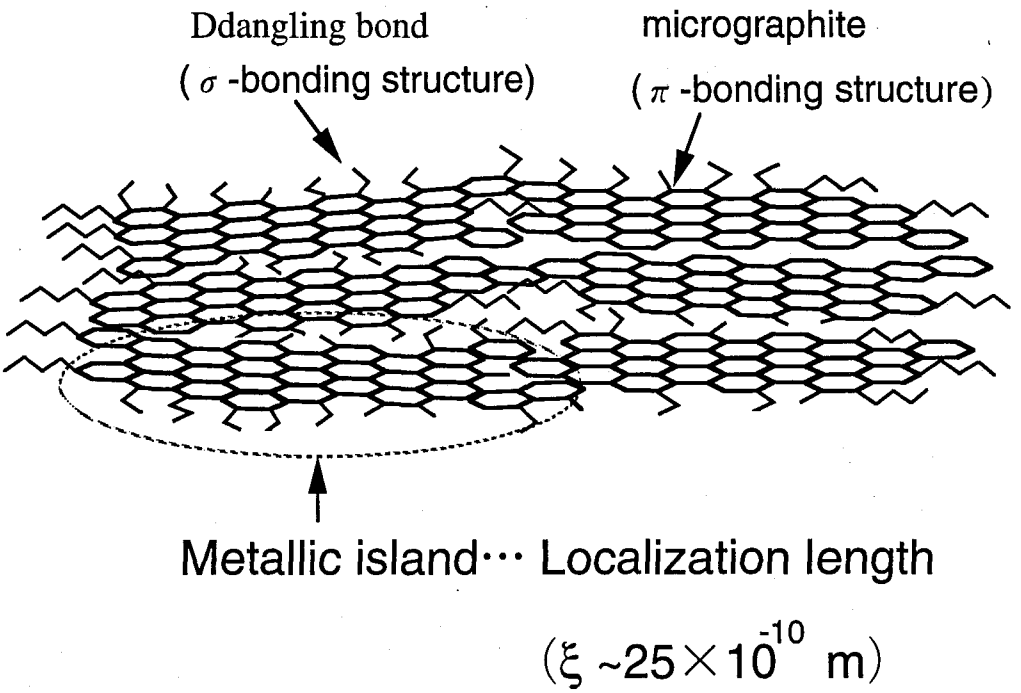

Fig. 6 Metallic islands and these network structure. One micrographite corresponds to the metallic island of ACF. π-bondings composing micrographites are connected by the bridges of σ-bondings consisting of the edge structure of micrographites.

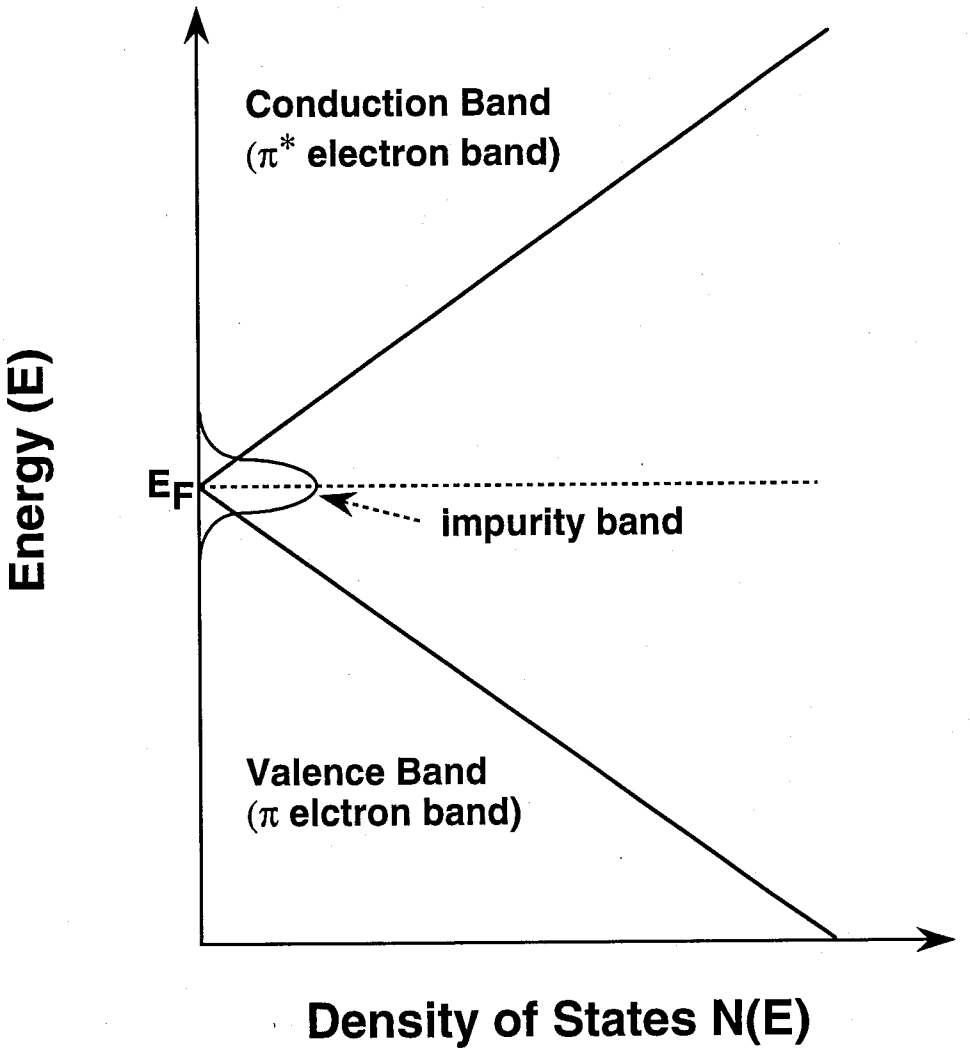

Fig. 7 The electronic structure of ACFs.

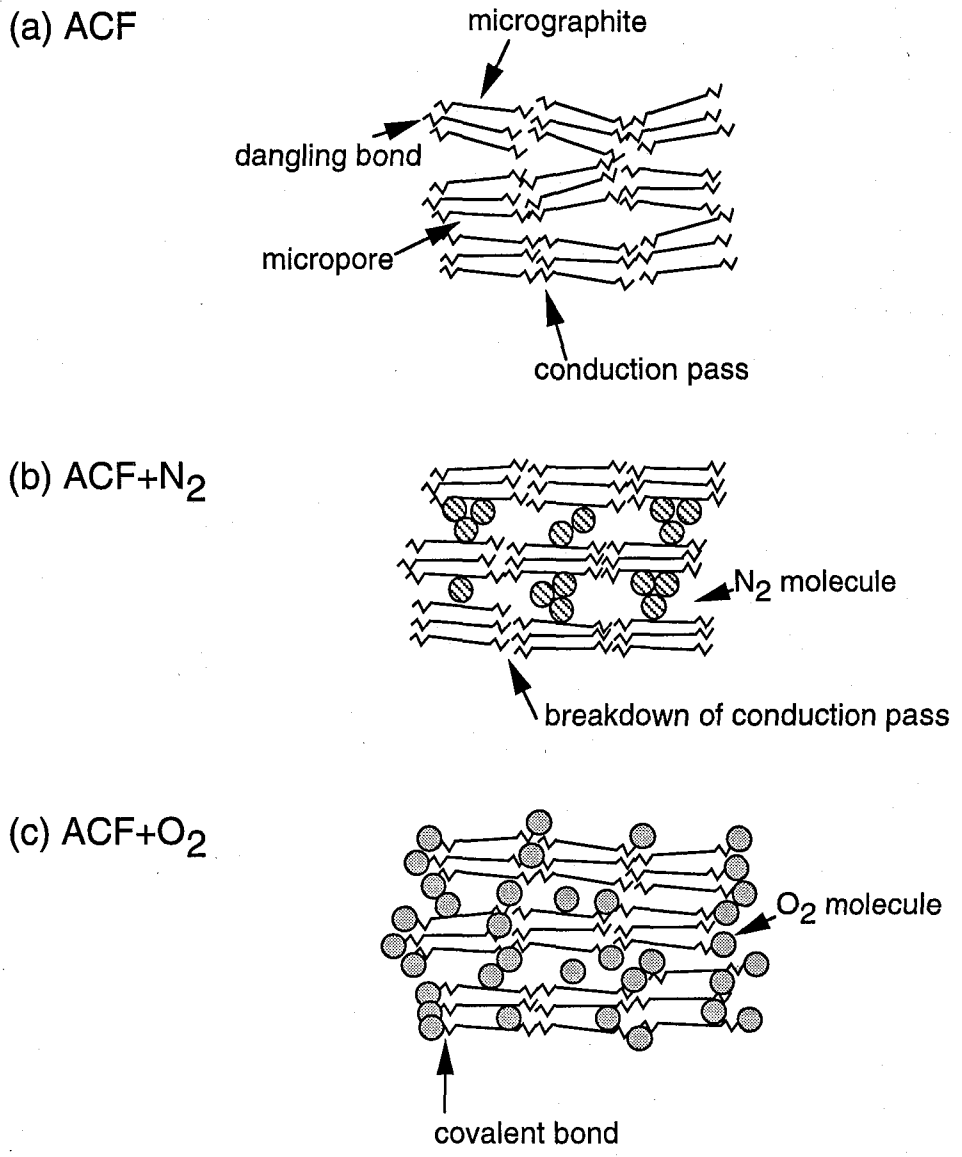

Fig. 8. Gas adsorption model of ACF. (a) The micropore of ACF is characterized by the wedge-type pore. (b) Adsorption of nitrogen gas changes the micropore shape from the wedge-type to the slit-type which causes a slight expansion of the ACF network structure.(c) Oxygen molecule is introduced into the parts in which the functional groups are located, and forms the weak covalent bonds with dangling bonds.

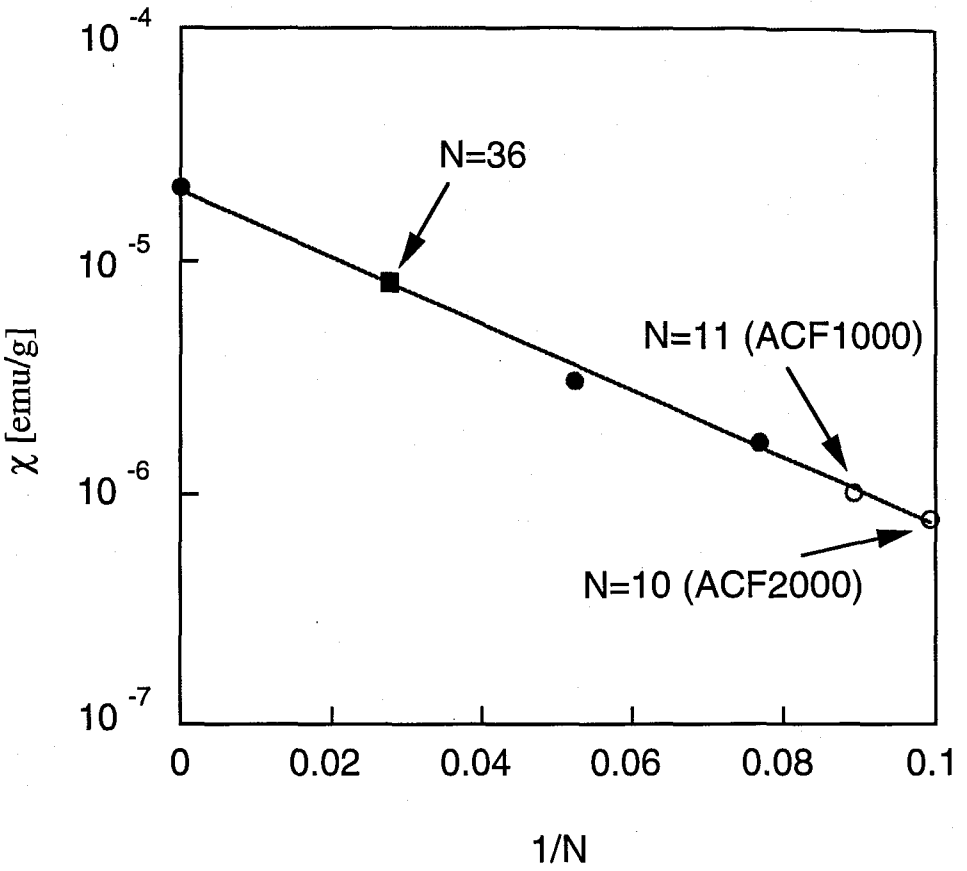

Fig. 9. The relation between the number of benzene rings N and the value of the orbital diamagnetic susceptibility χ_{orb} for condensed polycyclic acomatic compounds. ACF1000 (N=10) and ACF2000 (N=11) marked with ○ denote the position corresponding to the experimentally obtained orbital susceptibility for ACF1000 and ACF2000, respectively, while■ with N=36 corresponds to the number of benzene rings for the average structure of the micrographitc domain in ACF. The data for polycyclic compounds denoted by ● are referred from ref. 20. N=11 and N=10 mean that the observed values of χorb correspond to the orbitalsusceptibilities of the compounds with 11 and 10 benzene rings for ACF1000 and ACF2000, respectively.

Part V

General Conclusion

Pitch based activated carbon fibers (ACF) are microporous carbons with huge specific surface areas (SSA) ranging from 700 to 3000m^2/g, and have random structures consisting of an assembly of the micrographites with a dimension of a ca. 20×20Å. Magnetic and electronic properties of ACFs were investigated by the measurements of the ESR spectra, the magnetic susceptibility, and the electrical conductivity. In addition, their results of pristine samples are compared to that of gas adsorbed samples and heat-treated samples. Then the characters of dangling bonds, pore structures, microfraphites and their network structure which characterize properties of ACFs are summarized in this thesis. In addition to the introduction of ACFs, preparations and characterizations of ACF samples supplied from Osaka Gas Chemical Co., Ltd. are introduced in Part I. One of remarkable processes in the sample preparation is a activation process which produces huge SSAs of ACFs, resulting in pores, micrographites, and dangling bonds.

Properties determined by dangling bonds are clarified by magnetic measurements of ACF3000, which are summarized in Part II. Not only ACF3000 pristine sample but also heat-treated sample are investigated by the measurements of ESR spectra and magnetic susceptibility in order to investigate the spin species within ACF3000. In addition, mass spectra in the range of room temperature to 800°C are observed to obtain a structural information of dangling bonds. ACF3000 has isolated dangling bond spins and conduction electron spins, and linewidthes of ESR spectra show 40G and 800G, respectively. The magnetic susceptibility of isolated dangling bond spins obeys the Curie law, and that of conduction electron spins shows a weak temperature dependence. respectively. Heat-treatment of ACF removes functional groups in the micrographites, and

modifies disordered structure of micrographites, resulting in the more regular stacking of micrographites. However the temperature below 800°C does not occur the graphitization. Enlargement of the magnetic susceptibility of ACF3000 by heat-treatment below 800°C shows the increase of the number of new dangling bond spins after the decomposition process of functional groups above 400°C or the precursor of graphitization process, resulting in the enhancement of the value of a weak temperature dependent spin paramagnetic component.

Properties originated from pore structure are clarified from the ESR spin-lattice relaxation rate T_1^{-1} for ACF3000 in the presence of the He, Ne, Ar, H_2, N_2, and O_2 gases by using the dangling bond spins as a testing probe, which are summarized in Part III. We found the enhancement of the spin-lattice relaxation rate induced by the collisional process of the gas atoms to the dangling bonds where T_1^{-1} s are almost identical among ACFs adsorbing foreign gases with different molecular weight and size except helium and oxygen. The finding that the T_1^{-1}s for diatomic molecules are identical to those for inert gas atoms suggests that the internal degrees of freedom such as rotations and vibrations do not participate in the acceleration of T_1^{-1}. In the case of oxygen adsorption, the saturation curve behaves as a homogeneous spin system, different from the behavior of the curves in other gases. This suggests that the adsorbed oxygen molecules form weak covalent bonds to the dangling bonds in micropores.

In particular, helium gas is found to cause a marked enhancement in the spin-lattice relaxation rate. In addition, extraordinarily strong condensation of helium gas occurs in the pore even at room temperature. This anomalous phenomenon proves the novelty of the structure of micropores in ACF having ultra micropores, which

can accommodate only smallest diameter helium atoms. The extraordinarily strong condensation of helium gas in the ultra micropores has never been reported before and are prodigious from the point of physysorption phenomena in microporous materials. Anomalous helium-gas-induced spin-lattice relaxation is explained by the collision of the helium gas governed by electric dipole-dipole interaction which was discovered for the first time as a new spin-lattice relaxation mechanism. This is realized by the remarkably large helium gas condensation at room temperature in microporous materials.

To get information on the micrographite network structure and the internal structure of the mocrographitic domain, transport and magnetic properties of pitch-based ACF1000 and ACF2000 with SSA~1000 and 2000 m^2/g are investigated are summarized in Part IV. The temperature dependence of conductivities for both ACF1000 and ACF2000 are described in terms of the two-dimensional variable range hopping mechanism, whose behaviors are extrapolated to the ordinary thermally activation hopping conduction with the activation energy E_a=60 ~ 80 meV in the higher temperature range. The dimensionality of the transport properties of ACF is supposed to be caused by the specific network structure of micrographitic domains which are linked to each other through bridges composed of σ-bonding carbons. Assuming that the localization length is regarded to be equal to the domain size, the densities of states at the Fermi energy level are estimated at $N(E_F)\sim10^{18}$ $eV^{-1}m^{-2}$ for both ACF1000 and ACF2000. Introduced nitrogen gas or oxygen gas changes the electrical conductivity, which is caused by a change in the micrographite network structure. In addition to the structural modification by the introduced gas, oxygen affects the electronic structure of ACF

through the formation of weak chemical bonding between dangling bonds and oxygen molecules. The magnetic susceptibilities for both ACF1000 and ACF2000 show the Curie-Weiss temperature dependent susceptibility below 40 K, which suggests the presence of 10^{19}/g localized magnetic moments associated with dangling bond spins attached to the peripheries of micrographite. The orbital diamagnetic susceptibilities $\chi_{//orb}$ of ACF1000 and ACF2000 were estimated at -1.2×10^{-7} emu/g and -1.1×10^{-7} emu/g, respectively, which are about one order of magnitude as small as that expected for the condenced polycyclic aromatic hydrocarbons having the same number of benzene rings to the average number of benzene rings of ACF1000 and 2000. This proves that the graphene sheet of ACF is deformed with some degree of nonplanarity caused by defects and distortions of the in-plane structure.

Publication List

This thesis was written principally based on the papers listed as follows:

1."**MAGNETIC PROPERTIES OF ACTIVATED CARBON FIBERS**" ,
Synthetic Metals, 57(1) p3736-3741(1993),
A. Nakayama, S. L. di Vittorio, K. Koga, K. Suzuki, T. Enoki,
M. S.Dresselhaus. M. Endo, and N. Shindo,

2. "**ESR study of activated carbon fibers**",
J. Mater. Res. 8 (9)p2282-2287 (1993),
S.L.di Vittorio, A. Nakayama, T. Enoki, M. S. Dresselhaus, M. Eddo, and
N. Shindo.

3. "**Vector EPR studies on Carbon Fibers**",
Rep. Prog. Polym. Phys. Jpn., 36, p465-468 (1993),
K. Matsushita, Y. Shimoyama, A. Nakayama, T. Enoki, M. Endo, and
N. Shindo.

4."**Anomalous helium-gas-induced energy relaxation and the evidence for ultra micropores in microporous carbon**",
Solid. State. Commun., 93 (4) p323-326 (1995),
A. Nakayama, K. Suzuki, T. Enoki, C. Ishii, K. Kaneko, M. Endo, and
N. Shindo.

5."**NOVEL STRUCTURE OF MICROPOROUS ACTIVATED CARBON FIBERS ANDTHEIR GAS ADSORPTION**",
Mat. Res. Soc. Symp. Proc. Vol. 349, p73-78, Mat. Res. Soc. (1995),

T. Enoki, A. Nakayama, N. Kobayashi, K. Suzuki, C. Ishii, K. Kaneko, and M. Endo.

6. "**Anomalous spin-lattice relaxation induced by helium gas in microporous carbon**",

   J. Phys. Soc. Jpn., 64 (7) p2614-2620 (1995),

   K. Sugihara, A. Nakayama, and T. Enoki.

7. "**Electronic and Magnetic Properties of Activated Carbon Fibers**",

   Bull. Chem. Soc. Jpn., 69, p333-339 (1996).

   A. Nakayama, K. Suzuki, T. Enoki, K. Koga, M. Endo, and N. Shindo.